國 立 交 通 大 學

土 木 工 程 學 系

博 士 論 文

以福衛三號及GRACE低軌衛星GPS資料推算時變地球重力場

Temporal Gravity Changes from FORMOSAT-3 and GRACE GPS Tracking Data

研究生：林廷融

指導教授：黃金維

中華民國九十九年六月

以福衛三號及 GRACE 低軌衛星 GPS 資料推算時變地球重力場

Temporal Gravity Changes from FORMOSAT-3 and GRACE GPS Tracking Data

研　究　生：林廷融　　　Student : Ting-Jung Lin
指導教授：黃金維　博士　　Advisor : Dr. Cheinway Hwang

國立交通大學
土木工程學系
博士論文

A Dissertation
Submitted to Department of Civil Engineering
College of Engineering
National Chiao Tung University
in partial Fulfillment of the Requirements
for the Degree of
Doctor of Philosophy
in
Civil Engineering
June 2010
Hsinchu, Taiwan, Republic of China

中華民國九十九年六月

以福衛三號及 GRACE 低軌衛星 GPS 追蹤資料推算時變地球重力場

研究生：林廷融　　　　　　　　指導教授：黃金維 博士

國立交通大學土木工程學系

摘　要

本論文內容是結合福衛三號及 GRACE 衛星高-低衛星追蹤資料反衍時變地球重力場。為了估算時變重力地位係數，吾人已成功發展兩種重力反衍方法:軌道擾動解析法及殘餘加速度法，此兩種方法分別應用殘餘軌道擾動量(動態軌道及動力軌道之差值)及殘餘加速度(觀測加速度及參考加速度之差值)兩種不同觀測量,分別建立與時變重力地位係數之線性關係後進行估算時變重力地位係數。

吾人首先使用 Bernese 5.0 軟體計算福衛三號及 GRACE 衛星公分級動態軌道。此後，以標準力模式進行計算作用於福衛三號及 GRACE 衛星上之各種擾動力，此部分使用之主要計算軟體為 NASA Goddard 研發之 GEODYN II 軟體。福衛三號表面擾動力如大氣阻力、輻射壓及其他微小表面擾動力須以力模式進行求解，並於每飛行一圈即解算一組適當表面力參數。所解算之原始 5 秒一筆之六顆福衛三號衛星及 10 秒一筆之兩顆 GRACE 衛星動態及動力軌道重新取樣為一分鐘一筆之軌道位置資料,及後以數值微分得到加速度資料分別以為重力場反衍之用。

吾人以 2006 年 8 月一個月福衛三號及 GRACE 動態及動力軌道資料求解時變重力地位係數,分別使用軌道擾動解析法及殘餘加速度法處理福衛三號單一解及合併 GRACE 成果解，福衛三號及 GRACE 平均動態及動力軌道差異量分別約

為 7.5 公分及 6.5 公分。福衛三號單一解可解出某些已知的時變重力訊號，但仍含有雜訊，合併解則可看出某些程度提升了 GRACE 單一解某些區域時變重力訊號。

此外，吾人處理自 2006 年 9 月至 2007 年 12 月共 16 個月的福衛三號及 GRACE 精密定軌資料進行每月低階時變重力係數求解至 5 階，使用軌道擾動解析法及殘餘加速度法所得到之大地起伏變化將與 CSR RL04 解進行比較分析，15 階之合併 GRACE 解也將進行求解。吾人使用軌道擾動解析法及殘餘加速度法所得到之低階帶諧係數 $\Delta\overline{C}_{20}, \Delta\overline{C}_{30}$ 及 $\Delta\overline{C}_{40}$ 之變化與 SLR 及 CSR RL04 解同期觀測比較，發現四者變化趨勢極為相似，由 SLR、軌道擾動解析法殘餘加速度法、及 CSR RL04 解算之 $\Delta\overline{C}_{20}$ 年變率分別為 $(-0.94\pm045)\times10^{-10}$、$(-1.06\pm0.86)\times10^{-10}$、$(0.15\pm0.78)\times10^{-11}$ 及 $(-1.98\pm0.86)\times10^{-10}$，CSR RL04、軌道擾動解析法及殘餘加速度法解算之 $\Delta\overline{C}_{30}$ 年變率為 $(-1.58\pm6.07)\times10^{-11}$、$(-5.13\pm7.09)\times10^{-11}$ 及 $(-7.07\pm8.14)\times10^{-11}$，$\Delta\overline{C}_{40}$ 年變率為 $(3.46\pm3.06)\times10^{-11}$、$(-0.20\pm2.91)\times10^{-11}$ 及 $(2.33\pm3.01)\times10^{-11}$。

Temporal Gravity Changes from FORMOSAT-3 and GRACE GPS Tracking Data

Student : Ting-Jung Lin Advisor : Dr. Cheinway Hwang

Department of Civil Engineering
National Chiao Tung University

Abstract

This dissertation is aimed at temporal gravity field recovery from the analyses of the high-low satellite-to-satellite tracking (hl-SST) data from the COSMIC and GRACE satellite missions. In order to estimate the time-varying geopotential coefficients, two efficient methodologies, the analytical orbital perturbation (AOP) approach and the residual acceleration (ACC) approach, are developed in the research. With the reference orbits removed, orbital perturbations (difference between kinematic and reference orbits) and residual accelerations (difference between observed and reference accelerations) from the residual orbits are linear functions of the time-varying geopotential coefficients. Such linear functions enable convenient establishments of observation equations to estimate geopotential coefficients.

The Bernese 5.0 software is used to compute the cm-level kinematic orbits of COSMIC and GRACE. The NASA Goddard's GEODYN II software is used to compute the perturbing forces acting on COSMIC and GRACE satellites based on the standard models of orbit dynamics. The accelerations due to the atmospheric drag, solar radiation pressure and other minor surface forces are estimated by some relevant model parameters over one orbital period from COSMIC's kinematic and reduced dynamic orbits. The 5s kinematic and dynamic orbits from six COSMIC and the 10s orbits from two GRACE satellites are re-sampled into 1 minute normal point

positional data and then converted to acceleration data by numerical differential for gravity recovery.

To validate the theories and computer programs associated with the AOP and ACC approaches, some experimental solutions of time-varying geopotential coefficients are carried out using one-month (August 2006) of COSMIC and GRACE kinematic and dynamic orbits. The average RMS in RTN directions of reduced COSMIC and GRACE (1 minute) between kinematic orbits and dynamic orbits are about 7.5 and 6.5 cm. The COSMIC solutions reveal several well-known temporal gravity signatures, but contain artifacts. The combined COSMIC-GRACE solutions enhance some local features in the GRACE solutions.

The monthly COSMIC and GRACE precise orbit data from September 2006 to December 2007 (16 months) are processed to recover monthly low-degree (up to degree 5) geopotential coefficients by the AOP and ACC approaches. The geoid variations from such low-degree geopotential coefficients are compared with the CSR RL04 solutions. Two combined solutions by the AOP and ACC approaches (up to degree 15) are also carried out. The monthly variations of the zonal geopotential coefficients $\Delta\overline{C}_{20}$, $\Delta\overline{C}_{30}$ and $\Delta\overline{C}_{40}$ from the AOP and ACC solutions (degree 5) closely resemble the SLR-derived and CSR RL04 solutions. The rates of $\Delta\overline{C}_{20}$ from SLR, AOP, ACC, and CSR RL04 are $(-0.94\pm045)\times10^{-10}$, $(-1.06\pm0.86)\times10^{-10}$, $(0.15\pm0.78)\times10^{-11}$ and $(-1.98\pm0.86)\times10^{-10}$, respectively. The rates of $\Delta\overline{C}_{30}$ from CSR RL04, AOP and ACC solutions are $(-1.58\pm6.07)\times10^{-11}$, $(-5.13\pm7.09)\times10^{-11}$, and $(-7.07\pm8.14)\times10^{-11}$, and the rates of $\Delta\overline{C}_{40}$ are $(3.46\pm3.06)\times10^{-11}$, $(-0.20\pm2.91)\times10^{-11}$, and $(2.33\pm3.01)\times10^{-11}$, respectively.

Table of Contents

List of Tables

List of Figures

Chapter 1
Introduction

1.1 Background

The Earth's gravity field is the sum of gravitational attraction and centrifugal force and it would vary in space and time due to the mass redistributions caused by atmospheric circulation, oceanic circulation, ground water-level variation, melting ice and other factors (Torge 1989). Gravity variations will result in satellite orbital perturbations, and variations in Earth rotational velocity and vertical datum of the Earth etc..

The precise Earth's gravity field model can be applied to several disciplines of Earth sciences including geodesy, atmosphere, oceanography, aerospace engineering and geophysics. It can be determined with a variety of techniques and observation data types including surface gravity measurements, satellite tracking measurements and satellite radar altimetry measurements (Nerem 1995). Surface gravity measurements by terrestrial absolute/relative gravimetry, superconducting gravimetry, and airborne/ship-borne gravimetry can obtain the highest point-wise accuracy or regional information about the Earth's gravity field. Satellite radar altimetry data can monitor the global sea surface height to derive gravity anomalies and geoid over the oceans or lake areas. Satellite tracking measurements are popular for global gravity field modeling and mainly acquired by Satellite Laser Ranging (SLR), Doppler Orbitography and Radio positioning Integrated by satellite (DORIS), Precise Range and Range Rate Experiment (PRARE), high-low satellite-to-satellite tracking (hl-SST), low-low satellite-to-satellite tracking (ll-SST) and Satellite Gravity Gradiometry (SGG).

Low Earth orbiters (LEOs) have become one of the basic and efficient tools for determining global time-varying gravity field in 21th century. A number of satellite missions have been launched in order to accomplish time-varying gravity field determination such as CHAMP (CHAllenging Minisatellite Payload) (Reigber et al. 1996), GRACE (The Gravity Recovery and Climate Experiment) (Tapley 1997), FORMOSAT-3/COSMIC (Constellation Observing System for Meteorology, Ionosphere and Climate) (Chao et al. 2000) and GOCE (Gravity Field and Steady-State Ocean Circulation Explorer) (ESA 1999). Although these missions employ different measurement techniques, the common feature of all missions is the use of GPS (Global Positioning System) observations for the precise orbit determination. The GPS-determined precise orbit data contains all information of orbital perturbation forces due to the Earth's non-sphericity, air drag, solar radiation, N-body, solid Earth tide, ocean tide, Earth's radiation (albedo), and relativistic effects (Seeber 2003). With appropriate methods removing the non-gravitational forces and constraints, the time-varying gravity can be derived from precise orbit data.

The FORMOSAT-3/COSMIC mission is a joint Taiwan-USA satellite mission launched in April 2006 for meteorological and ionospheric research and geodetic applications. Each of the six COSMIC satellites is equipped with two POD (Precise Orbit Determination) GPS antennas with a code-less, dual-frequency BlackJack GPS receiver (Dunn et al. 2003; Wu et al. 2005; Schreiner 2005; Montenbruck et al. 2006) developed by the Jet Propulsion Laboratory (JPL), which yield data for precise orbit and gravity determinations (Fig. 1-1). For abbreviation, the six COSMIC satellites will be named FM1- FM6, following the convention of NSPO (National Space Organization). With 6 satellites in the constellation, COSMIC configuration will provide a strong geometry in determining Earth's gravity fields. COSMIC GPS data can be used to compute orbit perturbations and/or accelerations so that they may recover the Earth's temporal gravity fields and derive the spatial and time variations of the Earth's mass. The origin of the spacecraft coordinate frame is at the geometric center of the ring. The angle between the line of coordinate origin- physical center of POD antenna and either the +X or -X axis is 30°. The angle between the normal to the antenna patch and the +X or –X axis is 15°. The COMs (center of mass) of the six satellites have been determined in a NSPO laboratory, in the configurations of full load and empty propellant fuel with stowed solar panels. The Attitude and Orbit Control System (AOCS) of a COSMIC satellite is a combination of outputs from a three-axis magnetometer, an one-axis Earth sensor and a three-axis Coarse Sun sensor but without the star-camera. The phase center offset and phase center variation (PCV) of the two POD antennas were both determined in an anechoic chamber using a mockup of COSMIC satellite, built by UCAR (the University Corporation for Atmospheric Research). The L1 and L2 phase centers were estimated for L1 and L2 frequencies and for 8 different solar arrays drive (SAD) orientations.

The geopotential parameters can be estimated from the LEO's centimeter-precise POD data. The GPS data processing is performed at two stages for gravity recovery. In the first step, a reference orbit is computed from hl-SST data; the hl-SST data are applied to linearize the observational equations for the gravity coefficients estimation. In the second step, gravity recovery is carried out. Combining with different types of space measurements, the second step may use one of the three methods: (i) Kaula's linear perturbation theory (Kaula 1966); (ii) direct numerical integration (Hwang 2001; Visser et al. 2001; Rowlands et al. 2002); (iii) energy balance approach (Wolff 1969; Wagner 1983; Jekeli 1999; Visser et al. 2003; Visser 2005).

The GRACE mission, a joint effort of NASA (USA) and DLR (German), was launched on March 17, 2002. This mission consists of two satellites, GRACE-A and GRACE-B, operating at an altitude of about 500 km as a formation at a distance of about 200 km apart. The orbit inclination is 89° as a near polar orbit and the period of 1 revolution is 94 minutes. The purpose of choosing such an orbit is mainly to obtain a homogeneous and complete global coverage for gravity field recovery. The primary objective of GRACE mission is to determine the high precision and high spatial resolution Earth's gravity field, with an emphasis on its temporal changes (Tapley et al. 2004). The secondary objective is to determine total electron content and/or refractivity from the excess delay or bending angle of GPS measurements caused by the atmosphere and ionosphere. Both GRACE satellites are equipped with the following instruments: K-Band Ranging System (KBR), Accelerometer, GPS Space Receiver, Laser Retro-Reflector (LRR), Star Camera Assembly (SCA), Coarse Earth and Sun Sensor (CES), Ultra Stable Oscillator (USO) and Center of Mass Trim Assembly (CMT) (Fig.1-2) (GFZ homepage). The KBR system is to measure the inter-satellite distance forming the ll-SST observation, derived range-rates, and range-accelerations between two satellites. The accuracies of the inter-satellite distance and the range rate are 10μm and 1μm/s, respectively. On-board GPS TurboRogue Space Receivers receive GPS data to determine precise satellite orbits and to synchronize time tags of KBR measurements. The SuperSTAR accelerometer measures non-gravitational satellite accelerations. The satellite attitudes are controlled and determined by the SCA and CES systems. The LRR system is to measure distances between dedicated laser ground stations and the satellites with an accuracy of 1-2 cm. The USO system is built for the frequency generation of the KBR system. The CMT system is developed to adjust the offset between the satellite's COM and the center of the accelerometer proof-mass.

Three alternative monthly GRACE gravity models published by different institutions CSR, GFZ and JPL are available at the web site of Center for Space Research (CSR), The University of Texas at Austin (http://www.csr.utexas.edu/grace). The static gravity solutions, GGM02S (Tapley et al. 2005) and GGM03S (Tapley et al. 2007) derived from GRACE KBR and GPS measurements, is also available at the website. The monthly solutions issued by CSR have three versions: Release 01 (RL01), Release 02 (RL02) and Release 04 (RL04). The CSR RL04 monthly solutions based on one-step variational equations approach contain fully normalized spherical harmonic coefficients up to degree and order 60. The solution is obtained through an optimally weighted combination of GPS and KBR data with one-day dynamic arcs for a designated month. More details of the RL04 model development can be found in the documents released with the GRACE products (Bettadpur 2007).

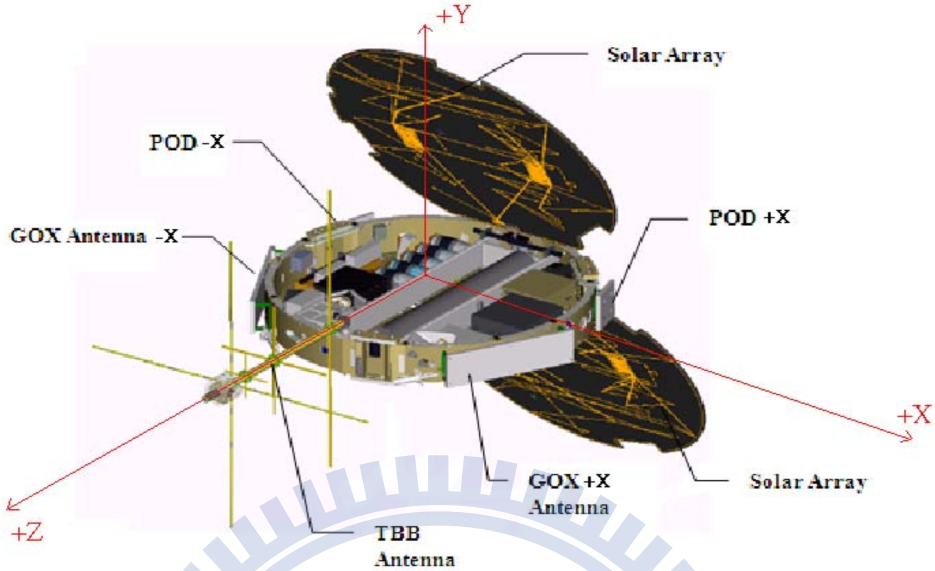

Fig. 1-1: A COSMIC spacecraft, payloads and spacecraft-fixed coordinate system, the origin is at the center of the main body (cylinder) (Hwang et al. 2008)

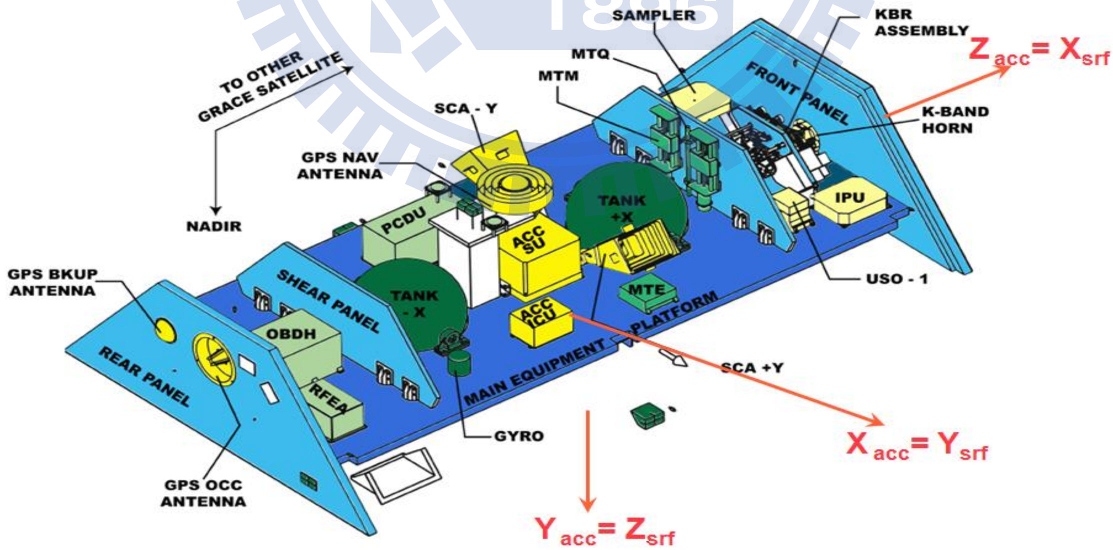

Fig. 1-2: GRACE science instrumentation

(http://www-app2.gfz-potsdam.de/pb1/op/grace/index_GRACE.html)

1.2 Research objectives

The primary objective of this research is to develop efficient techniques and data processing procedures to process the hl-SST observations from COSMIC and GRACE to recover the temporal Earth's gravity field models represented in the form of spherical harmonic series. Based on this objective, the first research regarding with the hl-SST data processing starts from a so-called analytical orbital perturbation (AOP) approach developed by Kaula (1966). For gravity recovery, the geometrically determined kinematic orbits are functions of orbit dynamic parameters, including geopotential coefficients, can be regarded as observations, and would be used in the least-squares estimation of these parameters.

The residual acceleration (ACC) approach is the second technique related to hl-SST data processing using satellites accelerations derived from precise kinematic and reference dynamic orbits by numerical differentiations. After removing accelerations other than the Earth's gravity-induced accelerations, linear relations between LEO accelerations and gravity coefficients can be established. The residual acceleration differences between kinematic and reference orbits are assumed to be linear functions of time-varying geopotential coefficients and further used as observations for the geopotential coefficients estimation.

The second objective of this thesis is to derive time series of low-degree, zonal term gravity changes using COSMIC and GRACE GPS data. The combined COSMIC and GRACE solutions are also computed which are expected to enhance local temporal gravity signatures contained in the GRACE only solutions. The time series of zonal geopotential coefficients derived by AOP and ACC methods will also be assessed by those derived by tracking data.

1.3 Outline of Thesis

This dissertation comprises seven chapters. The detailed introductions of two gravity field recovery methods, analytical orbital perturbation approach and residual acceleration approach, are described in Chapter 2. This chapter starts from the analytical orbital perturbation approach which makes use of the relationship between the positional variations of orbits and variations in the six Keplerian elements from hl-SST observations. After that, the residual acceleration approach is proposed for gravity solutions.

In Chapter 3, since the precise orbits play an important role in gravity field recovery, the main principle of precise orbit determination is presented. The descriptions of orbit dynamics are discussed especially about the surface forces including atmospheric drag, solar radiation pressure and the Earth's radiation pressure acting on COSMIC satellites. The procedures of precise dynamic orbit determination using GEODYN II software (Pavlis et al. 1996) and precise kinematic orbit determination using Bernese 5.0 software (Dach et al. 2007) are also provided. To reduce noises and data volume, the normal-point reduction is therefore introduced.

Chapter 4 is devoted to gravity field modeling using analytical orbital perturbation approach. The procedure of processing kinematic orbit and the orbit accuracy assessment is presented in this chapter. Both COSMIC and combined COSMIC and GRACE gravity solutions are computed using the post-processed orbit data.

Chapter 5 focuses on gravity field modeling derived from combined COSMIC and GRACE POD data and residual acceleration approach was applied. Position data screening and computation of residual accelerations are discussed in this chapter. The results from simulations and real data processing are carried out and compared with the results from AOP solution and CSR RL04 solution.

A time-series analysis of the estimated COSMIC and GRACE monthly low-degree temporal gravity solution is the subject of Chapter 6. The time span is from September 2006 to December 2007. The COSMIC and GRACE monthly low-degree temporal gravity solutions and combined solutions are presented in this chapter. Moreover, a comparison of some zonal geopotential coefficients with SLR and CSR RL04 solutions is also covered in this chapter.

Chapter 7 contains summaries, conclusions, future researches and suggestions.

Chapter 2
Methods for gravity field modeling using GPS observations

2.1 Introduction

A conventional one-step approach to model the gravity field is to use the raw GPS measurements directly in the equations of motion for estimation of geopotential coefficients. In this case, the relationship between geopotential coefficients and SST measurements is not linear, so the linearlization of observation equations is required. After linearization and with some iterations, the orbits of LEOs and GPS satellites and gravity field parameters can be determined by the method of least-squares adjustment with inputs from GPS ground and space-borne data, SLR data, accelerometer data, K-band observation data, etc. (Zhu et al 2004). The GGM and EIGEN series of static gravity field models based on GRACE KBR and GPS measurements are computed in this way (Tapley et al. 2004; Reigber et al. 2005; Förste et al. 2006).

At present, the two-step approach, i.e. computing orbit first and estimating gravity fields using such orbits, is widely adopted for gravity field modeling. Compared to the one-step approach, this two-step procedure avoids the time-consuming computations of associated partials with respect to parameters. Two basic important physical laws are applied: the energy conservation law and Newton's second law of motion. In this thesis, we focus on the two-step approach using GPS observations based on Newton's second law of motion. See Section 2-2 for the description of the two-step approach where the analytical orbital perturbation approach is involved (Kaula 1966). The residual acceleration approach linking the acceleration vector to the gradient of the gravitational potential is discussed in Section 2.3.

2.2 Theory of analytical orbital perturbation approach

To establish the linear relationship between the satellite positions and geopotential coefficients, Kaula (1966) demonstrated the analytical orbital perturbation method for gravity field recovery in terms of the six Keplerian elements. The six Keplerian elements (a, e, i, ω, Ω, M) are semi-major axis, eccentricity, inclination, argument of perigee, right ascension of the ascending node, and mean anomaly. To use the three-dimensional positional data for gravity field recovery, orbital perturbations in radial, along-track and cross-track (RTN) directions should be transformed to perturbations in the Keplerian elements.

The radial distance r of a LEO from the geocenter is

$$r = a(1 - e\cos E) \tag{2-1}$$

where E is eccentricity anomaly, which is related to the mean anomaly by $M = E - e \cdot \sin E$. The perturbations in the RTN directions, shown in Fig. 2-1, can be expressed as

$$\Delta x_1 = \frac{\partial r}{\partial a}\Delta a + \frac{\partial r}{\partial e}\Delta e + \frac{\partial r}{\partial E}\Delta E = (1 - e\cos E)\Delta a - (a\cos E)\Delta e + (ae\sin E)\Delta E \tag{2-2}$$

$$\Delta x_2 = r(\Delta u + \Delta\Omega\cos i) = r[\Delta\omega + \Delta f + (\cos i)\Delta\Omega] \tag{2-3}$$

$$\Delta x_3 = r[(\sin u)\Delta i - (\sin i\cos u)\Delta\Omega] \tag{2-4}$$

where f is true anomaly and $u = \omega + f$ is argument of latitude.

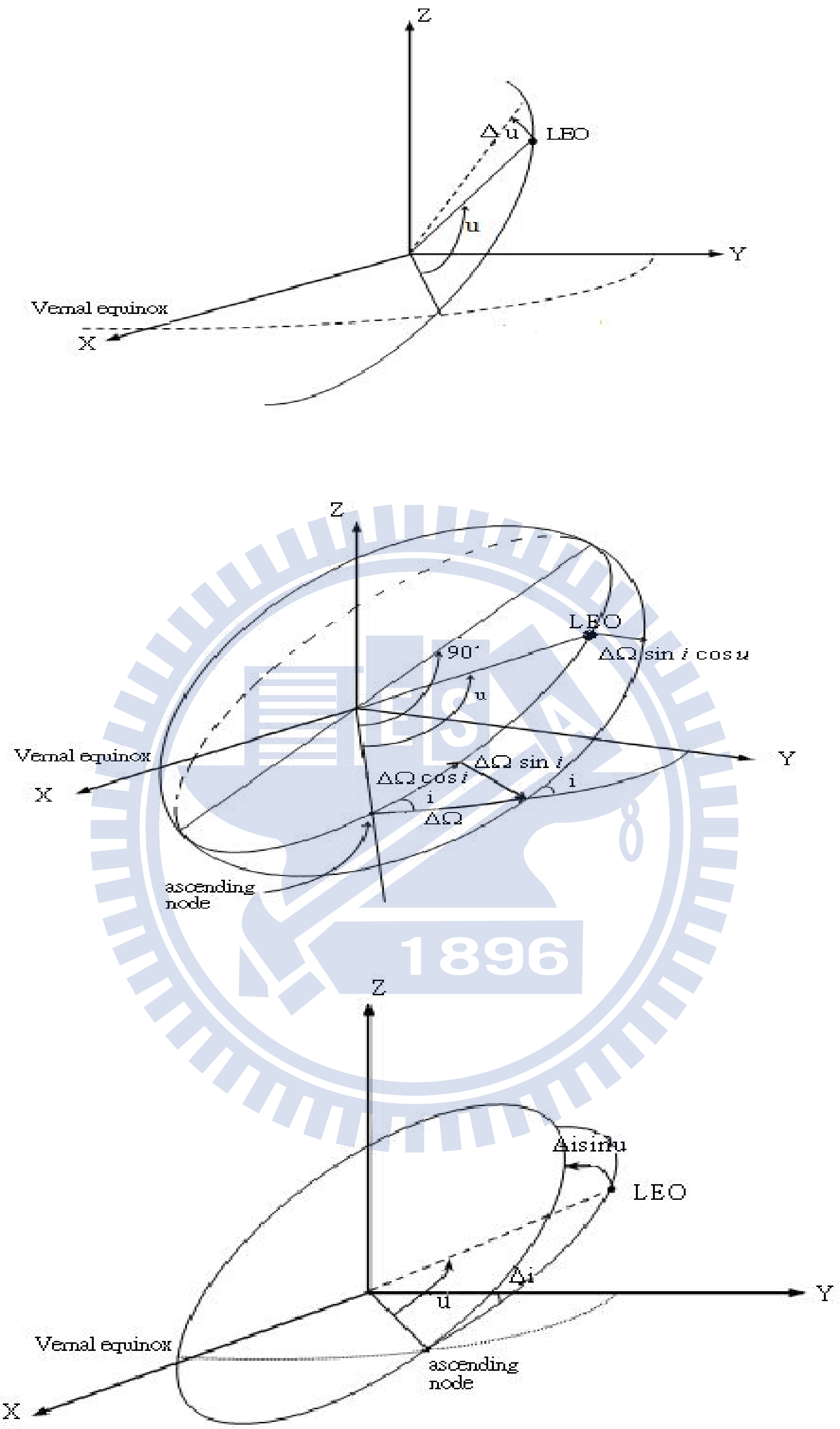

Fig. 2-1: Geometry showing the effects of perturbations in argument of perigee (top), right ascension of the ascending node and inclination (bottom) on the radial, along-track, and cross-track perturbations at a satellite position (Hwang 2001)

The potential due to the Earth (called geopotential) at the satellite position, V, is expanded into a spherical harmonic series as (Heiskanen and Moritz 1985)

$$
\begin{aligned}
V(r,\phi,\lambda) &= \frac{GM}{r}\left[1+\sum_{n=1}^{K}\left(\frac{a_e}{r}\right)^n \sum_{m=0}^{n}(\overline{C}_{nm}\cos m\lambda+\overline{S}_{nm}\sin m\lambda)\overline{P}_{nm}(\sin\phi)\right] \\
&= \frac{GM}{r}+V_{ns}
\end{aligned}
\tag{2-5}
$$

where (r,ϕ,λ) are the spherical coordinates (radial distance, geocentric latitude and longitude), a_e is the semi-major axis of the Earth's reference ellipsoid, K is the maximum degree of expansion depending on the satellite altitude, $(\overline{C}_{nm},\overline{S}_{nm})$ are geopotential coefficients, $\overline{P}_{nm}$ is the fully normalized associated Legendre function of degree n and order m, and V_{ns} is the potential due to the Earth's non-sphericity (perturbing potential). From eq. (2-5), the perturbing potential V_{ns} can be expressed in terms of the six Keplerian elements as (Kaula 1996; Balmino 1994; Hwang 2001):

$$
V_{ns} = R = \sum_{n=2}^{K}\sum_{m=0}^{n}\sum_{p=0}^{n}\sum_{q=-Q}^{Q} R_{nmpq} \tag{2-6}
$$

$$
R_{nmpq} = \frac{GMa_e^n}{a^{n+1}}\overline{F}_{nmp}(i)G_{npq}(e)S_{nmpq}(\omega,M,\Omega,\theta) \tag{2-7}
$$

where Q is the number depending on the orbital eccentricity, and θ is Greenwich sidereal time (GST). $\overline{F}_{nmp}$ is the fully normalized inclination function, and is defined by (Balmino 1994; Hwang and Hwang 2002)

$$\bar{F}_{nmp} = H_{nm} F_{nmp} \tag{2-8}$$

where

$$F_{nmp}(i) = (-1)^{E\left(\frac{n-m+1}{2}\right)} \frac{(n+m)!}{2^n p!(n-p)!} \times \sum_{j=\max\{n-2p-m,0\}}^{\min\{n-m,2n-2p\}} (-1)^j \binom{2n-2p}{j} \binom{2p}{n-m-j} c^{2n-a} s^a \tag{2-9}$$

$$H_{nm} = \left[(2-\delta(m))(2l-1)(l-m)!/(l+m)!\right]^{1/2} \tag{2-10}$$

$c = \cos(i/2)$, $s = \sin(i/2)$, and $a = m - n + 2p + 2j$. $G_{npq}(e)$ is the eccentricity function, which is a polynomial of e about the order $e^{|q|}$ (Kaula 1966). S_{nmpq} is defined by

$$S_{nmpq}(\omega, M, \Omega, \theta) = \begin{pmatrix} \bar{C}^{+}_{nm} \\ -\bar{S}^{-}_{nm} \end{pmatrix} \cos(\psi_{nmpq}) + \begin{pmatrix} \bar{S}^{+}_{nm} \\ \bar{C}^{-}_{nm} \end{pmatrix} \sin(\psi_{nmpq}) \tag{2-11}$$

$$\psi = (n-2p)\omega + (n-2p+q)M + m(\Omega - \theta) \tag{2-12}$$

where $\bar{C}^{+}_{nm}$ is $\bar{C}_{nm}$ when (*n-m*) is even and $\bar{C}^{-}_{nm}$ is $\bar{C}_{nm}$ when (*n-m*) is odd (the same is true for $\bar{S}_{nm}$).

The Lagrange's equation of motion (LEOM) is (Kaula 1966)

$$\frac{da}{dt}=\frac{2}{\bar{n}a}\frac{\partial R}{\partial M}$$

$$\frac{de}{dt}=\frac{1-e^2}{\bar{n}a^2e}\frac{\partial R}{\partial M}-\frac{\sqrt{1-e^2}}{\bar{n}a^2e}\frac{\partial R}{\partial \omega}$$

$$\frac{di}{dt}=\frac{\cos i}{\bar{n}a^2\sqrt{1-e^2}\sin i}\frac{\partial R}{\partial \omega}-\frac{1}{\bar{n}a^2\sqrt{1-e^2}\sin i}\frac{\partial R}{\partial \Omega} \tag{2-13}$$

$$\frac{d\omega}{dt}=-\frac{\cos i}{\bar{n}a^2\sqrt{1-e^2}\sin i}\frac{\partial R}{\partial i}+\frac{\sqrt{1-e^2}}{\bar{n}a^2e}\frac{\partial R}{\partial e}$$

$$\frac{d\Omega}{dt}=\frac{1}{\bar{n}a^2e\sqrt{1-e^2}\sin i}\frac{\partial R}{\partial i}$$

$$\frac{dM}{dt}=\bar{n}-\frac{1-e^2}{\bar{n}a^2e}\frac{\partial R}{\partial e}-\frac{2}{\bar{n}a}\frac{\partial R}{\partial a}$$

where $\bar{n}=\sqrt{GM/a^3}$ is the mean angular velocity. An approximate solution of eq. (2-13) with a closed form can be derived for a near-circular orbit ($e\approx 0$).In such a solution, it is assumed that a ,e and i are invariant with time (denoted as $\bar{a}$,$\bar{e}$ and $\bar{i}$) and ω ,Ω and M vary linearly with time, so that (Hwang and Hwang 2002)

$$\omega(t)=\omega_0+\dot{\omega}(t-t_0)$$

$$\Omega(t)=\Omega_0+\dot{\Omega}(t-t_0) \tag{2-14}$$

$$M(t)=M_0+\dot{M}(t-t_0)$$

where ω_0 ,Ω_0 and M_0 are the mean elements and $\dot{\omega}$,$\dot{\Omega}$ and $\dot{M}$ are the linear rates. Because the C_{20} term (or $-J_2$) is the order of 10^{-3} and it is at least 1000 times larger than any other geopotential coefficients, the major contribution to the perturbing potential is due to this term and can be expressed as

$$R_{20} = \frac{GMC_{20}}{a}\left(\frac{a_e}{a}\right)^2 \sum_{p=0}^{2}\sum_{q=-\infty}^{\infty} F_{20p}(i)G_{2pq}(e)\cos\left((2-2p)\omega + (2-2p+q)M\right) \quad (2\text{-}15)$$

The term with M in eq. (2-15) has a period much smaller than other terms, and hence can be neglected provided that long-period perturbations are sought, that is,

$$2-2p+q=0 \quad (2\text{-}16)$$

The (p, q) terms with (0, -2) and (2, 2) do not exist (Kaula 1966), thus the only term left is

$$R_{2010} = \frac{GMC_{20}}{a}\left(\frac{a_e}{a}\right)^2 F_{201}(i)G_{210}(e) \quad (2\text{-}17)$$

Based on Kaula (1966), the values of $F_{201}(i)$ and $G_{210}(e)$ are

$$\begin{aligned} F_{201}(i) &= 3\sin^2 i/4 - 1/2 \\ G_{210}(e) &= (1-e^2)^{-3/2} \end{aligned} \quad (2\text{-}18)$$

Thus, the secular perturbation due to C_{20} is

$$\frac{da}{dt} = \frac{de}{dt} = \frac{di}{dt} = 0 \tag{2-19}$$

$$\dot{\omega} = \frac{d\omega}{dt} = \frac{3nC_{20}a_e^{\ 2}}{4(1-e^2)a^2}\left(1-5\cos^2 i\right)$$

$$\dot{\Omega} = \frac{d\Omega}{dt} = \frac{3nC_{20}a_e^{\ 2}}{2(1-e^2)a^2}\cos i \tag{2-20}$$

$$\dot{M} = \frac{dM}{dt} = n - \frac{3nC_{20}a_e^{\ 2}}{4(1-e^2)a^2}\left(3\cos i - 1\right)$$

A reference orbit at the reference epoch t_0 based on nine orbital parameters ($\bar{a}$,$\bar{e}$,$\bar{i}$,ω_0 ,Ω_0 ,M_0 ,$\dot{\omega}$,$\dot{\Omega}$,$\dot{M}$) is used. Integrating eq. (2-13) with respect to time yields

$$\Delta\alpha = \sum_{n=2}^{K}\sum_{m=0}^{n}\sum_{p=0}^{n}\sum_{q=-Q}^{Q}\Delta\alpha_{nmpq} \tag{2-21}$$

where α denotes any of the six Keplerian elements. Integrating eq. (2-11), we get

$$S^{*}_{nmpq}(\omega, M, \Omega, \theta) = \begin{pmatrix} \bar{C}^{+}_{nm} \\ -\bar{S}^{-}_{nm} \end{pmatrix}\sin(\psi_{nmpq}) - \begin{pmatrix} \bar{S}^{+}_{nm} \\ \bar{C}^{-}_{nm} \end{pmatrix}\cos(\psi_{nmpq}) \tag{2-22}$$

The perturbations in a ,e ,i are

$$\Delta s_k = \sum_{n=2}^{K}\sum_{m=0}^{n}\sum_{p=0}^{n}\sum_{q=-Q}^{Q}\alpha^{i}_{nmpq}S_{nmpq} \tag{2-23}$$

And the perturbations in ω ,Ω and M are

$$\Delta s_k = \sum_{n=2}^{K} \sum_{m=0}^{n} \sum_{p=0}^{n} \sum_{q=-Q}^{Q} \alpha^{i}_{nmpq} S^{*}_{nmpq} \tag{2-24}$$

The coefficients α^{i}_{nmpq} in the order of six Keplerian elements a , e , i, ω, Ω, M are

$$\alpha^{1}_{nmpq} = 2ab\overline{F}_{nmp} G_{npq} (n-2p+q)$$

$$\alpha^{2}_{nmpq} = b\frac{(1-e^2)^{1/2}}{e}\overline{F}_{nmp} G_{npq} \times [(1-e^2)^{1/2}(n-2p+q)-n+2p]$$

$$\alpha^{3}_{nmpq} = b\overline{F}_{nmp} G_{npq} \frac{[(n-2p)\cos I - m}{\sin I (1-e^2)^{1/2}}$$

$$\alpha^{4}_{nmpq} = b\frac{\overline{F}'_{nmp} G_{npq}}{\sin I (1-e^2)^{1/2}} \tag{2-25}$$

$$\alpha^{5}_{nmpq} = b\left[\frac{(1-e^2)^{1/2}}{e}\overline{F}_{nmp} G'_{npq} - \frac{\cos I}{\sin I (1-e^2)^{1/2}}\overline{F}'_{nmp} G_{npq}\right]$$

$$\alpha^{6}_{nmpq} = b\overline{F}_{nmp}\left[2(n+1)G_{npq} - \frac{(1-e^2)^{1/2}}{e}G'_{npq} - 3G_{npq}(n-2p+q)\frac{\overline{n}}{\dot{\psi}_{nmpq}}\right]$$

where

$$b = \frac{\overline{n}}{\dot{\psi}_{nmpq}}\left(\frac{a_e}{a}\right)^{n} \tag{2-26}$$

$$\dot{\psi}_{nmpq} = (n-2p)\dot{\omega} + (n-2p+q)\dot{M} + m(\dot{\Omega} - \dot{\theta}) \tag{2-27}$$

$$\overline{F}'_{nmp} = \frac{\partial \overline{F}_{nmp}}{\partial i}, G'_{npq} = \frac{\partial G_{npq}}{\partial e} \tag{2-28}$$

where $\dot{\psi}$ is the frequency of the perturbations, and $\dot{\theta}$ is the velocity of the GST (about $7.292115 \times 10^{-5} rads^{-1}$).

Let Δx_i and Δs_k represents the perturbations in the RTN directions and of the six Keplerian elements. We have

$$\Delta x_i = \sum_{k=1}^{6} c_k^i \Delta s_k \,, \quad i = 1,2,3 \tag{2-29}$$

where c_k^i are the coefficients used to transform the Keplerian perturbations to the RTN perturbations (Hwang 2001). The coefficients are

$$c_3^1 = c_4^1 = c_5^1 = 0, c_1^1 = 1 - e\cos E,$$
$$c_2^1 = -a\cos E + \frac{ae\sin^2 E}{1 - e\cos E}, c_6^1 = \frac{ae\sin E}{1 - e\cos E},$$

$$c_1^2 = c_1^2 = 0, c_3^2 = \frac{r(2 - e^2 - e\cos E)\sin E}{\sqrt{1-e^2}(1 - e\cos E)^2},$$
$$c_4^2 = r\cos I, c_5^2 = r, c_6^2 = \frac{r\sqrt{1-e^2}}{(1 - e\cos E)^2}, \tag{2-30}$$

$$c_1^3 = c_2^3 = c_5^3 = c_6^3 = 0,$$
$$c_3^3 = \frac{r[\sin\omega(\cos E - e) - \sqrt{1-e^2}\cos\omega\sin E]}{1 - e\cos E},$$
$$c_4^3 = r\sin I\frac{\cos\omega(\cos E - e) - \sqrt{1-e^2}\sin\omega\sin E}{1 - e\cos E},$$

The above relationships between orbit perturbations and geopotential coefficients can be used for least-squares estimation of the later given GPS-determined satellite orbits.

2.3 Theory of residual acceleration approach

A residual acceleration method is employed to determine the time variation of the Earth's gravity field. In this method, the accelerations of LEOs are determined by numerical differentiations of the positions of LEOs. All perturbing forces caused by the static gravity field, Earth's non-sphericity, N-body, solid Earth tide, ocean tide, air drag, solar radiation pressure, Earth radiation and relativity are modeled first. After removing accelerations other than the Earth's gravity-induced accelerations, linear relations between LEO accelerations and gravity coefficients can be established. Empirical parameters can be used to model the residual non-gravitational accelerations.

The total gravitational force is the gradient of *V*. The acceleration vector expressed in the Earth-fixed coordinate system is (GSFC 1989)

$$\mathbf{a}_{ns}^{b}=\begin{bmatrix}\dfrac{\partial V_{ns}}{\partial x_b}\\ \dfrac{\partial V_{ns}}{\partial y_b}\\ \dfrac{\partial V_{ns}}{\partial z_b}\end{bmatrix}=\begin{bmatrix}\dfrac{\partial r}{\partial x_b} & \dfrac{\partial \phi}{\partial x_b} & \dfrac{\partial \lambda}{\partial x_b}\\ \dfrac{\partial r}{\partial y_b} & \dfrac{\partial \phi}{\partial y_b} & \dfrac{\partial \lambda}{\partial y_b}\\ \dfrac{\partial r}{\partial z_b} & \dfrac{\partial \phi}{\partial z_b} & \dfrac{\partial \lambda}{\partial z_b}\end{bmatrix}\begin{bmatrix}\dfrac{\partial V_{ns}}{\partial r}\\ \dfrac{\partial V_{ns}}{\partial \phi}\\ \dfrac{\partial V_{ns}}{\partial \lambda}\end{bmatrix} \tag{2-31}$$

where x_b , y_b and z_b are the Earth-fixed coordinates and r, ϕ, and λ are the spherical coordinates. The partial derivatives of the non-spherical portion of the Earth's potential with respect to r, ϕ, and λ are given by

$$\frac{\partial V_{ns}}{\partial r} = -\frac{GM}{r^2}\sum_{n=2}^{\infty}\left(\frac{a_e}{r}\right)^n (n+1)\sum_{m=0}^{n}(\overline{C}_{nm}\cos m\lambda + \overline{S}_{nm}\sin m\lambda)\overline{P}_{nm}(\sin\phi) \quad (2\text{-}32)$$

$$\begin{aligned}\frac{\partial V_{ns}}{\partial \phi} = \frac{GM}{r}\sum_{n=2}^{\infty}\left(\frac{a_e}{r}\right)^n \sum_{m=0}^{n}(\overline{C}_{nm}\cos m\lambda + \overline{S}_{nm}\sin m\lambda)\cdot \\ \left[\sqrt{(n-m)(n+m+1)/(1+\delta(m))}\overline{P}_{n,m+1}(\sin\phi) - m\tan\phi\overline{P}_{nm}(\sin\phi)\right]\end{aligned} \quad (2\text{-}33)$$

$$\frac{\partial V_{ns}}{\partial \lambda} = \frac{GM}{r}\sum_{n=2}^{\infty}\left(\frac{a_e}{r}\right)^n \sum_{m=0}^{n} m(\overline{S}_{nm}\cos m\lambda - \overline{C}_{nm}\sin m\lambda)\overline{P}_{nm}(\sin\phi) \quad (2\text{-}34)$$

where $\delta(m)=1$ when m is zero and $\delta(m)=0$ when m is not zero. Substituting eq. (2-32) through eq. (2-34) into eq. (2-31) and transforming the Earth-fixed coordinates (x_b , y_b , z_b) into the spherical coordinates (r , ϕ , λ), eq. (2-31) can be rewritten as

$$\mathbf{a}_{ns}^{b} = \begin{bmatrix} \frac{x_b}{r} & \frac{-x_b z_b}{r\sqrt{x_b^2+y_b^2}} & \frac{-y_b}{\sqrt{x_b^2+y_b^2}} \\ \frac{y_b}{r} & \frac{-y_b z_b}{r\sqrt{x_b^2+y_b^2}} & \frac{x_b}{\sqrt{x_b^2+y_b^2}} \\ \frac{z_b}{r} & \frac{\sqrt{x_b^2+y_b^2}}{r} & 0 \end{bmatrix} \begin{bmatrix} \frac{\partial V_{ns}}{\partial r} \\ \frac{\partial V_{ns}}{r\partial \phi} \\ \frac{\partial V_{ns}}{r\cos\phi\partial\lambda} \end{bmatrix} = \mathbf{Ma} \quad (2\text{-}35)$$

where $\mathbf{a}$ is the acceleration vector $[\mathbf{A_r}, \mathbf{A_\varphi}, \mathbf{A_\lambda}]$ expressed in a local rotating frame which are the radial, latitudinal, and longitudinal accelerations, respectively. $\mathbf{M}$ is an orthogonal matrix. The transformation of eq. (2-35) can be simplified by neglecting precession, nutation, and polar motion to obtain the acceleration vector $\mathbf{a}^I$ in the inertial coordinate system (Hwang and Lin 1998):

$$\mathbf{a}^I = \begin{bmatrix} \dfrac{x}{r} & \dfrac{-xz}{r\sqrt{x^2+y^2}} & \dfrac{-y}{\sqrt{x^2+y^2}} \\ \dfrac{y}{r} & \dfrac{-yz}{r\sqrt{x^2+y^2}} & \dfrac{x}{\sqrt{x^2+y^2}} \\ \dfrac{z}{r} & \dfrac{\sqrt{x^2+y^2}}{r} & 0 \end{bmatrix}^{-1} \begin{bmatrix} \dfrac{\partial V_{ns}}{\partial r} \\ \dfrac{\partial V_{ns}}{r\partial \phi} \\ \dfrac{\partial V_{ns}}{r\cos\phi \partial \lambda} \end{bmatrix} \tag{2-36}$$

where x, y and z are the inertial coordinates, $r = \sqrt{x^2+y^2+z^2}$. The longitude and latitude are calculated as follows:

$$\lambda = \tan^{-1}(y/x) - \mathrm{GAST} \tag{2-37}$$

$$\phi = \sin^{-1}(z/r) \tag{2-38}$$

where GAST is Greenwich apparent sidereal time.

Chapter 3

Force modeling and precise orbit determination for COSMIC

3.1 Introduction

Precise orbits of a satellite position are important for positioning the satellite and for estimation of the Earth's gravitation. Owing to the development of GPS, the spacecraft equipped with hl-SST receiver can collect position data continuously. The dynamic method (using force models) and the kinematic method (not using force models) (Švehla and Rothacher 2003; Jäggi et al. 2006 and 2007; Hwang et al. 2009) are two popular methods using GPS data applied for POD of LEOs. In addition, the so-called reduced-dynamic orbit determination, which is a compromising method between the dynamic method and the kinematic method, requires simplified force models. All above procedures for POD require GPS satellite ephemeris, Earth rotation information, and LEO GPS observation data as input for processing.

In Section 3.2, we focus on the perturbation force models acting on a COSMIC spacecraft. Without an accelerometer on the COSMIC spacecraft, the non-gravitational accelerations due to atmospheric drag and solar radiation need to be modeled. Section 3.3 and 3.4 describe the kinematic and dynamic orbit determination methods, complete with the principles, computation procedures and some analysis of results. The procedure of observed orbit data compression applied in gravity recovery is presented in the last part of this chapter.

3.2 Orbit dynamics of COSMIC satellite

The perturbing forces (accelerations) can be classified into gravitational forces and surface forces (or non-gravitational forces). The gravitational forces include the

Earth's non-sphericity, N-body, solid Earth tide, ocean tide, and relativistic effect, and the surface forces include atmospheric drag, solar radiation pressure and the Earth's radiation pressure. General accelerations, or empirical accelerations, are used to absorb the mis-modeled and un-modeled gravitational and surface forces. The algorithms of N-body, solid Earth tide, ocean tide, and relativistic effects can be found in a standard textbook of orbit dynamics such as Seeber (2003), and they will not be elaborated here. In this section, we focus on the parameters related to Earth's non-sphericity, atmospheric drag and solar radiation pressure.

3.2.1 Equations of motion and perturbing potential force

In a geocentric inertial rectangular coordinate system, the equations of motion of an artificial Earth satellite such a COSMIC spacecraft can be expressed as (Long et al. 1989; Montenbruck and Gill 2001; Seeber 2003)

$$\ddot{\mathbf{r}} = -\frac{GM}{r^3}\mathbf{r} + \mathbf{a}_{\mathbf{ns}} + \mathbf{a}_{\mathbf{Pert}} \tag{3-1}$$

where

$\mathbf{r}$: vector of satellite coordinates in the inertial frame

$\ddot{\mathbf{r}}$: acceleration vector

GM: Earth's gravitational constant

$\mathbf{a}_{\mathbf{ns}}$: acceleration due to Earth's non-sphericity

$\mathbf{a}_{\mathbf{Pert}}$: accelerations due to other perturbing forces

The first term in eq. (3-1) is called the point mass effect of the Earth given by Newton's law of gravity and is 1000 times larger than any other acceleration. Eq. (3-1) contains a system of second order differential equations which can be integrated to obtain the satellite positions and velocity at any epoch giving the initial state vector. The direct integration known as Cowell's method (Balmino 1989) is selected for the simplicity and capacity for incorporating additional perturbations easily (Pavlis et al. 1996). The accelerations in eq. (3-1) are associated with certain parameters and can be adopted from existing values or estimated by satellite tracking data.

The acceleration $\mathbf{a}_{\text{earth}}$ due to the geopotential is the gradient vector of the geopotential:

$$\mathbf{a}_{\text{earth}} = \frac{\partial V}{\partial \mathbf{r}} = -\frac{GM}{r^3}\mathbf{r} + \mathbf{a}_{\text{ns}} \tag{3-2}$$

The first term in eq. (3-2) corresponds to the potential of a spherically symmetric Earth and the potential can be considered static. In fact, due to mass re-distribution in the Earth system, the geopotential is time-dependent so that the time-varying part should be considered. This is equivalent to dividing the coefficients in eq. (2-5) into a static part and a time-varying part as

$$\overline{C}_{nm}(t) = \overline{C}^0_{nm} + \Delta\overline{C}_{nm}(t), \quad \overline{S}_{nm}(t) = \overline{S}^0_{nm} + \Delta\overline{S}_{nm}(t) \tag{3-3}$$

where t is time. Thus, by recovering temporal gravity we mean estimating the time-varying coefficients $(\Delta\overline{C}_{nm}(t), \Delta\overline{S}_{nm}(t))$ with respect to a mean gravity field.

3.2.2 Atmospheric drag and solar radiation effects on COSMIC satellites

The acceleration vector of a LEO due to atmospheric drag is given by

$$\mathbf{a}_{\mathbf{drag}} = -\frac{1}{2} C_D \rho \frac{A_d}{m} |\dot{\mathbf{r}} - \dot{\mathbf{r}}_{\mathbf{d}}| (\dot{\mathbf{r}} - \dot{\mathbf{r}}_{\mathbf{d}}) \tag{3-4}$$

where C_D is drag coefficient depending on the LEO shape and atmospheric composition, ρ is atmospheric density at the LEO position, A_d is effective (cross-sectional) area and m is the mass of the LEO, $\dot{\mathbf{r}}, \dot{\mathbf{r}}_d$ are the velocity vectors of the LEO and atmosphere in the inertial frame, and $(\dot{\mathbf{r}} - \dot{\mathbf{r}}_{\mathbf{d}})$ is the velocity vector of the LEO relative to atmosphere. For each of the six COSMIC spacecrafts, the mass (with full thrust fuel) has been determined in the chamber test before the launch (April 2006). The remaining thrust fuel during the flight is observed and is used to adjust the time-dependent mass after the launch (Hwang et al. 2006 and 2009). The effective area A_d is the projected area of the area of the satellite in the flight direction onto a plane perpendicular to the direction $(\dot{\mathbf{r}} - \dot{\mathbf{r}}_{\mathbf{d}})$. A COSMIC spacecraft travels in a manner that the POD+X antenna points to the flight direction (Fig. 3-1). Therefore, the total area in the flight direction is

$$A_T = A_{main} + A_{panel} \tag{3-5}$$

where A_{main} is the area of the main body and A_{panel} is the area of two solar panels, which are computed as

$$A_{main} = 1.034 \times 0.132 \ (\mathrm{m}^2)$$
$$A_{panel} = 2 \times \pi (\frac{0.974}{2})^2 \sin\theta \ (\mathrm{m}^2) \tag{3-6}$$

where θ is the rotational angle of the solar panel (Fig. 3-1). Here we assume the thickness of the solar panels is negligible. The effective area was then computed by

$$A_d = A_T \cos^{-1}(\dot{\mathbf{r}} \cdot (\dot{\mathbf{r}} - \dot{\mathbf{r}}_{\mathbf{d}}) / |\dot{\mathbf{r}}||\dot{\mathbf{r}} - \dot{\mathbf{r}}_{\mathbf{d}}|) \tag{3-7}$$

The velocity vector of atmosphere was computed as

$$\dot{\mathbf{r}}_{\mathbf{d}} = \begin{bmatrix} -\omega_h y \\ -\omega_h x \\ 0 \end{bmatrix} \tag{3-8}$$

where x and y are geocentric coordinate components of the LEO in the inertial frame, and ω_h is the rotational velocity of atmosphere at an altitude of h computed as (King-Hele and Walker 1983)

$$\omega_h = \omega_e(1 - 1.588187\times10^{-3}h + 1.88539\times10^{-5}h^2 - 5.108229\times10^{-8}h^3 + 3.917401\times10^{-11}h^4) \tag{3-9}$$

where ω_e is the mean rotational velocity of the Earth (7.292115×10^{-5} rad/sec), and h is in km.

The acceleration vector due to solar radiation pressure is

$$\mathbf{a}_{\mathbf{srp}} = \nu P_s C_r \frac{A_s}{m}(au)^2 \frac{\mathbf{r}-\mathbf{r_s}}{|\mathbf{r}-\mathbf{r_s}|^3} \tag{3-10}$$

where ν is the eclipse factor, P_s is solar flux at one astronomical unit (au) (4.560×10^{-6} N/m^2), C_r is reflectivity coefficient depending on the characteristics of the LEO, A_s is the effective area (different from the effective area for atmospheric drag) and $\mathbf{r_s}$ is the position vector of the Sun. The method to compute the effective area for the solar radiation pressure is the same as that used in the atmospheric drag. In this case, the effective area lies in a plane perpendicular to the vector ($\mathbf{r}-\mathbf{r_s}$). C_r can be expressed as (1+ε), where ε is reflectivity (from 0 to 1), which depends on the material of satellite parts. The eclipse factor depends on the position of LEO; ν=0 when the LEO is in the Earth's shadow, and ν=1 when the LEO is illuminated by the Sun. The orbit dynamic modeling software we used is able to determine the eclipse factor in the cases of umbra and penumbra based on the ratio of the sunlight received at the LEO location, so that in practice the eclipse factor for a COSMIC satellite varies from zero to one.

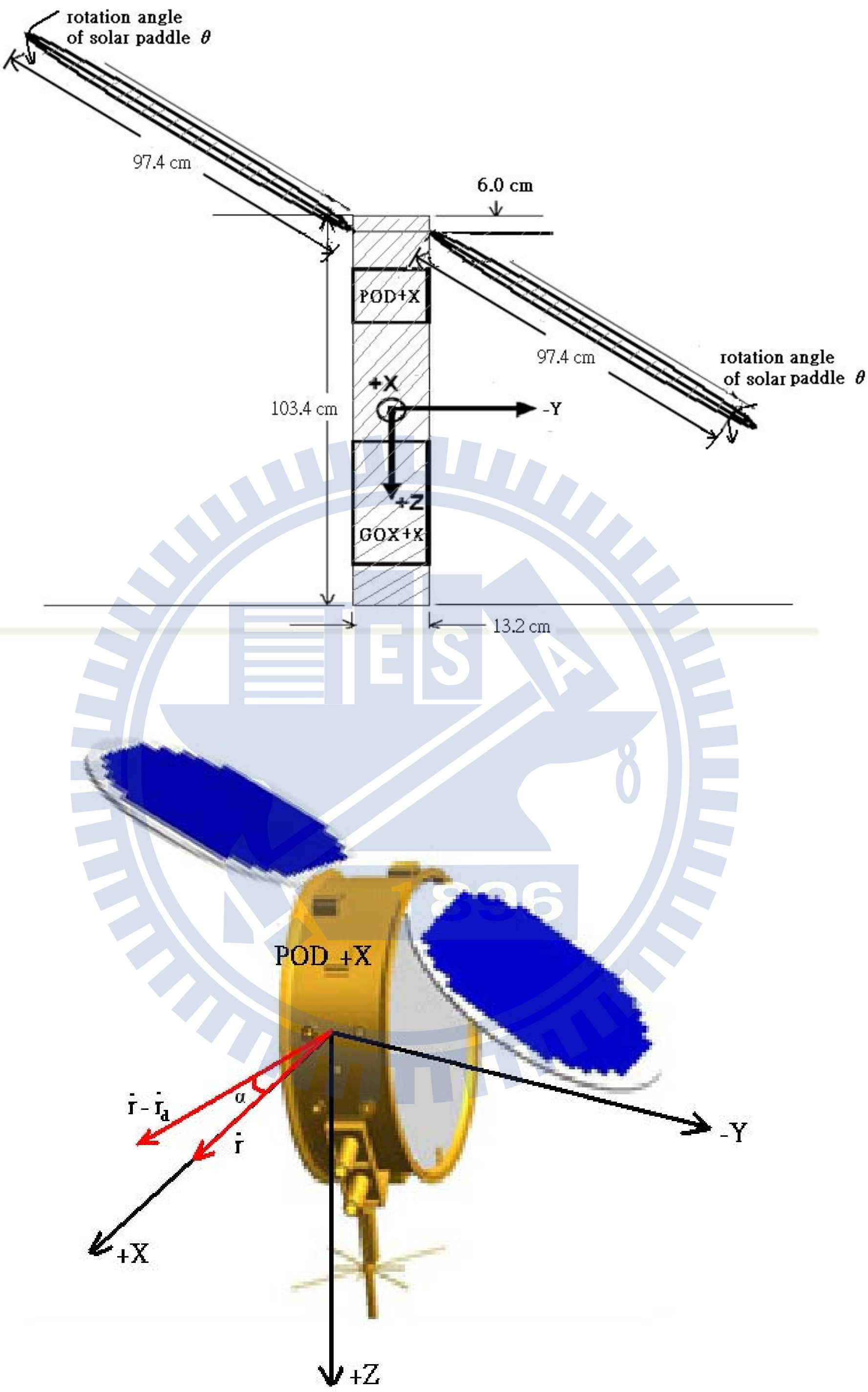

Fig. 3-1: The dimensions of the main part and solar panels of a COSMIC LEO (top), velocity vector $\dot{\mathbf{r}}$ and LEO-to-atmosphere vector $(\dot{\mathbf{r}} - \dot{\mathbf{r}}_{\mathbf{d}})$ (Hwang et al. 2008)

3.3 Kinematic orbit determination using Bernese 5.0

The precise kinematic orbits of LEOs in this research were determined by the Bernese Version 5.0 GPS software (Dach et al. 2007). The reduced dynamic and kinematic approaches are available in Bernese 5.0 for POD with GPS observations. The reduced dynamic approach estimates orbit arc-dependent parameters including the initial state vector (6 Keplerian elements), 9 solar radiation coefficients and three stochastic pulses in the radial, along-track and cross-track directions. The kinematic approach estimates the kinematic parameters of an orbit arc, including epoch coordinate components, receiver clock errors and phase ambiguities. Both the reduced dynamic and kinematic orbit determinations require high precision GPS satellite orbits and clocks. The GPS satellite precise orbits and high-rate clocks can be downloaded on the website provided by the Center for Orbit Determination in Europe (CODE, http://www.aiub.unibe.ch/igs.html). In the kinematic orbit determination with Bernese 5.0, the reduced dynamic orbit serves as a priori orbit for the kinematic orbit. Fig. 3-2 shows the steps of precise kinematic orbit determination using real GPS data.

The zero-differenced ionosphere-free GPS measurements are usually used for point-wise calculation of the satellite positions in the kinematic approach. The limitations of orbit accuracy associated with kinematic orbits are based on the GPS satellite observation numbers and relative GPS-LEO geometry (Byun and Schutz 2001). Satellite coordinates are estimated together with one GPS receiver clock parameter every epoch. Comparing with SLR observations, the kinematic POD with accuracy of 1–3 cm was demonstrated for the GRACE mission (Švehla and Rothacher 2004). Using an overlapping analysis, the orbit accuracy of COSMIC is about 3 cm, compared to 1 cm in the case of GRACE satellites (Hwang et al. 2009). We find that the quality of GPS data depends on the quality of satellite attitude data. For the case of COSMIC satellite at an altitude of 800 km, typical standard errors of attitude measurements over the equator and the polar regions are 0.5° and 3°, respectively, and are larger at a lower altitude. When the attitude of a satellite is poorly determined, the uncertainties in the estimated GPS phase ambiguities are relatively large, leading to degraded orbital accuracy. The detail of GPS-determined orbits of GRACE and COSMIC satellites using the kinematic approaches by Bernese have been documented by Švehla and Rothacher (2005), Jäggi et al. (2007) and Hwang et al. (2009).

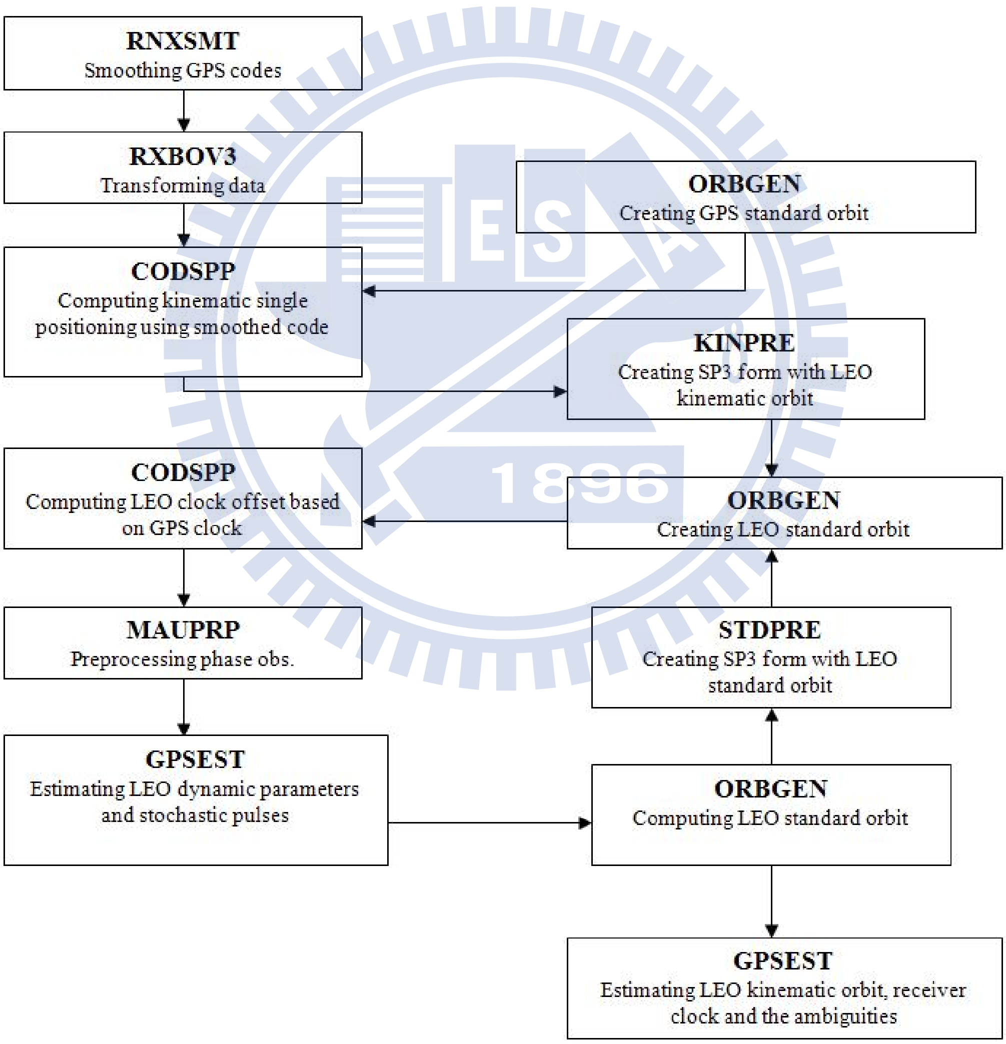

Fig. 3-2: Steps of precise kinematic orbit determination using GPS data

3.4 Dynamic orbit determination using GEODYN II software

The dynamic orbit determination strategy for LEO based on GPS double-difference tracking data is demonstrated for the first time for TOPEX/Poseidon mission (Bertiger et al. 1994; Schutz et al. 1994). The equations of motion are solved by numerical integration. The dynamic model errors will lead to systematic errors growing with the arc length (Bock 2003).

In this research, we use NASA Goddard GEODYN II software to model the perturbing forces described in Section 3.2.1. GEODYN II is used extensively for satellite orbit determination, geodetic parameter estimation, tracking instrument calibration, satellite orbit prediction, as well as for other applied research in satellite geodesy using virtually all types of satellite tracking data (Pavlis et al. 1996). For direct numerical integration, GEODYN II uses Cowell's summation method to obtain the position and velocity at epoch and uses the Bayesian's least-squares method for parameter estimation. The mathematical models of the perturbing forces used in GEODYN II can be found in Long et al. (1989), Pavlis et al. (1996) and McCarthy (1996). GEODYN II has been used for precise orbit determination/prediction and force modeling in various Earth resource satellites such as TOPEX/Poseidon and GRACE. Temporal gravity fields from such satellite tracking data as SLR and GRACE KBR have been derived with GEODYN II (Cox and Chao 2002; Luthcke et al. 2006).

GEODYN II is divided into three major components: the Tracking Data Formatter (TDF), GEODYN IIS and GEODYN IIE. The flow of running GEODYN II can be found in Hwang (2002). The TDF program takes in the one of several tracking data forms. In this research, the tracking data format is PCE data format containing the information of satellite position and velocity as a priori orbit.

In preparation for the execution of GEODYN II, a file containing the ephemeris of the planets and a file containing A1UTC, polar motion, solar flux and magnetic flux must be made ready. A1UTC is the difference between the atomic time (A1) used in GEODYN II and the universal time (UTC), which is available from http://hpiers.obspm.fr/eop-pc/. Solar flux and magnetic flux are obtained from NOAA's web site ftp://ftp.ngdc.noaa.gov under the directory STP/ GEOMAGNETIC_DATA/INDICE. These raw data are processed to produce binary files suitable for input to GEODYN IIS program.

The GEODYN IIS program is mainly used to read and process the option cards, the input observation data, optional gravity model, station geodetics, area/mass files, ephemeris and table data. The default gravity model is stored in the file ftn12. In this research, we choose GGM03S gravity models up to degree/order 70 derived from GRACE GPS and KBR observations.

The JPL export ephemeris as input file ftn01 is used in GEODYN IIS for nutations, positions, and velocities of the Moon, Sun, and planets. In this research, we use the JPL binary DE-403 ephemeris. GEODYN II interpolates for the ephemeris in the mean of 1950.0 reference system by Chebyshev interpolation. This step gives greater accuracy than interpolating in the reference system (the true of date coordinate system) because the high-frequency perturbations due to nutations are absent. After interpolation, the coordinates are then rotated to the true of date system using the precession and nutation matrices (Seeber 2003). More details on the transformations between different coordinate systems can be found in the textbooks or manuals like Long et al. (1989), Pavlis et al. (1996) and Seeber (2003).

The file ftn05 contains all option cards determining the force and non-force model parameters to be used in the program execution. These option cards are divided into two major categories: the Global Set and the Arc Set (Pavlis et al. 1996; Hwang

2002). The Global Set consisting of four groups provides all of the common arcs processing information. The first group, Global Set Mandatory Cards, is the mandatory run description on other three cards. The second set of Global Set Option cards is used to define and/or estimate conditions which are common to all the arcs being processed. This group contains the information and estimations of the Earth's gravitational potential and/or new Earth constants, application and/or adjustment of time dependent gravity coefficients, dynamic polar motion, the third body gravitational potential and/or new constants, solid Earth tide model, ocean tide model, atmosphere drag model, solar flux, and tectonic plate motion. The third group is the Position Card Group containing the information of tracking stations. The last group is the Global Set Terminator to end the Global Set.

One or more Arc Set contains information defining its arc in ftn05 file. The Arc Set also has four groups in this order. The first group, Arc Set Mandatory Cards, is to decide the reference coordinate system and time and spacecraft parameters in this arc. The second group, Arc Option Set cards, is specified to make use of GEODYN II's individual arc capabilities. The third group is the Data Selection/Deletion Subgroup used to edit input observations. The last group is the Arc Set Terminator to end the Arc Set.

The parameters in the Global Set for the force models of COSMIC given in Table 3-1 are defined by input option cards in the file ftn05. For surface forces in the Arc set, we solve for atmospheric drag coefficient, radiation coefficient and 9 empirical coefficients of general acceleration along the radial, along-track and cross-track directions every 1.5 hours (one orbital period) using COSMIC kinematic orbits. As an example, Fig. 3-3 shows the estimated atmospheric drag coefficients and reflectivity coefficients for FM5. These estimated coefficients vary over time, and the mean values/standard deviations of the drag and reflectivity coefficients are 2.12/0.29

and 1.23/0.30, respectively. The general accelerations for COSMIC (Table 3-1) at an altitude of 520 km are on the order of $10^{-11} ms^{-2}$. GEODYN IIE performs the computation of satellite orbit and geodetic parameter estimations. The output from IIE contains all necessary information for data analysis.

The main purpose of precise dynamic orbit determination is to generate a reference orbit to compute the residual orbit perturbations for gravity field recovery. The residual orbit perturbation is a function of the perturbing force due to the perturbing geopotential. Like satellite position, satellite acceleration contains the effect due to the geopotential, plus other perturbing forces which must be modeled for gravity field recovery.

Table 3-1: Standards for the orbit dynamics of COSMIC satellites

Model/parameter	Standard
Conventional inertial reference frame	J2000
N-body	JPL DE-403
Earth gravity model	GGM03S
Polar motion	IERS standard 2000
Reference ellipsoid	a_e = 6378136.3 m, f=1/298.257
GM	396800.4415 km^3s^{-2}
Ocean tides	GOT00.2 (Ray 1999)
Solid Earth tides	IERS standard 2000
Atmosphere density	Mass Spectrometer Incoherent Scatter (MSIS) Empirical Drag Model (Hedin, 1991)
Earth radiation pressure	Second-degree zonal spherical harmonic model (Knocke et al. 1988)
Solar radiation pressure	one coefficient every 1.5 hours
Atmosphere drag	one coefficient every 1.5 hours
General accelerations	9 parameters every 1.5 hours

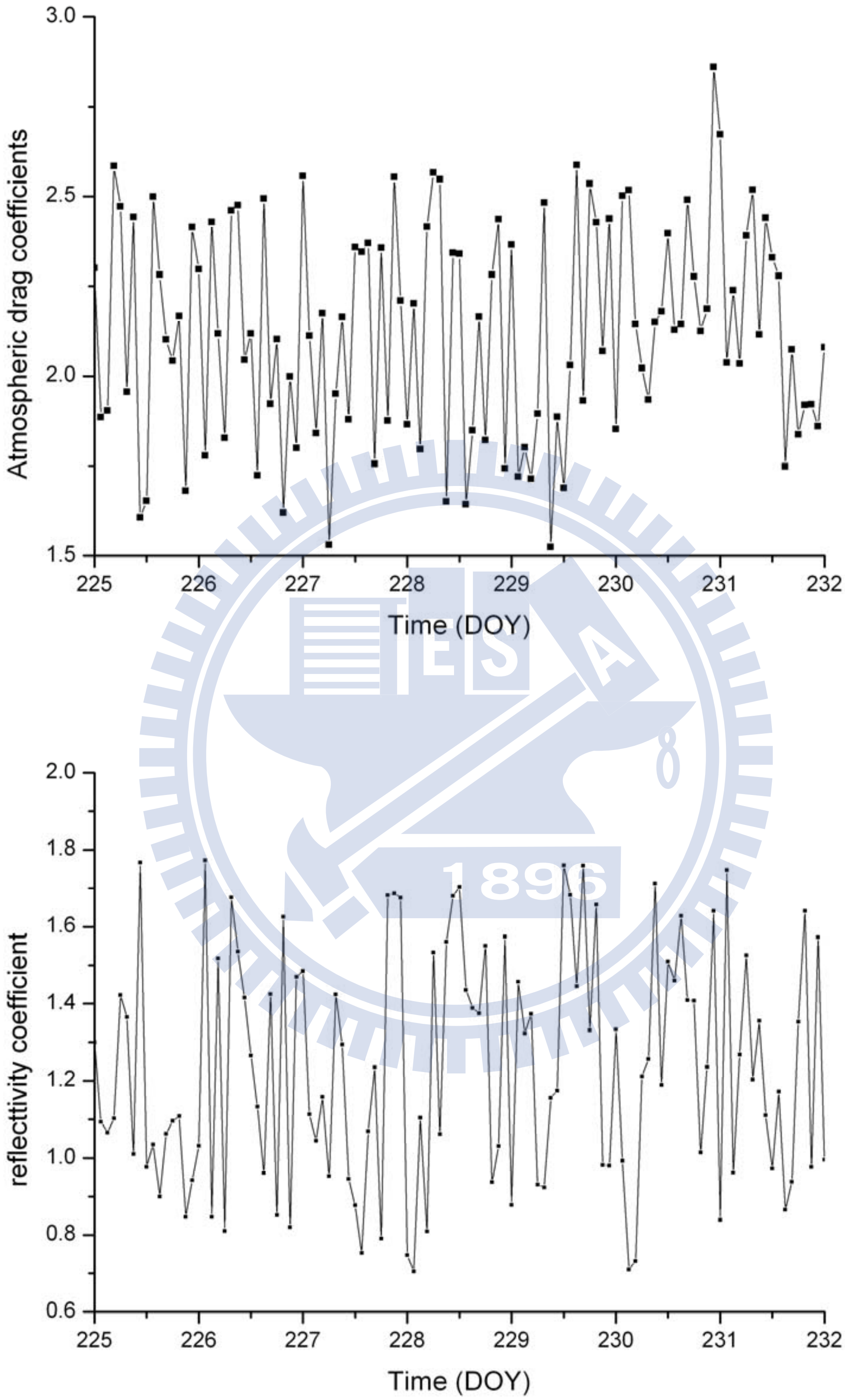

Fig. 3-3: Estimated atmospheric drag coefficients (top) and solar reflectivity coefficients of FM 5 from Day 225 to 232, 2006

3.5 Normal-point reduction

The original sampling interval of COSMIC and GRACE GPS POD carrier-phase and code observables is 1 second. In practice, a 5-s (0.2 Hz) is used in the reduced-dynamic and kinematic orbit computations. To reduce noises and data volume, the 5-s kinematic orbits can be compressed and filtered at a greater item interval by an algorithm similar to that used in the normal-point reduction of satellite laser ranging. In this research, we adopt the Herstmonceux algorithm (Sinclaire 1997) to compress the COSMIC and GRACE precise orbits. Specifically, we use the following steps to generate normal-point kinematic orbits:

(1) Use the reduced-dynamic orbit as the reference orbit to generate differenced orbit. A differenced orbit component is

$$p_i = x_i^k - x_i^r, \quad i = 1, 2, 3 \tag{3-11}$$

where x_i^k and x_i^r are components of kinematic and reduced-dynamic orbits, respectively.

(2) Remove large outliers in the kinematic orbit, which will not be used in the subsequent computations. An outlier is defined as $|p_i| \geq 20\,\text{cm}$.

(3) Within a bin (a window containing many differenced orbits), the differenced orbits are fitted by a polynomial in time using least-squares. The polynomial is called the trend function $f(t)$

(4) For each orbit component, compute the residuals at the times of observations as

$$v_i = p_i - f(t_i) \tag{3-12}$$

(5) Compute the root-mean-square value RMS of the residuals. Identify outliers using a rejection level of 2.5 times of RMS, and neglect these outliers in step (3) of the next iteration

(6) Repeat steps (3)-(5) until no outlier is found

(7) Divide the accepted residuals into bins starting from 0^h UTC.

(8) Compute the mean value $\bar{v}_m$ and the mean time of the accepted residuals within each bin. The number of accepted residuals within bin *m* is denoted as n_m.

(9) For each orbit component, locate the kinematic orbit x_m^k and its residual v_m, whose observation time t_m is nearest to the mean time of the accepted residuals in bin *m*.

(10) Compute the normal-point kinematic orbit as

$$NP_m = x_m^k - v_m + \bar{v}_m \tag{3-13}$$

(11) Compute the standard error of normal points as (if $n_m = 1$, this bin is neglected)

$$\sigma_m = \sqrt{\frac{\sum_1^{n_m} v_j^2}{n_m(n_m - 1)}} \tag{3-14}$$

The bin size can be adjusted according to the desired spatial resolution of gravity solution and data compression ratio. The degree of the fitted polynomial increases with the bin size. For a one-minute bin, a second-degree polynomial is found to be optimal. Statistically, the standard errors of normal points will be smaller than those of raw orbits. For example, Fig. 3-4 shows the normal-point residuals (differences between reduced-dynamic and kinematic orbits) are smaller than raw residuals in Y-direction of FM5 satellite in DOY 216, 2006.

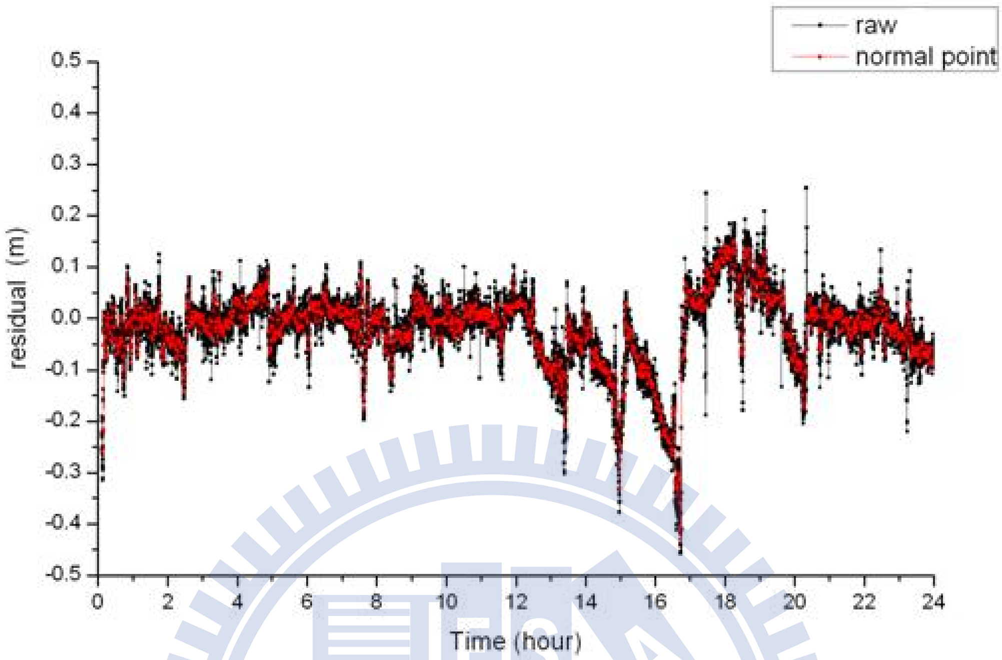

Fig. 3-4: Raw and normal-point residuals in Y-direction (FM5, DOY216)

Chapter 4

Recovery of temporal gravity field using analytical orbital perturbation approach

4.1 Introduction

In the previous chapter, two different approaches for gravity field modeling are developed. In this chapter, we employ the analytical orbital perturbation approach to compute temporal gravity field using COSMIC and GRACE GPS data. The experimental solutions of time-varying geopotential coefficients are computed using one month (August 2006) of COSMIC and GRACE kinematic orbits. According to Hwang et al. (2009), the current orbital accuracies of COSMIC and GRACE kinematic orbit are 3 and 1 cm respectively and the accuracies of the 60-s normal points are further improved. The perturbing forces other than the Earth gravity that act on COSMIC spacecrafts are modeled by GEODYN II using the standard models of orbit dynamics (Table 3-1), yielding pure dynamic orbits that serve as reference orbits. With the reference orbits and GPS-derived kinematic orbits, three-dimensional residual orbital perturbations (difference between kinematic and reference orbits) are assumed to be linear functions of time-varying geopotential coefficients (Chapter 2) and are used as observations to estimate the latter. Both COSMIC and combined COSMIC and GRACE gravity solutions were computed.

4.2 Kinematic orbits of COSMIC and accuracy assessment

In this study, the kinematic orbits of the six COSMIC satellites used for gravity recovery are over the time span from August 2 to August 31, 2006. In this time span, the altitudes of the six COSMIC satellites are 512, 543, 521, 515, 800 and 505 km for FM1, FM2, … and FM6, respectively. The inclinations of all COSMIC orbits are 72° and the eccentricities are nearly zero. Fig 4-1 shows the trajectory of FM5 satellite in August 2006. The coverage of satellite ground tracks of FM5 is uniform, but the 72°-inclination angle a naturally lead to polar gaps.

According to the sampling theorem (Meskó 1994), the along-track sampling interval Δt can be computed as

$$\Delta t = \frac{T}{2K} \approx \frac{\pi a^{3/2}}{K\sqrt{GM}} \tag{4-1}$$

where T is the period time of one revolution, K is the maximum degree of the geopotential field, and a is the semi-major axis. At the altitude of 800 km, use of a maximum harmonic degree 50 of the geopotential is sufficient for COSMIC (Hwang 2001), so the sampling interval is about 60 seconds. The raw GPS kinematic orbits of COSMIC spacecrafts are computed at a 5-s interval. Due to presence of outliers in the GPS data and the need to compress the high-rate orbit data for gravity recovery, the raw GPS kinematic orbits were pre-processed as follows:

Step 1: Removing outliers. An outlier is a kinematic orbit component whose difference with the reduced dynamic orbit (prior orbit) exceeds 20 cm.

Step 2: Compressing 5-second orbits to one-minute normal-point orbits.

The detail of normal-point compression (Step 2) is given in Section 3-5. The normal-point kinematic orbits in Step 2 are actually used for gravity recovery. Fig.

4-2 shows the percentages of accepted 5-second kinematic orbits in August 2006 after removing outliers (Step 1). The average percentages of acceptance are 74.3, 76.5, 73.4, 66.0, 82.5 and 69.5% for FM1, FM2, …, and FM6, respectively. In most cases, data are rejected due to bad attitude control and/or poor clock resolution. FM5 has the largest percentage of acceptance, due to its 800-km altitude where the attitude control is better than other five spacecrafts. Fig. 4-3 shows daily standard errors of the one-minute normal orbits, which will be used as data weights in the gravity recovery. On average, the accuracy of the normal-point orbits is 7 mm, compared to the 3 cm orbit error for the raw 5-s orbits. Table 4-1 shows the statistics of the standard errors for the six COSMIC satellites in August 2006. FM5 has the least standard error of all satellites in the normal-point data.

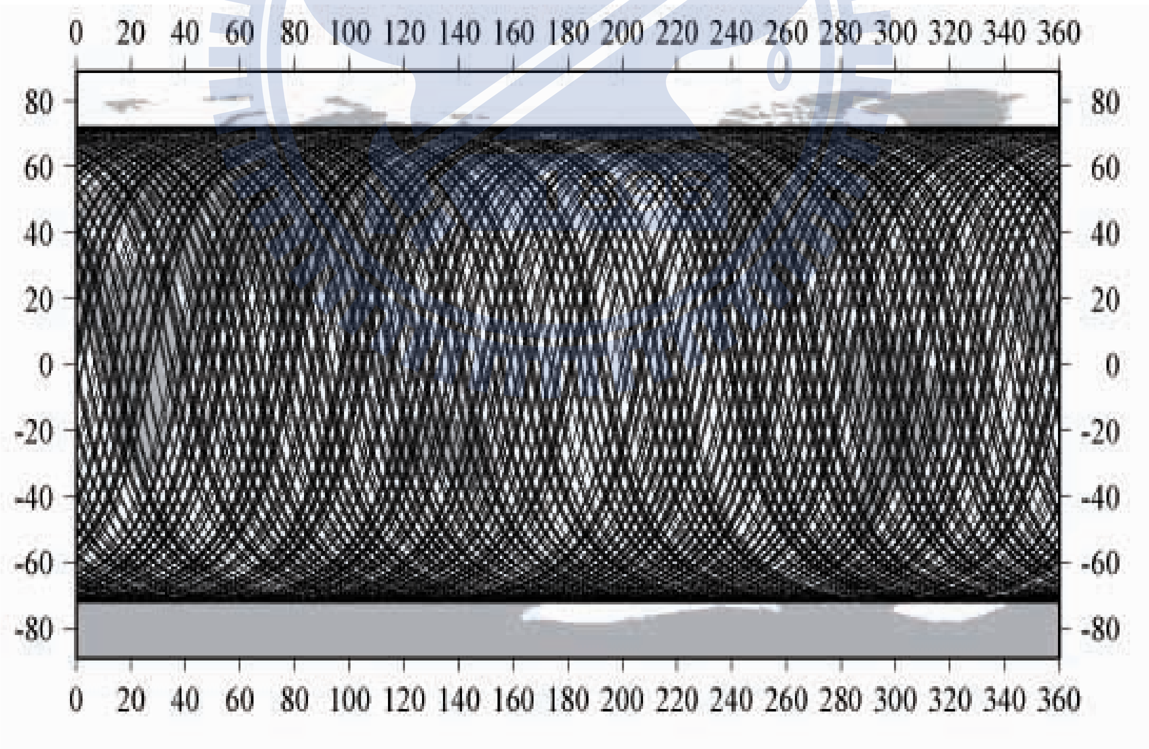

Fig. 4-1: Trajectory of FM5 satellite (August 2006)

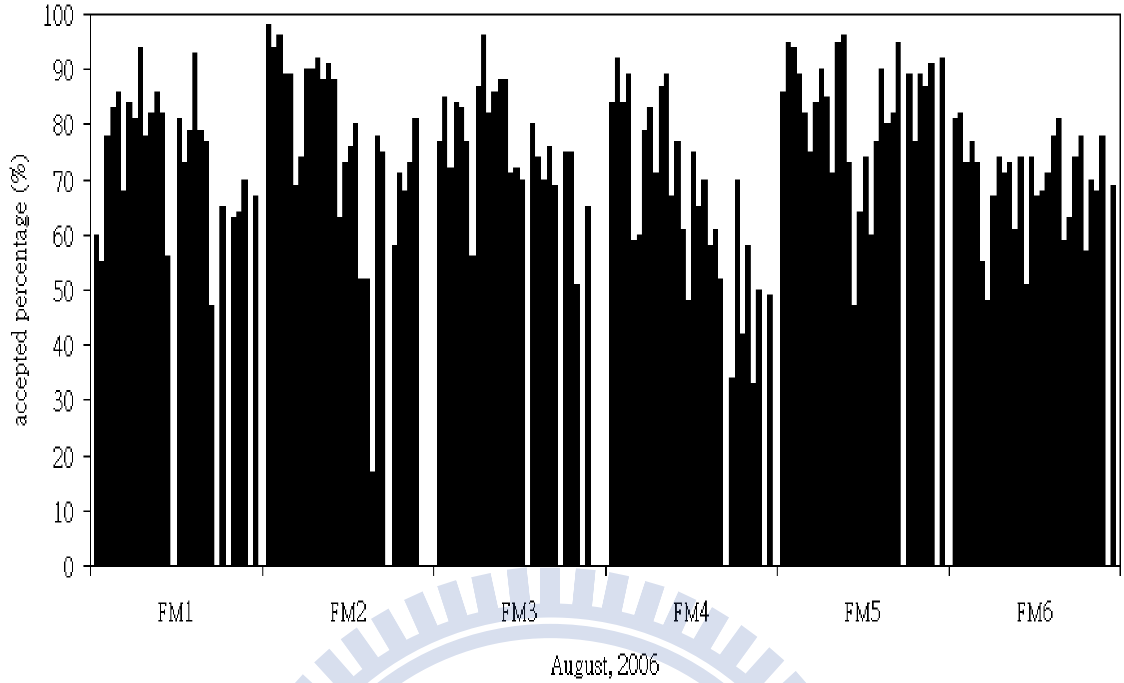

Fig. 4-2: Percentages of acceptance of kinematic orbits for normal-point computations

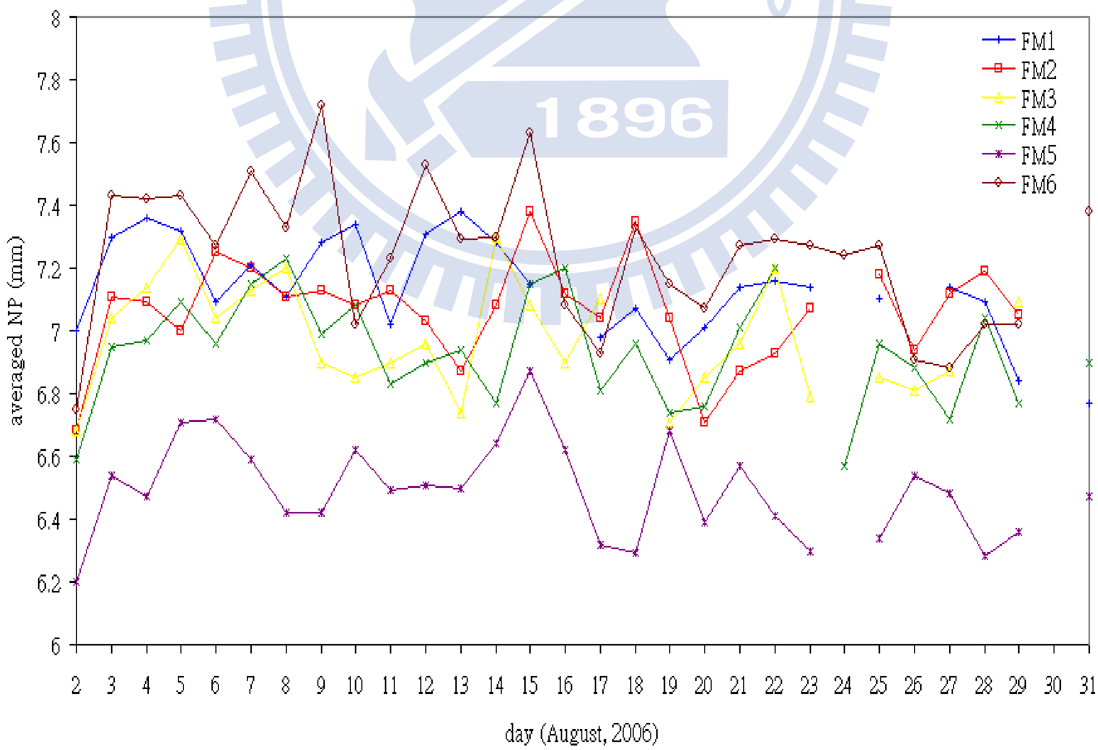

Fig. 4-3: Standard errors of normal-point kinematic orbits in August 2006

Table 4-1: Statistics of standard errors of normal-point kinematic orbits

	MAX. (mm)	MEAN (mm)	MIN. (mm)
FM1	7.38	7.13	6.77
FM2	7.38	7.06	6.68
FM3	7.30	6.98	6.68
FM4	7.23	6.93	6.57
FM5	6.87	6.49	6.20
FM6	7.72	7.24	6.75

4.3 Reference dynamic orbits for COSMIC and GRACE

The geometry of COSMIC spacecraft is simple compared to that of GRACE, and its surface forces can be with a sufficient degree of confidence. The NASA Goddard GEODYN II is used to determine the COSMIC dynamic orbits and the parameters for the force models of COSMIC are given in Section 3.4 and Hwang et al. (2008).

The reference dynamic orbit data of GRACE in August 2006 is provided by CSR. The software used for GRACE dynamic POD is the CSR MSODP software (Rim 1992) and the double-differenced GRACE GPS carrier-phase observations are processed to convert range measurements using a network of 51 International Global Navigation Satellite System (GNSS) Service (IGS) ground stations (Beutler et al., 1999). An aggressive force model parameterization is used to estimate many empirical parameters including the GRACE satellite initial positions and velocities, ambiguity parameters, troposphere zenith delays, center of mass offset in the nadir direction, atmosphere drag parameters, 1 cycle-per-revolution (1-cpr) (along-track) and normal (cross-track) empirical accelerations, and the previously mentioned GPS orbit element correction to improve the orbit accuracy (Kang et al. 2003). The orbit dynamic standard of GRACE is listed in the paper of Kang et al. (2006). The GPS-based dynamic orbits have about 1-cm radial orbit accuracy and better than 2.5-cm accuracy in the along-track and cross-track directions (Kang et al. 2006).

Due to different satellite sizes and altitudes, we choose different orbit dynamic standards for each mission to produce a precise orbit. Table 4-2 shows the different standards for the orbit dynamics between COSMIC and GRACE satellites. The gravity content that is sensible at the altitude of 800 km will be about harmonic degree 50 (Hwang and Lin 1998). The ocean tide effect on satellite contains the leading diurnal and semi-diurnal constituents including Q1, O1, M1, S1, P1, K1, J1, N2, M2, S2, K2 and other long-period constituents using different ocean tide models. The selection of other force standards is based on past experience and tests.

Table 4-2: Different standards for the orbit dynamics of COSMIC and GRACE satellites

Model/parameter	COSMIC	GRACE
Earth gravity model	GGM03S (70×70)	GGM02C (120×120)
N-body	JPL DE-403	JPL DE-405
Ocean tides	GOT00.2	FES2004
Atmosphere density	Mass Spectrometer Incoherent Scatter (MSIS) Empirical Drag Model	Density temperature model (DTM)
Earth radiation pressure	Second-degree zonal spherical harmonic model	Albedo and infrared
Solar radiation pressure	one coefficient every 1.5 hours	Box-wing model

4.4 Formulae used in gravity recovery

Following Section 4.2, the observables are now normal point kinematic orbits of COSMIC at a one-minute interval for gravity recovery. For determining temporal gravity variation, the unknown parameters are time-varying geopotential coefficients $(\Delta\overline{C}_{nm}(t), \Delta\overline{S}_{nm}(t))$. An empirical model is used to compensate partially the deficiency of the linear orbital perturbation and absorb the error in the initial state vector and errors in the force models in the parameter estimation. Specifically, for each of the radial, along-track and cross-track residual orbit components, we use the following empirical model:

$$
\begin{aligned}
\Delta r_i &= a_0 + a_1 \cos u + a_2 \sin u + a_3 \cos 2u + a_4 \sin 2u + a_5 t \cos u + a_6 t \sin u + a_7 t \sin 2u \\
&+ a_8 t \cos 2u + a_9 t + a_{10} t^2
\end{aligned}
\tag{4-2}
$$

where i = 1, 2 and 3 (three orbit components), u is argument of latitude, a_k is the coefficient for the perturbation component, and t is the time elapsed with respect to a reference epoch. Eq. (4-2) is based on the results in Colombo (1984), Engelis (1987) and Hwang (1995).

With GEODYN II, the reference orbits of COSMIC and GRACE are determined by numerically integrating the equations of motion that take into account all perturbing forces acting on COSMIC and GRACE satellites. The GRACE-derived gravity model GGM03S is used as the Earth's static gravity model containing geopotential coefficients $(\overline{C}^0_{nm}, \overline{S}^0_{nm})$. The CSR RL04 products are used in this chapter for comparison and analysis. If the reference orbits are generated using an optimal static gravity model such as GGM03S and all other perturbing forces are properly modeled, we can assume that the residual orbits are linear functions of time-varying geopotential coefficients.

For parameter estimation, the matrix representation is

$$\mathbf{L} = \mathbf{AX} - \mathbf{V} \tag{4-3}$$

where **A** is the design matrix containing the partials of residual orbit components with respect to time-varying geopotential coefficients and empirical parameters, vectors **V**, **X** and **L** contain random errors, unknowns (geopotential coefficients and empirical parameters) and observations (residual orbits), respectively. Given a priori values of the unknowns and the associated weight matrix, $\mathbf{P_X}$, the least-squares solution of **X** is

$$\mathbf{X} = -(\mathbf{A}^{\mathrm{T}}\mathbf{PA} + \mathbf{P_X})^{-1}\mathbf{A}^{\mathrm{T}}\mathbf{PL} \tag{4-4}$$

where **P** is the weight matrix containing inverses the squared standard errors (Fig. 4-2 and Table 4-1). Because COSMIC is not in a polar orbit, it is necessary to use $\mathbf{P_x}$ to stabilize the estimation of **X**. For the geopotential coefficient part of $\mathbf{P_x}$, it is a diagonal matrix containing the variances of time-varying geopotential coefficients. The variances were computed as follows. The geopotential coefficients of GGM03S were subtracted from the monthly coefficients of GRACE gravity models in August 2006 to obtain monthly time-varying coefficients. The degree variances of the monthly time-varying coefficients were computed and the average degree variances determined. The average degree variances were then least-squares fit to a model whose expression is similar to that of the Kaula rule (Kaula 1966), i.e., $\alpha n^{-\beta}$, where n is the spherical harmonic degree. The result shows that the average degree variance follows (Fig. 4-4)

$$\bar{\sigma}_n^2 = \frac{1}{2n+1}\sum_{m=0}^{n}(\Delta\bar{C}_{nm}^2 + \Delta\bar{S}_{nm}^2) \approx 5.04\times10^{-21} n^{-1.7130} \tag{4-5}$$

where $\Delta\bar{C}_{nm}, \Delta\bar{S}_{nm}$ are coefficients. A diagonal element of $\mathbf{P_x}$ corresponding to any geopotential coefficient of the same degree is computed by

$$P_{c_{nm}} = P_{s_{nm}} = \frac{1}{\bar{\sigma}_n^2} \tag{4-6}$$

Because the orbital inclination of COSMIC is $72°$, it is expected COSMIC GPS data will enhance the current gravity models of GRACE and CHAMP. The GRACE and CHAMP missions are in polar orbits. We also carried out a combined COSMIC-GRACE solution. In this case, the least-squares solution of $\mathbf{X}$ is

$$\mathbf{X} = -(\mathbf{A}^{\mathrm{T}}\mathbf{PA} + \mathbf{\Sigma}_{\mathbf{g}}^{-1})(\mathbf{A}^{\mathrm{T}}\mathbf{PL} + \mathbf{\Sigma}_{\mathbf{g}}^{-1}\mathbf{g}) \tag{4-7}$$

where $\mathbf{g}$ is a vector of time-varying geopotential coefficients from GRACE and $\mathbf{\Sigma_g}$ is the error covariance of $\mathbf{g}$. Since the full error covariance matrices of GRACE gravity models are not released, only error variances of the time-varying geopotential coefficients are used for the diagonal elements, so $\mathbf{\Sigma_g}$ is in fact a diagonal matrix.

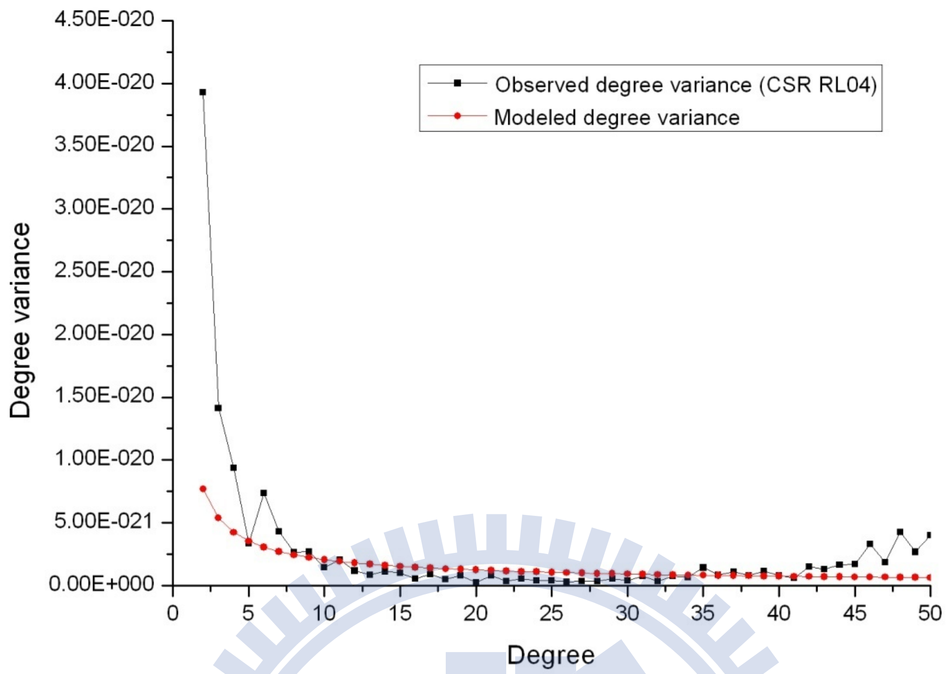

Fig. 4-4: Observed and modeled degree variances of CSR RL04 solution in August 2006

4.5 Results of gravity recovery

Several experimental gravity solutions were carried out using one month of normal-point kinematic orbits of COSMIC and GRACE. Fig. 4-5 shows the steps of gravity recovery from real GPS data using the analytical orbital perturbation approach. Based on numerous tests and the result of Hwang et al. (2008), we decide to adopt 15 as the maximum degree of expansion for the COSMIC-only and COSMIC-GRACE solutions. Fig. 4-6 shows degree variances and error degree variances from the COSMIC and COSMIC-GRACE solutions. The error degree variances of COSMIC and COSMIC-GRACE solutions increase with degree and are all less than the degree variances below degree 10 and 11, respectively. The COSMIC-GRACE solution yields error degree variances that are smaller than those from the COSMIC-only solution due to the use of more observations and better data coverage. For spherical harmonic components with degrees lower than 10, the signal-to-noise ratio is larger than 1.

Fig. 4-7 shows the geoid variation to spherical harmonic degree 15 from the CSR RL04 solution, and the high and low signatures of geoid variations are clearly seen. In Fig. 4-8, we compare geoid changes from the COSMIC-only and COSMIC-GRACE solutions to degree 15. The COSMIC-only solution shows more artifacts than the COSMIC-GRACE solution, but these two solutions reveal clear geoid highs and lows over Europe, Greenland, Amazon Basin, India continent and southern Africa, which resemble those given by the CSR RL04 solution in Fig. 4-7. The geoid variations at latitudes higher than 72º are probably not reliable due to the low inclination of COSMIC. Also, the GPS data used in the current solutions are from five of the six COSMIC satellites that are at altitudes of about 520 km, where the non-gravity forces are difficult to model and the attitude control is not optimal.

In order to compare the geopotential coefficients from COSMIC and from GRACE, we compute the relative differences of coefficients as follows (regarding GRACE-derived geopotential coefficients as the reference values):

$$\varepsilon_{nm}^{C} = \frac{\Delta\overline{C}_{nm}^{C} - \Delta\overline{C}_{nm}^{G}}{\Delta\overline{C}_{nm}^{G}} \quad , \quad \varepsilon_{nm}^{S} = \frac{\Delta\overline{S}_{nm}^{C} - \Delta\overline{S}_{nm}^{G}}{\Delta\overline{S}_{nm}^{G}} \tag{4-8}$$

where $(\Delta\overline{C}_{nm}^{C}, \Delta\overline{S}_{nm}^{C})$ and $(\Delta\overline{C}_{nm}^{G}, \Delta\overline{S}_{nm}^{G})$ are the estimated geopotential coefficients from COSMIC and GRACE, respectively, and $(\varepsilon_{nm}^{C}, \varepsilon_{nm}^{S})$ are the relative differences. The relative differences of all coefficients and those of the zonal coefficients from COSMIC-only and COSMIC-GRACE solutions are given in Figs. 4-9 and 4-10. The COSMIC-GRACE solution yields the relative errors that are smaller than those from the COSMIC-only solution. The recovered coefficients with relative differences smaller than one are considered as significantly close to the CSR RL04 coefficients. From Figs. 4-9 and 4-10, a large portion of the recovered geopotential coefficients from COSMIC-only and COSMIC-GRACE solutions are consistent with those of CSR RL04 solution. However, a significant portion of the COSMIC-derived coefficients disagree with the GRACE-derived coefficients, which is expected given the different data qualities from the two missions.

Fig. 4-11 shows the error degree variances (formal errors) of time-varying geopotential coefficients from the combined and the CSR RL04 solutions. The combined solution yields error degree variances that are smaller than those from the CSR RL04 solution. We also compute calibrated standard errors of COSMIC-GRACE geopotential coefficients using the method given in Schmidt et al. (2007), which was used to calibrate the error estimates of GRACE-derived geopotential coefficients. A scaling factor at degree n and order m is computed as

$$f_{nm} = \frac{C_{nm}^{C} - C_{nm}^{G}}{E_{nm}^{C}} \tag{4-9}$$

where C_{nm}^{C} and C_{nm}^{G} are the estimated geopotential coefficients from COSMIC-GRACE and GRACE, respectively, and E_{nm}^{C} is the un-calibrated error degree variance from COSMIC-GRACE. A calibrated standard error is obtained by multiplying the un-calibrated standard error by the factor in eq. (4-9). Fig. 4-12 compares the calibrated error degree variances from GRACE (available at the website, http://www.csr.utexas.edu/grace), COSMIC and combined solutions. Again, the combined solution yields smaller error degree variances than those from GRACE solutions.

Fig. 4-13 shows the geoid variations from the combined COSMIC and GRACE solution. The combined solution closely resembles the GRACE solution and this is due to the large weights of GRACE coefficients in the combination. Comparing Fig. 4-13 and 4-7, we note that the combined solution enhances the geoid signatures of the GRACE solution over central Africa, Russia and Greenland, and the geoid highs in North America, India and northern Amazon. Fig 4-14 shows the geoid signature enhanced in Amazon derived from combined solutions.

More quantitative assessments of accuracy and spatial resolution of COSMIC gravity solutions are yet to be carried out, for example, using terrestrial based gravity measurements at locations with large gravity changes. However, from the gravity solutions, the COSMIC mission shows a potential for gravity recovery. The COSMIC mission coincides with the GRACE mission since April 2006, and its lifetime is expected to be 5 years. Following the procedure of gravity recovery, we will produce monthly gravity fields from the combined COSMIC and GRACE data for a longer term in Chapter 6.

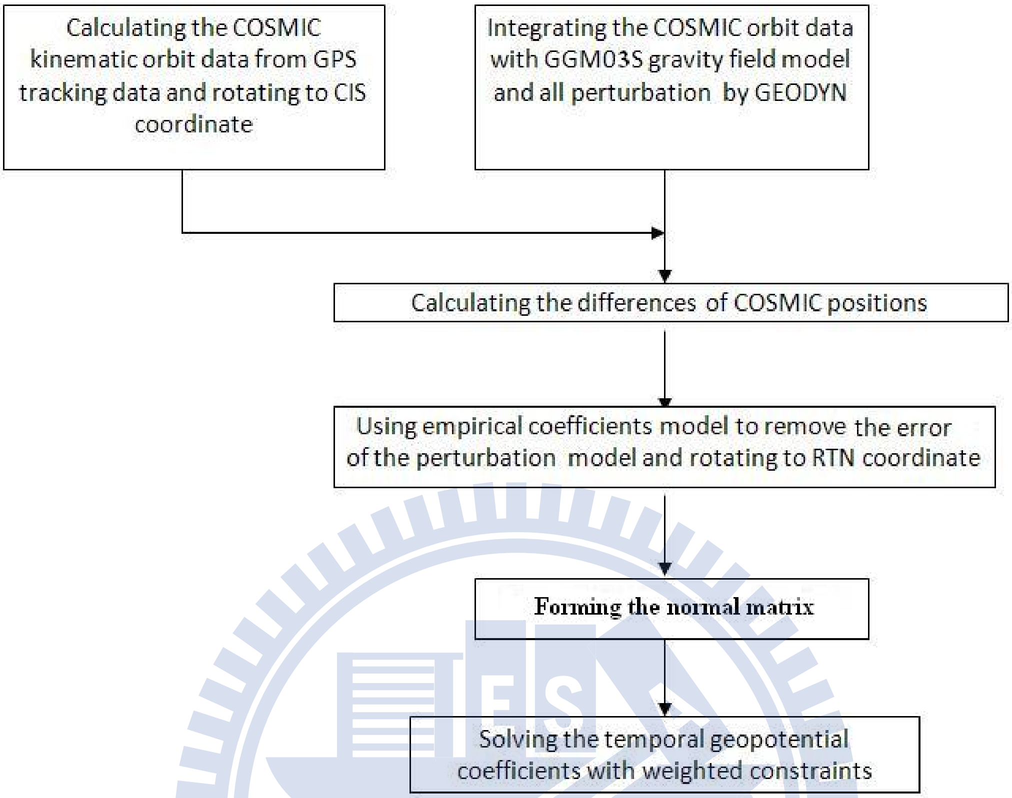

Fig. 4-5: Steps of gravity recovery from COSMIC GPS data using analytical orbital perturbation approach

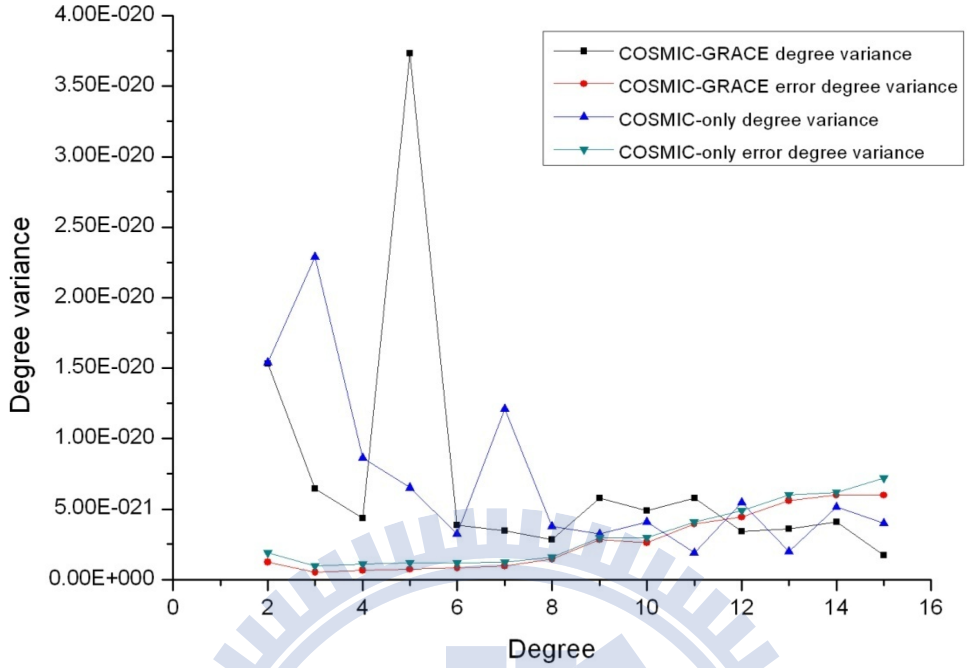

Fig. 4-6: Degree variance and formal error degree variances of time-varying geopotential coefficients from the COSMIC-only and COSMIC-GRACE solutions

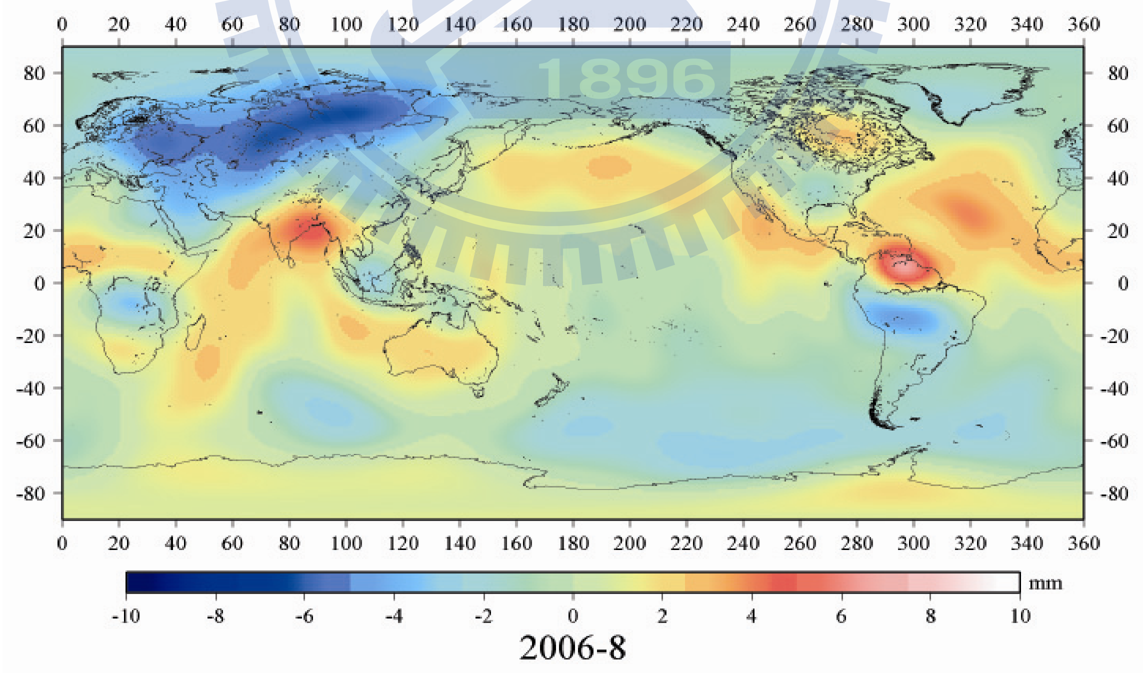

Fig. 4-7: Geoid variation to spherical harmonic degree 15 from the CSR RL04 solution

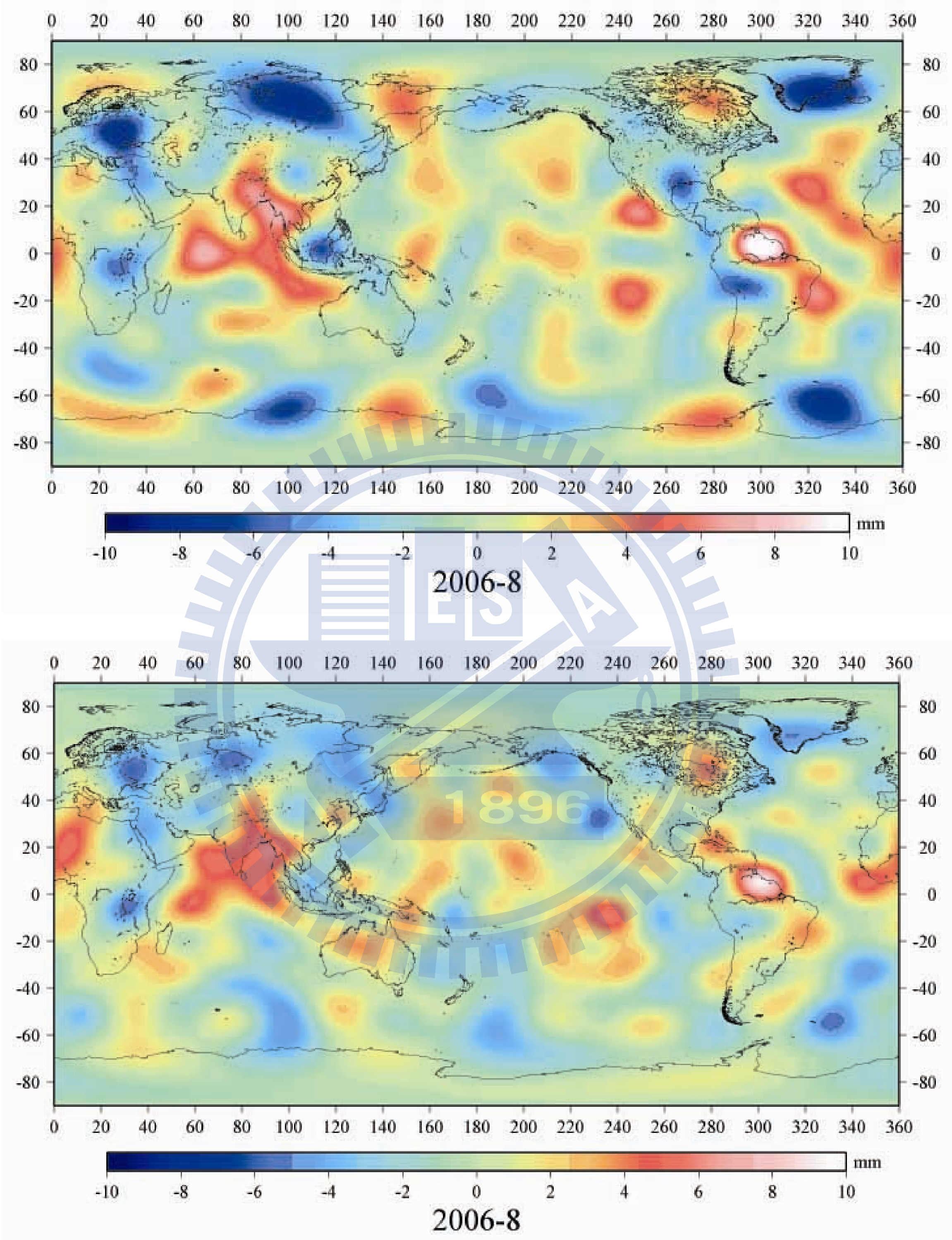

Fig. 4-8: Geoid variations to spherical harmonic degree 15 from COSMIC-only (top) and COSMIC-GRACE solutions

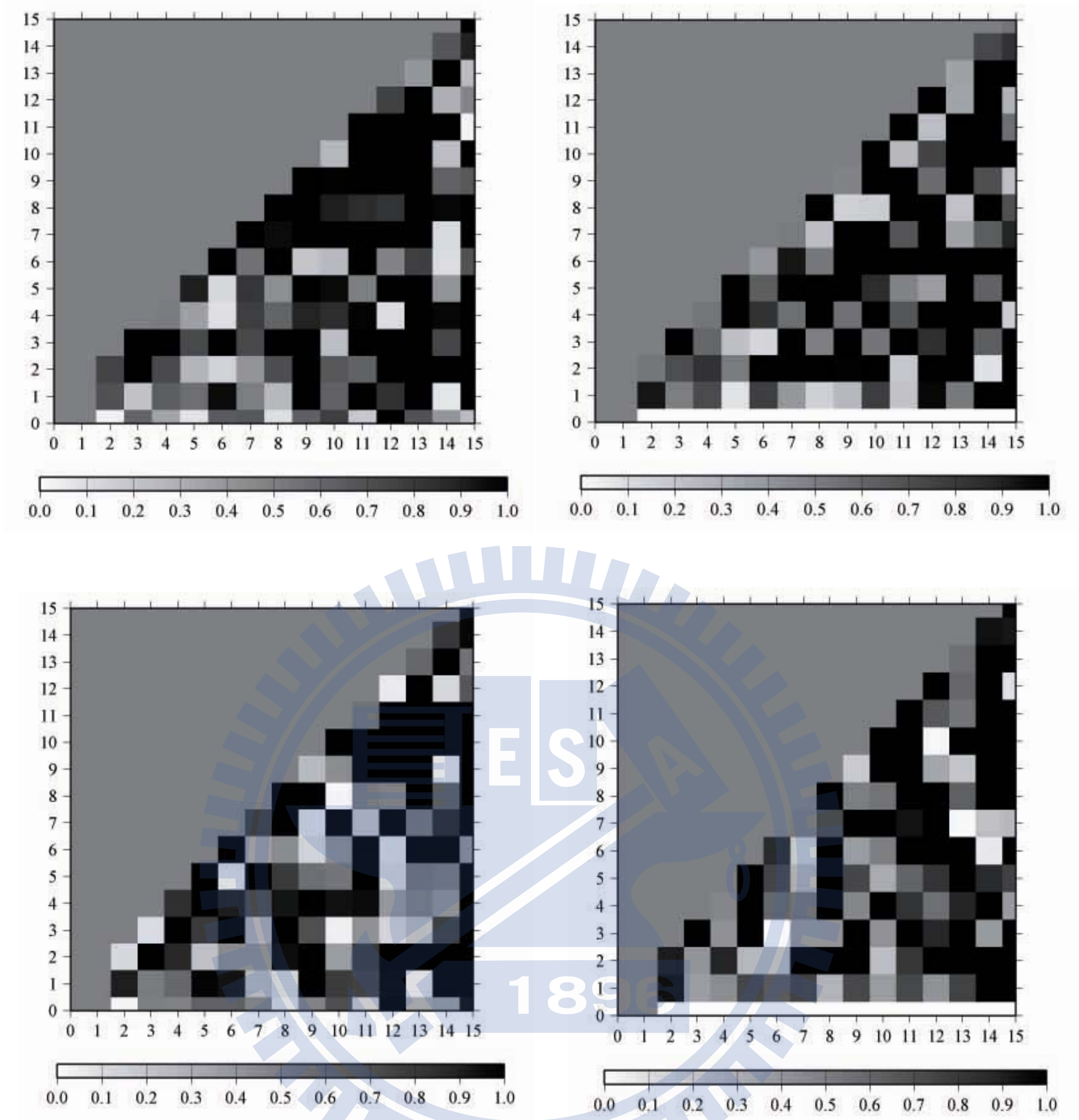

Fig. 4-9: Relative differences of the COSMIC-only (top) and COSMIC-GRACE coefficients with respect to the GRACE-derived coefficients of gravity variation for $\Delta\overline{C}_{nm}$ (left) and $\Delta\overline{S}_{nm}$ up to degree 15

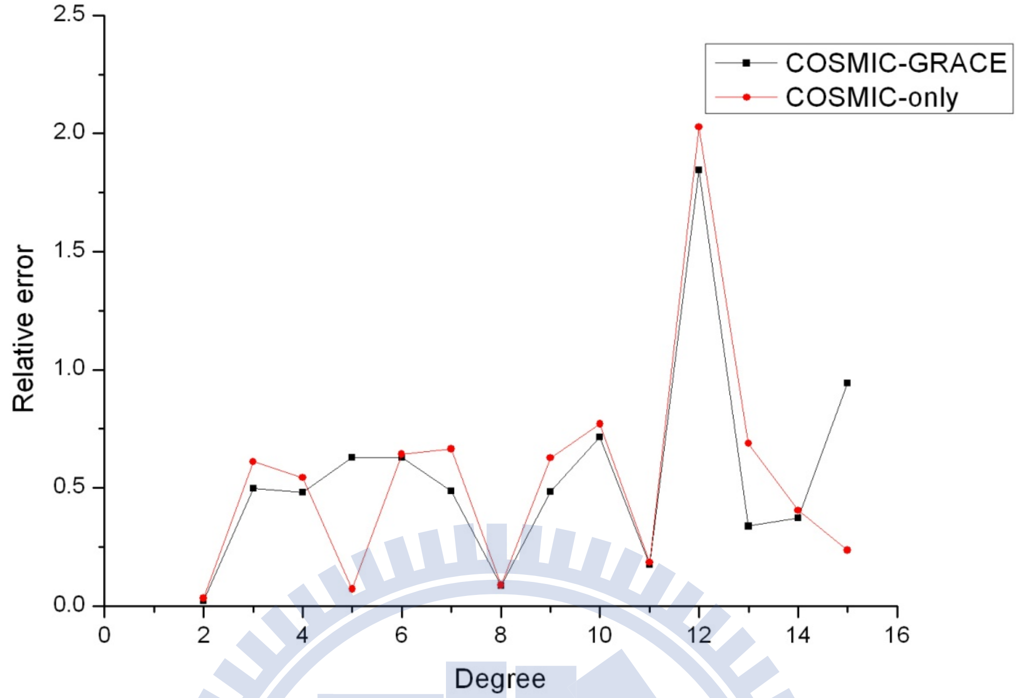

Fig. 4-10: Same as Fig. 4-9, but for the zonal coefficients

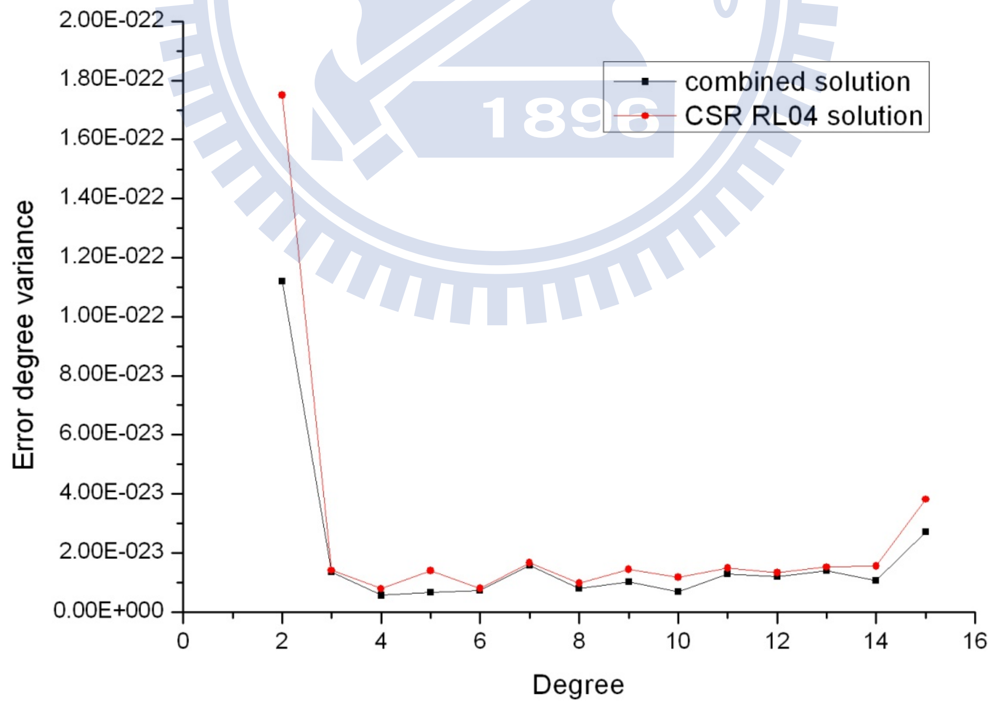

Fig. 4-11: Formal error degree variances of time-varying geopotential coefficients from the CSR RL04 and the combined solutions

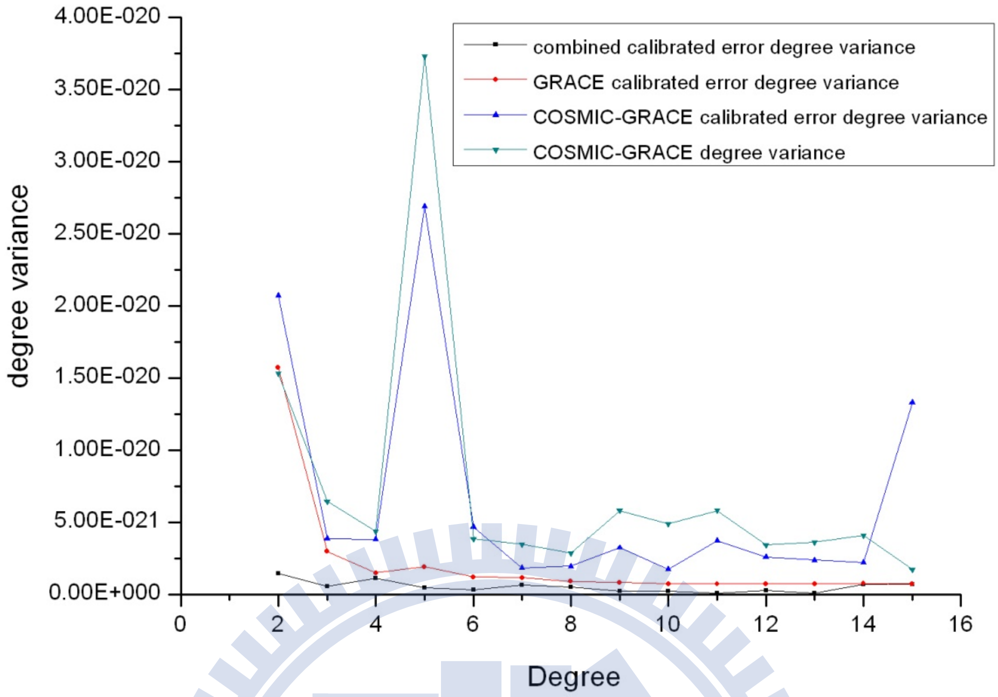

Fig. 4-12: Degree variances from COSMIC-GRACE, and calibrated error degree variances from COSMIC-GRACE, GRACE and combined solutions

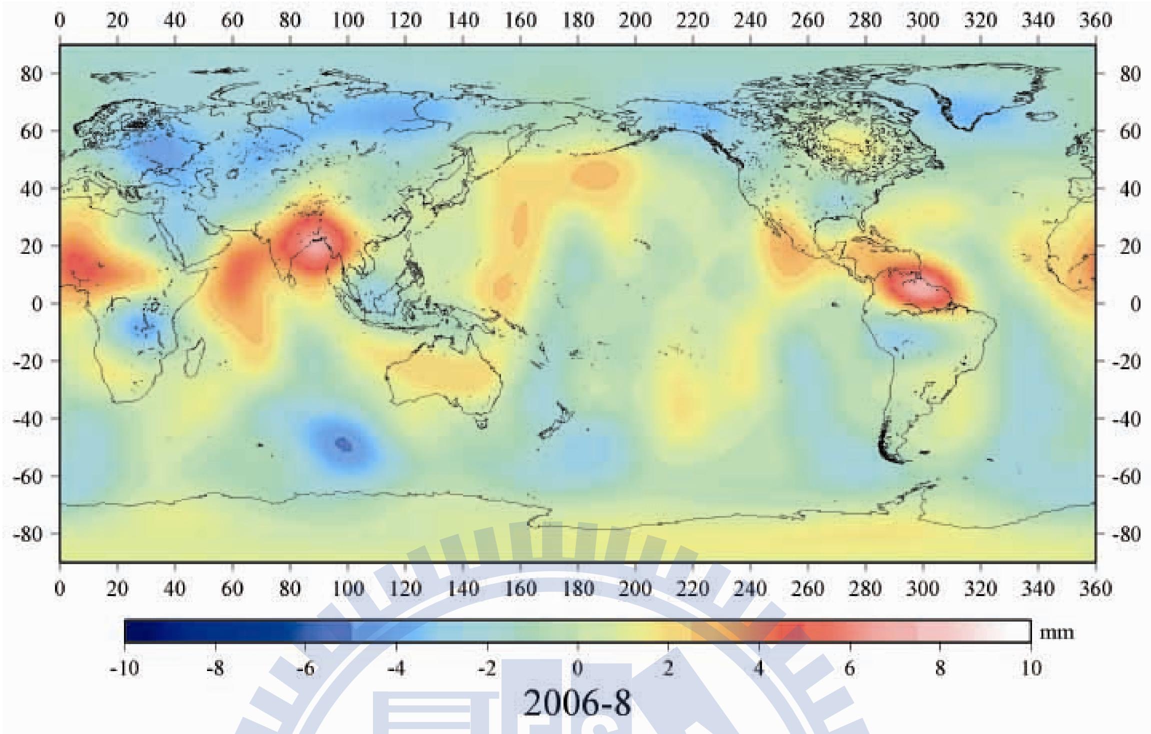

Fig. 4-13: Geoid variation to spherical harmonic degree 15 from the combined solution

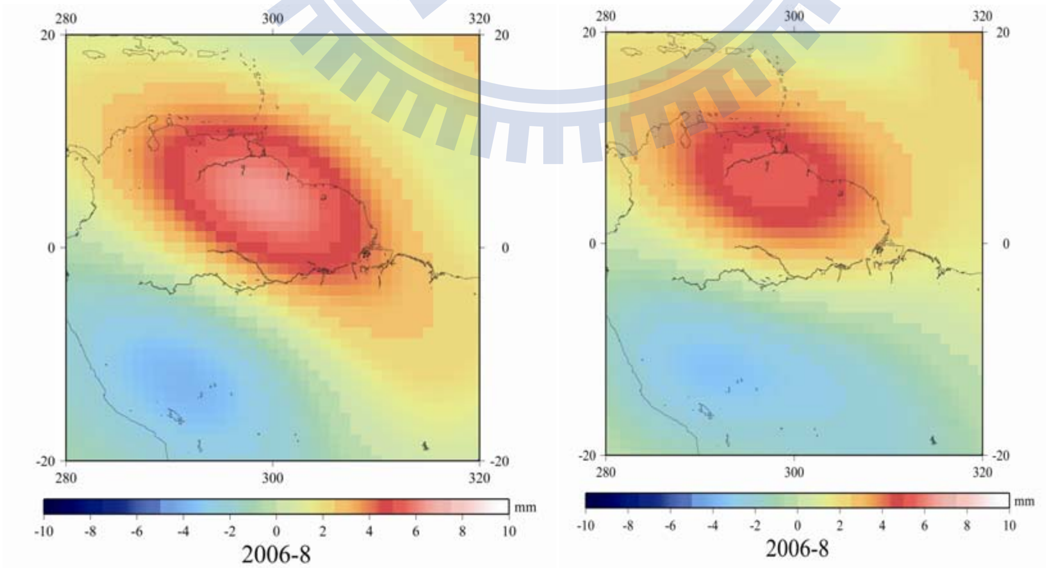

Fig. 4-14: Geoid changes in Amazon area derived from combined (left) and GRACE solutions

Chapter 5

Temporal gravity recovery based on satellite accelerations

5.1 Introduction

A residual acceleration approach is employed to determine the time variation of the Earth's gravity field by using the precise GPS high-low tracking data from two different inclination satellite missions –COSMIC and GRACE. It makes use of satellites accelerations derived from precise kinematic and reference dynamic orbits by numerical differentiations. We carried out experimental solutions of time-varying geopotential coefficients using one month of COSMIC and GRACE kinematic orbits (August 2006). The residual accelerations are derived from differencing kinematic and reference orbits. We also carried out a combined solution with CSR RL04 solution. The comparison between the results from this method and from the analytical orbital perturbation approach will be presented.

5.2 Processing of COSMIC and GRACE residual accelerations

5.2.1 Position data screening

Because kinematic orbits results in a series of satellite positions without force model assumptions, it is preferable for gravity field modeling. For the comparison of the gravity recovery result presented in Chapter 4, the kinematic orbits of the six COSMIC satellites and two GRACE satellites used for gravity recovery are over the time span from August 2 to August 31, 2006. The original sampling intervals of COSMIC and GRACE kinematic orbit is 5-s and 10-s, respectively. The 5-s COSMIC and 10-s GRACE kinematic data can be decimated and filtered to a coarser sampling interval to improve orbit quality (Hwang et al. 2008).

Again, to reduce noises and data volume, the original COSMIC and GRACE kinematic orbits were re-sampled at a 1-minute interval using the normal-point reduction procedure in Section 3.5. A typical way of removing outliers is to screen the orbit position differences between two successive epochs, and the kinematic orbits are not used if the differences exceed a certain threshold value (Ditmar et al. 2006). In this study, the threshold value is that 2.5 times of the RMS of orbit differences, with a tolerable maximum difference of 20 cm, which is an empirical value (Hwang et al. 2008).

Fig. 5-1 shows the RMS differences of GRACE-A and GRACE-B between NCTU kinematic orbits and CSR dynamic orbits. The average RMS values in RTN directions of reduced GRACE and COSMIC (1 minute) between kinematic orbits and dynamic orbits are listed in Table 5-1. The RMS differences of COSMIC are about 7 cm and uniform in all components. These differences are larger than those of GRACE. FM5 has the least RMS difference of all COSMIC satellites in the normal-point data. The larger RMS difference of COSMIC may come from the poor antenna position and bad attitude control compared to the GRACE satellite (Hwang et al. 2010). Fig. 5-2 shows the percentages of accepted COSMIC and GRACE kinematic orbits in August 2006 after removing outliers. The statistics of average percentages of acceptance are shown in Table 5-2. FM5 has the largest percentage of acceptance in COSMIC mission due to its 800-km altitude where the surface perturbation force is smaller and the attitude control is better than other those for other five spacecrafts. These normal-point kinematic orbits were used for gravity recovery.

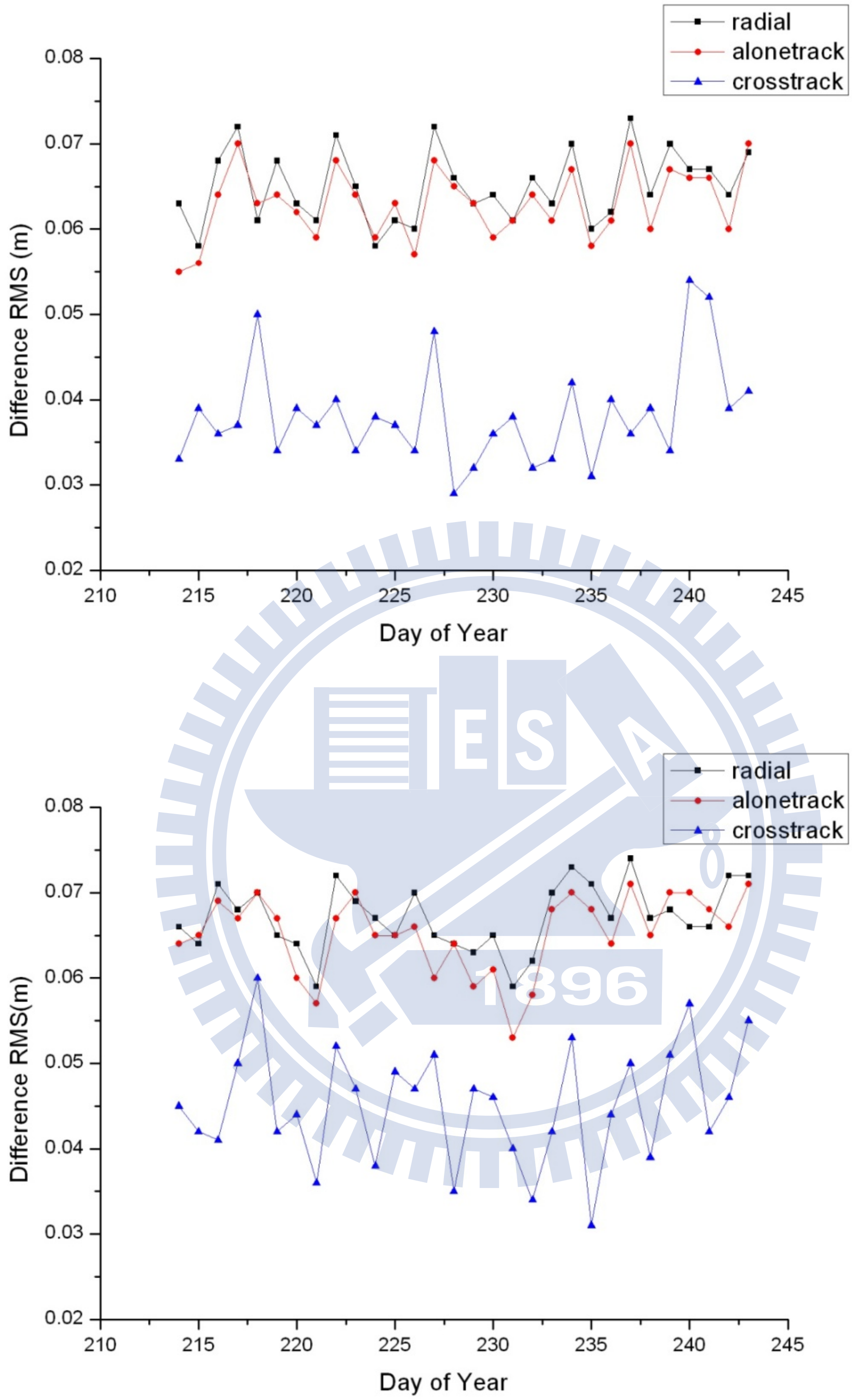

Fig. 5-1: RMS differences of GRACE-A (Top) and GRACE-B between NCTU kinematic orbits and CSR dynamic orbits

Table 5-1: Average RMS differences between kinematic orbits and dynamic orbits in RTN directions for six COSMIC and two GRACE satellites (unit: cm)

	radial	along-track	cross-track
FM1	7.74	7.52	7.30
FM2	7.55	7.44	7.19
FM3	7.54	7.62	7.24
FM4	7.87	7.65	7.53
FM5	7.27	7.11	6.85
FM6	7.77	7.73	7.58
GRA	6.50	6.30	3.81
GRB	6.71	6.53	4.52

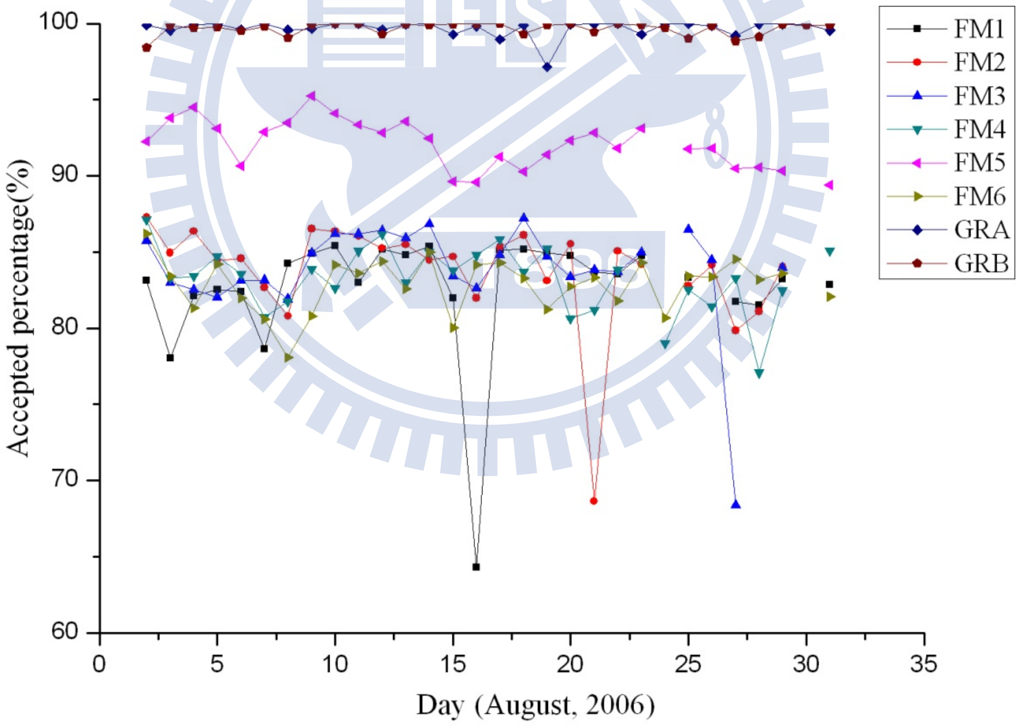

Fig. 5-2: Percentages of acceptance of kinematic orbits for normal point computations

Table 5-2: Statistics of percentages of accepted normal-point kinematic orbits (August, 2006)

	Min.	Max.	Ave.
FM1	64.31	85.42	82.62
FM2	68.65	87.30	83.77
FM3	68.37	87.22	83.85
FM4	77.08	87.15	83.22
FM5	89.41	95.24	92.10
FM6	78.09	86.18	82.84
GRA	97.15	100	99.68
GRB	98.43	100	99.66

5.2.2 Computation of residual accelerations

The key concept under consideration is the determination of the LEO acceleration derived from a kinematic orbit. Acceleration derived from GPS phase observations were first used in airborne gravimetry (Jekeli and Garcia 1997). Reubelt et al. (2004) have used the means of high-resolution nine-point scheme Newton interpolation and Ditmar et al. (2006) have used a three-point difference scheme to derive the accelerations from CHAMP satellite orbits for computing gravity field.

In this study, we employ a numerical differentiation technique to compute accelerations from COSMIC and GRACE normal-point kinematic and dynamic orbits. This technique is based on the divided-difference method (Gerald and Wheatley 2003) that requires less arithmetic operations than Lagrangian and Neville's methods.

Assuming the function values of $f(x)$ are given at several values for x, an nth-degree polynomial representing this function is (Gerald and Wheatley 2003):

$$P_n(x) = a_0 + (x-x_0)a_1 + (x-x_0)(x-x_1)a_2 + \cdots + (x-x_0)(x-x_1)\cdots(x-x_{n-1})a_n \quad (5\text{-}1)$$

If a_i is chosen so that $P_n(x) = f(x)$ at the $n+1$ known points, $(x_i, f_i), i = 0, \ldots, n$, then $P_n(x)$ is an interpolating polynomial. The first divided difference between x_s and x_t is

$$f[x_s, x_t] = \frac{f_t - f_s}{x_t - x_s} = f[x_t, x_s] \quad (5\text{-}2)$$

The higher-order difference is defined as

$$f[x_0, x_1, \cdots, x_n] = \frac{f[x_1, x_2 \cdots, x_n] - f[x_0, x_1 \cdots, x_{n-1}]}{x_n - x_0} \quad (5\text{-}3)$$

So we can establish that the a_i of eq. (5-1) are given by these divided differences and each $P_n(x_i)$ will equal $f(x_i)$ if $a_i = f[x_0, x_1, \cdots, x_i]$. Eq. (5-1) can be written as

$$P_n(x) = f_0^{[0]} + (x-x_0)f_0^{[1]} + (x-x_0)(x-x_1)f_0^{[2]} + \cdots + (x-x_0)(x-x_1)\cdots(x-x_{n-1})f_0^{[n]} \quad (5\text{-}4)$$

If the x-values are evenly spaced, ordinary differences are used instead of divided differences (Gerald and Wheatley 2003). It's called Newton-Gregory interpolation method and an interpolating polynomial of degree n with x evaluated at (x_s) can be represented as:

$$P_n(x_s) = f_0 + s\Delta f_0 + \frac{s(s-1)}{2!}\Delta^2 f_0 + \cdots + \frac{s(s-1)\cdots(s-n+1)}{n!}\Delta^n f_0^{[n]} \tag{5-5}$$

where $\Delta^n f_i$ is *n*-order difference, $s = (x - x_0)/h$ and *h* is the uniform spacing in *x*-values. We can write eq. (5-5) in terms of $s = (x - x_i)/h$:

$$P_n(s) = f_i + s\Delta f_i + \frac{s(s-1)}{2!}\Delta^2 f_i + \frac{s(s-1)(s-2)}{3!}\Delta^3 f_i^{[n]} + \cdots + \prod_{j=0}^{n-1}(s-j)\frac{\Delta^n f_i}{n!} \tag{5-6}$$

Therefore,

$$\frac{d}{dx}P_n(s) = \frac{d}{ds}P_n(s)\frac{ds}{dx} = \frac{1}{h}[\Delta f_i + \sum_{j=2}^{n}\left\{\sum_{k=0}^{j-1}\prod_{\substack{l=0 \\ l\neq k}}^{j-1}(s-l)\right\}\frac{\Delta^j f_i}{j!} \tag{5-7}$$

The derivation of *f*(*x*), denoted as $f'(x)$, can be approximated as

$$f'(x) = \frac{1}{h}\left[\Delta f_i - \frac{1}{2}\Delta^2 f_i + \frac{1}{3}\Delta^3 f_i - \cdots + (-1)^{n-1}\frac{\Delta^n f_i}{n}\right]_{x=x_i} \tag{5-8}$$

The second-order derivation of *f(x)* is

$$f''(x) = \frac{1}{h^2}\left[\Delta^2 f_i - \Delta^3 f_i + \frac{11}{12}\Delta^4 f_i - \frac{5}{6}\Delta^5 f + \cdots\right] \tag{5-9}$$

In this study, the default polynomial degree n is 14. The residual satellite accelerations vector $\mathbf{a}$ can be computed as follow:

$$\mathbf{a} = \mathbf{a}_{\mathbf{i}}^{(\mathbf{kin})} - \mathbf{a}_{\mathbf{i}}^{(\mathbf{dyn})} \tag{5-10}$$

where $\mathbf{a}_{\mathbf{i}}^{(\mathbf{kin})}$ is the observed kinematic acceleration and $\mathbf{a}_{\mathbf{i}}^{(\mathbf{dyn})}$ is the reference dynamic acceleration and the index **i** indicates a given component at a given epoch.

5.3 Validation of the acceleration method

In the following simulation, the true orbit perturbing noises are known and so are the true values of temporal gravity field. The purpose of this simulation is to validate the computer program for the acceleration method and assess the accuracy of the recovered gravity field.

We simulate the six FORMOSAT-3 satellite orbits using a computer program package, called CTODS (Chang 2003), developed for precise orbit and gravity determination. The perturbing forces caused by the Earth's non-sphericity, N-body, solid Earth tide, ocean tide, air drag, solar radiation pressure, Earth radiation and relativity are modeled. The data span is from June 1, 2002 to June 7, 2002 and the data sampling is 1 minute. The initial state vectors (six Keplerians) are $a =$ 7160.137km, $e = 0$, $i = 72°$, $\omega = 0°$, $\Omega = 0°, -24°, -48°, -72°, -96°, -120°$ and $M = 0°, 52.5°, 105°, 157.5°, 210°, 262.5°$. We assume the geopotential coefficients $\overline{C}_{nm}^{E}$ and $\overline{S}_{nm}^{E}$ of the reference gravity field GGM02C model and the temporal geopotential coefficients $\Delta\overline{C}_{nm}$ and $\Delta\overline{S}_{nm}$ derived from the ocean mass variation are true. The following data sets are used (See Fig.5-3)：

(1) Compute $\overline{C}_{nm}^{T} = \overline{C}_{nm}^{E} + \Delta\overline{C}_{nm}$ and $\overline{S}_{nm}^{T} = \overline{S}_{nm}^{E} + \Delta\overline{S}_{nm}$.

(2) Integrate 7-day orbits at a 1-minute interval using $\overline{C}_{nm}^{T}$ and $\overline{S}_{nm}^{T}$ up to degree 70 for each of the 6 COSMIC satellites. Random errors are added to the orbit based on a 1, 3, 5-cm standard deviation.

(3) Repeat (2), but using $\overline{C}_{nm}^{E}$ and $\overline{S}_{nm}^{E}$.

(4) Calculate the accelerations by quadratic differential of (2) and (3) positions.

(5) Subtract the accelerations in (4) to get the radial, along-track and cross-track perturbations due to mass variation.

(6) Sample the acceleration data at a 2-minute interval by using normal-point method.

(7) Compute $\Delta\hat{\overline{C}}_{nm}$ and $\Delta\hat{\overline{S}}_{nm}$, which are the estimates of $\Delta\overline{C}_{nm}$ and $\Delta\overline{S}_{nm}$, by using the residual acceleration approach.

One set of normal equation, geopotential coefficients and empirical coefficients is computed from a 7-day orbit arc for each satellite. These normal equations are considered uncorrelated and are combined to determine an averaged gravity field.

Fig.5-4(a) shows the gravity variation to spherical harmonic degree/order 5 from the ocean mass variation, and (b), (c) and (d) show the recovered gravity variation with 1, 3 and 5 cm random white noise, respectively. Fig. 5-4 suggests that the temporal gravity can be recovered well using a 7-day arc data of one satellite with 1 cm random white noise. With 3 cm random white noise, the recovered gravity signatures are less obvious compared to the case of 1-cm noise. Fig. 5-5 shows the relative differences for zonal terms of the simulation-derived coefficients with respect to the ocean mass variation derived coefficients of gravity variation with different random noises.

We can also combine normal equations from all satellites to recover the gravity field. The observation equation in such combination solution is

$$\mathbf{X} = (\sum c_i \mathbf{N}_i)^{-1} (\sum c_i \mathbf{U}_i) \tag{5-11}$$

where $\mathbf{N}_i$ is the individual normal equation, i is the number of satellites, c_i is the regularization factor of weighting matrix since the weighting of different kinds of observations is generally unknown. If the prior weighting matrix is unknown, we need to estimate the variance-covariance to estimate c_i (Koch 1987).

Fig. 5-6 shows the relative differences of the recovered harmonic coefficients of gravity variation up to degree/order 5, 10, 15, and 20 using one week of 6 satellites data with 3 cm white noise. The relative differences in the case of degree/order 5 are smaller than those in the cases of degree/order 10, 15, and 20. Fig. 5-7 presents the recovered gravity variation combining one week of six satellites data by adding 1, 3 and 5 cm white noise. The relative differences in these solutions are shown in Fig. 5-8. The gravity signatures can be recovered well if the orbit data contains 5-cm noise or smaller. Fig. 5-9 shows smaller relative differences for zonal terms when adding different random noises, in comparison to the results given in Fig. 5-5.

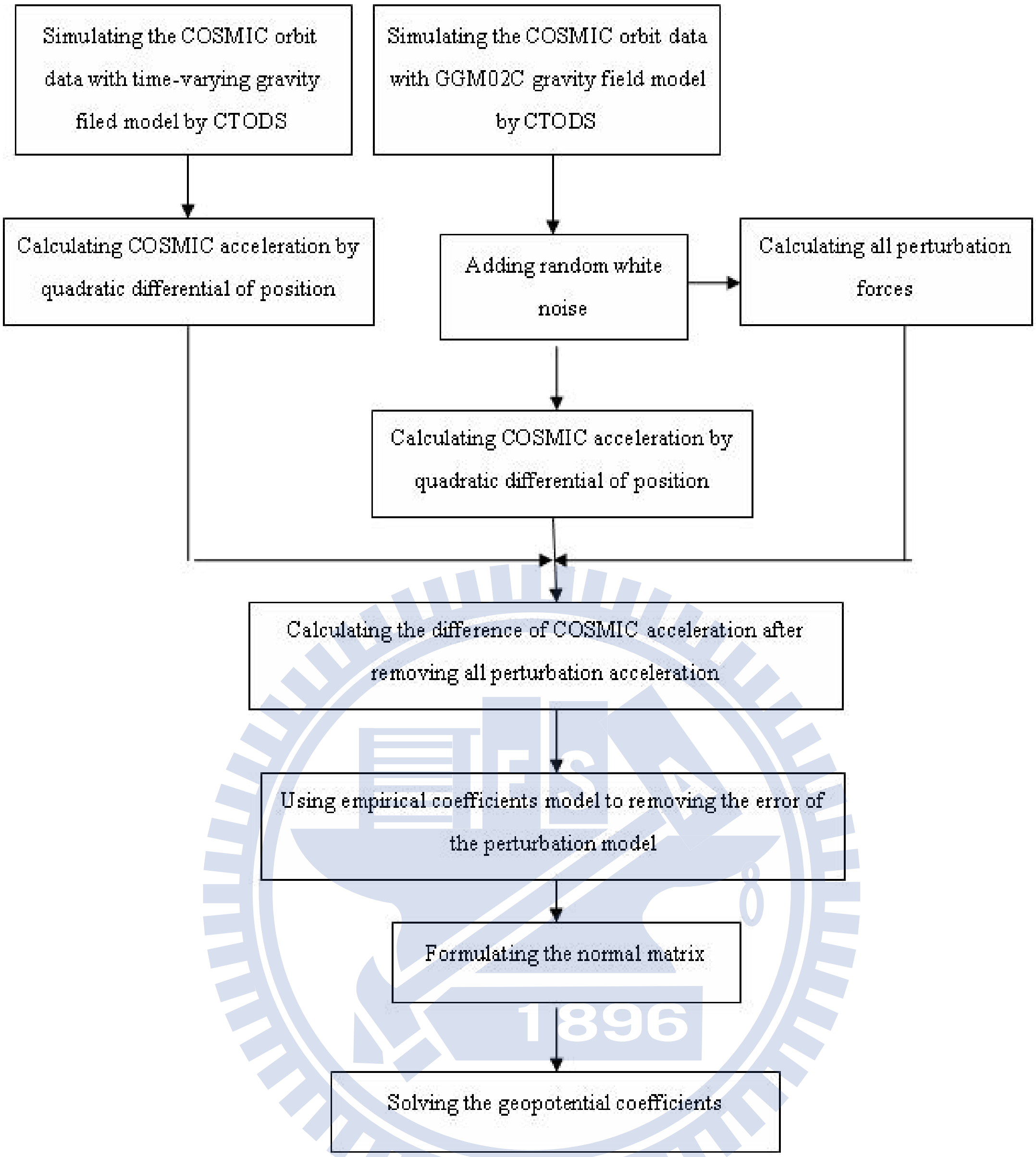

Fig. 5-3: The simulation procedure of residual acceleration approach

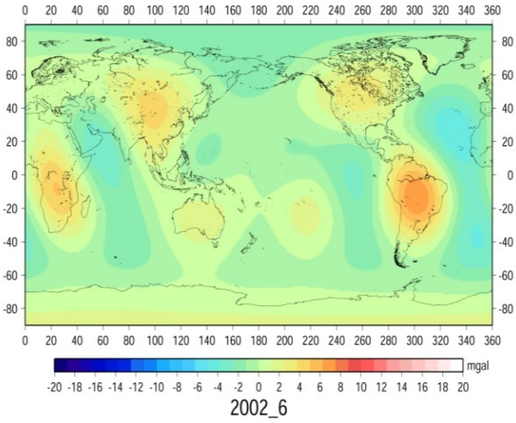

(a)

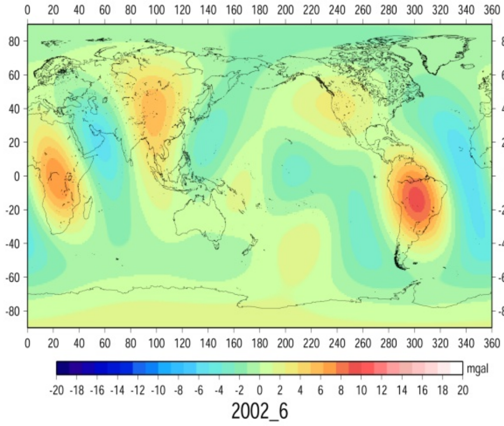

(b)

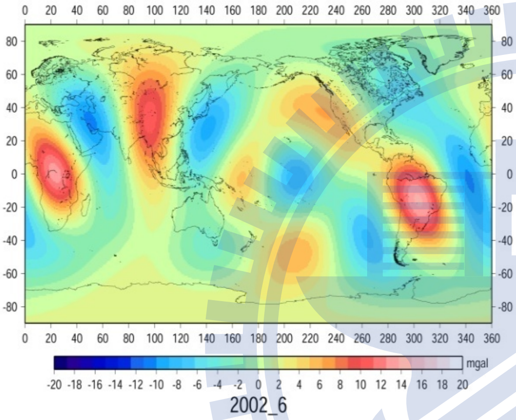

(c)

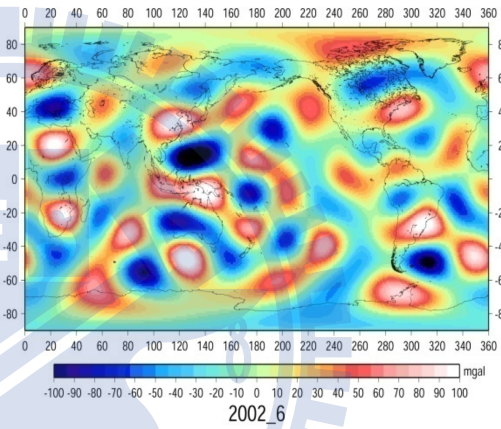

(d)

Fig. 5-4: Recovered gravity variation using one week of one COSMIC satellite data and degree-5 solutions by (a) oceanic mass variation (b) 1-cm white noise (c) 3-cm white noise (d) 5-cm white noise. Unit is mgal

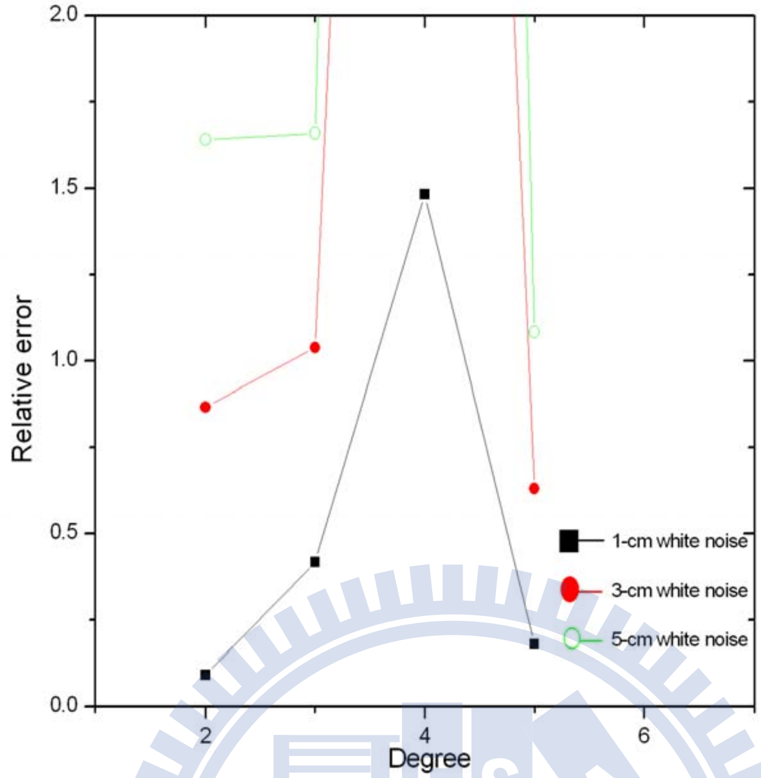

Fig. 5-5: Relative differences of recovered zonal coefficients from the degree-5 solutions (one COSMIC satellite)

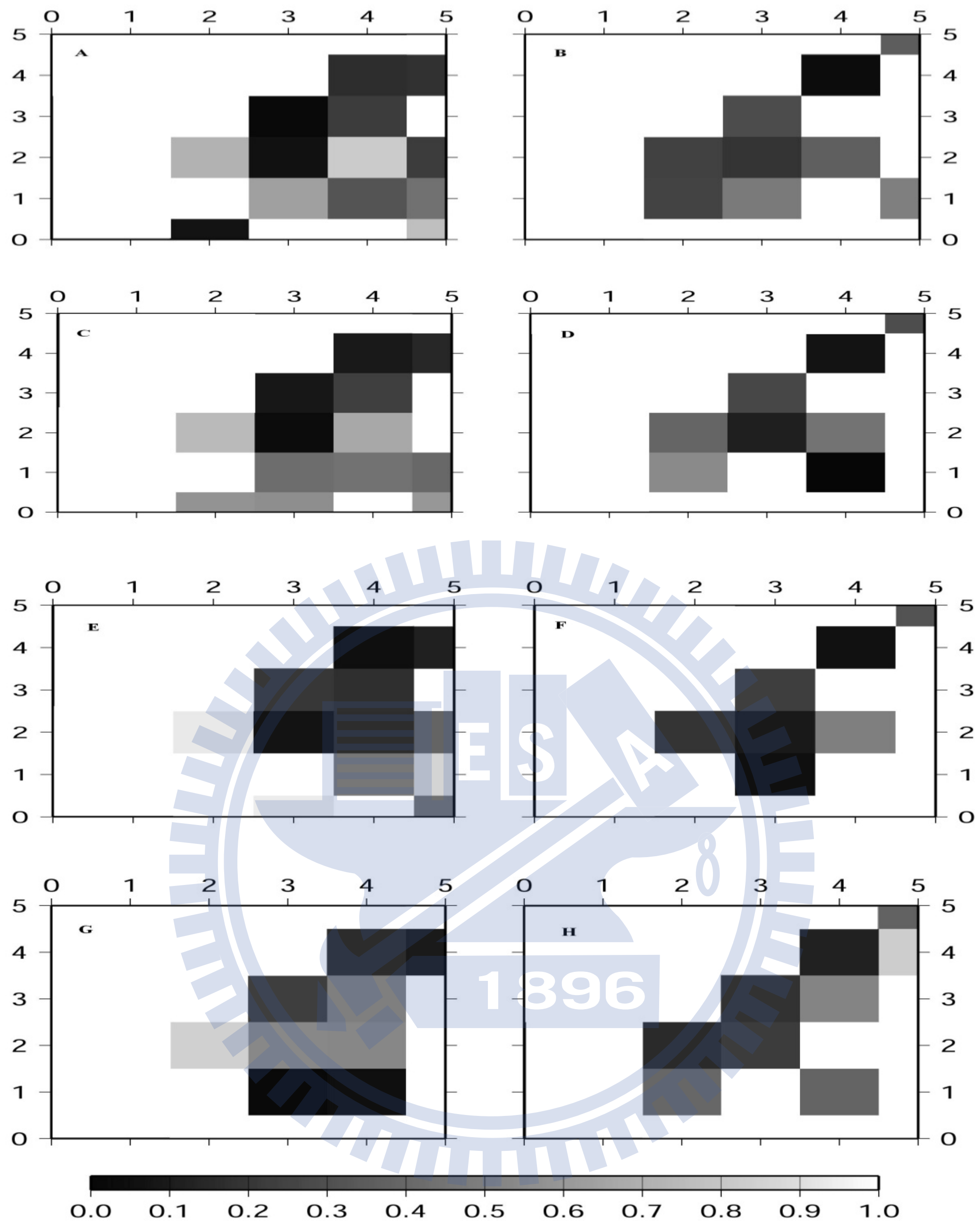

Fig. 5-6: Relative differences of the recovered harmonic coefficients of gravity variation for (A) $\Delta\hat{\hat{C}}_{nm}$ (degree-5 solution), (B) $\Delta\hat{\hat{S}}_{nm}$ (degree-5 solution), (C) $\Delta\hat{\hat{C}}_{nm}$ (degree-10 solution), (D) $\Delta\hat{\hat{S}}_{nm}$ (degree-10 solution), (E) $\Delta\hat{\hat{C}}_{nm}$ (degree-15 solution), (F) $\Delta\hat{\hat{S}}_{nm}$ (degree-15 solution), (G) $\Delta\hat{\hat{C}}_{nm}$ (degree-20 solution) and (H) $\Delta\hat{\hat{S}}_{nm}$ (degree-20 solution) using one week of six COSMIC satellite data with 3-cm white noise

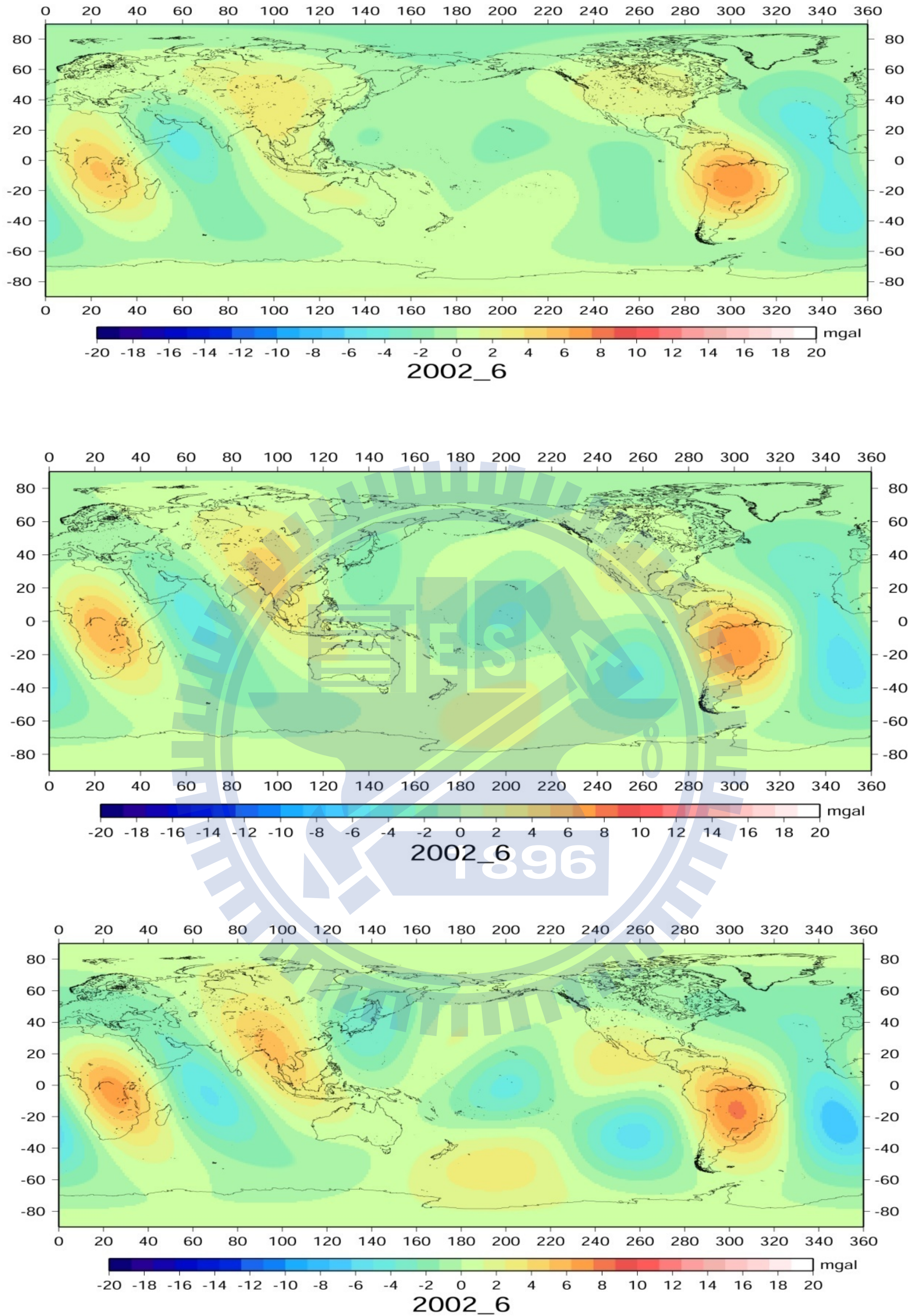

Fig. 5-7: Recovered gravity variation combining one week of six COSMIC satellite data by adding 1-cm white noise (top), 3-cm white noise (center) and 5-cm white noise (bottom). Unit is mgal

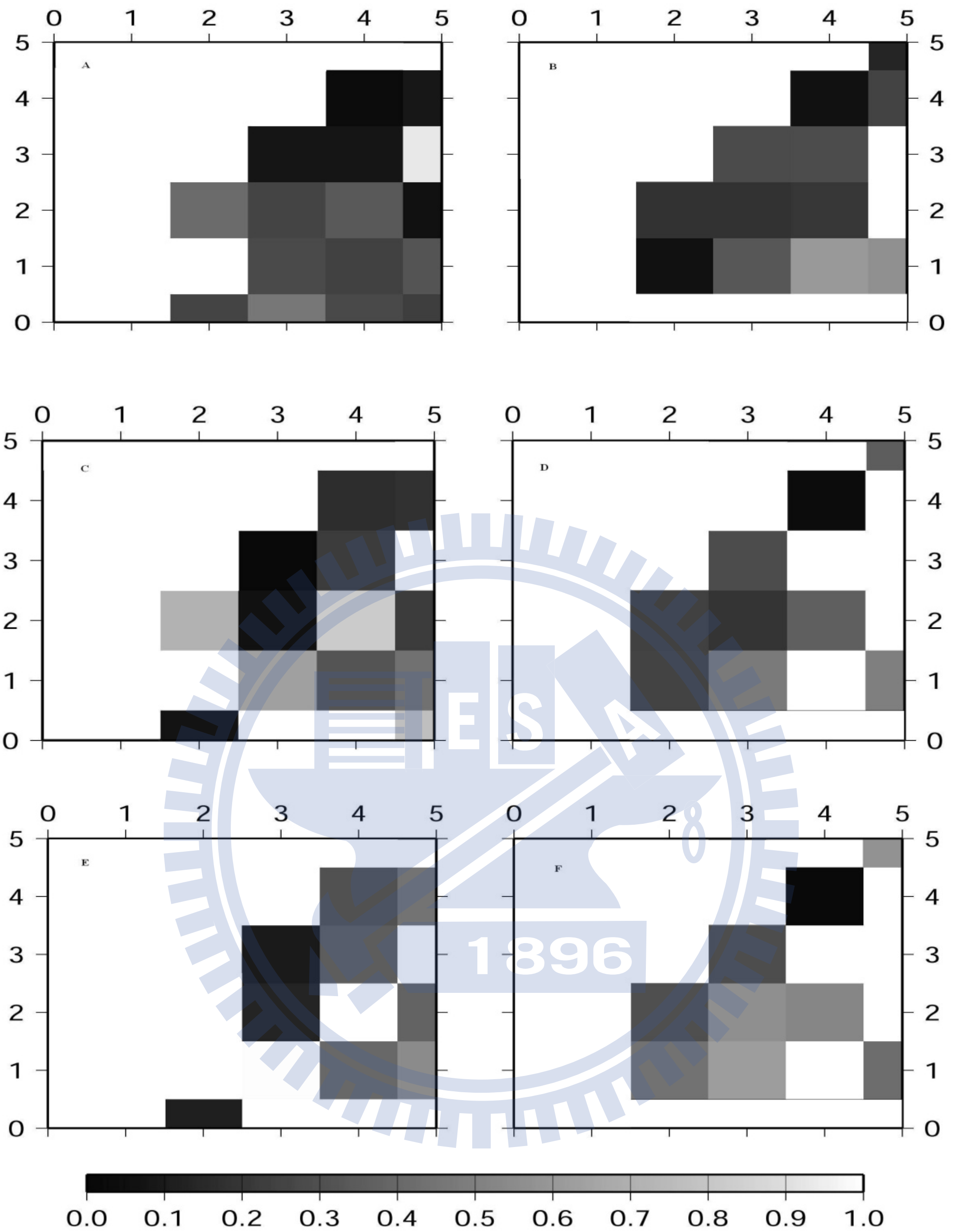

Fig. 5-8: Relative errors of the recovered harmonic coefficients up to degree 5 of gravity variation for (A) $\Delta\hat{\bar{C}}_{nm}$ (1 cm white noise), (B) $\Delta\hat{\bar{S}}_{nm}$ (1 cm white noise), (C) $\Delta\hat{\bar{C}}_{nm}$ (3 cm white noise), (D) $\Delta\hat{\bar{S}}_{nm}$ (3 cm white noise), (E) $\Delta\hat{\bar{C}}_{nm}$ (5 cm white noise) and (F) $\Delta\hat{\bar{S}}_{nm}$ (5 cm white noise) using one week of six COSMIC satellites data

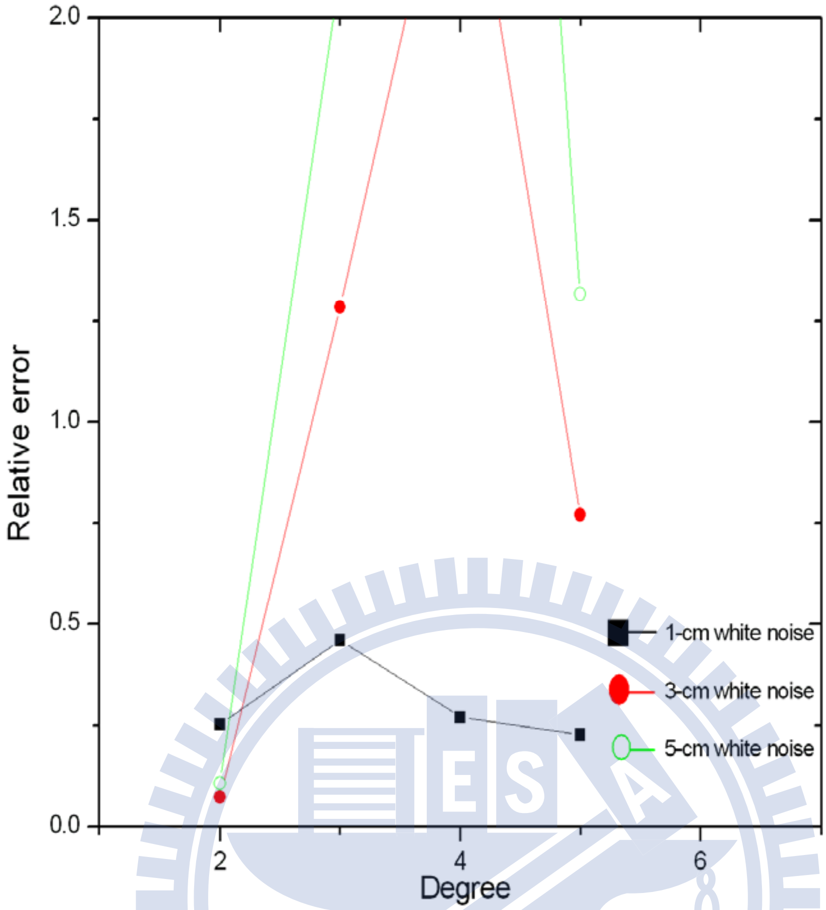

Fig. 5-9: Relative errors of recovered zonal coefficients from the degree-5 solutions (six COSMIC satellites)

5.4 Gravity recovery using COSMIC and GRACE GPS data

The CSR RL04 products are presented in this chapter for comparison and analysis. Following Hwang et al. (2008) and Xu et.al (2006) studies, the signal-to-noise ratio of COSMIC-derived spherical harmonic components is shown larger than 1 with degrees lower than 10. For efficient computation, we decide to adopt 15 as the maximum degree of expansion and carried out several experimental gravity solutions using one month of COSMIC and GRACE normal-point kinematic orbits with different combinations. Fig. 5-10 shows degree variances and error degree variances from the COSMIC, COSMIC-GRACE and CSR RL04 solutions.

We can clearly observe three features from Fig. 5-10: (i) The COSMIC and COSMIC-GRACE degree variances decrease and the error degree variances increase unapparently with degree; (ii) all error degree variances are less than the degree variances below degree 10; (iii) The degree variance of COSMIC-only solution is closer to the CSR RL04 solution but degree 2 may be affected by the constraint of Kaula's rule.

The geoid changes from the COSMIC-only and COSMIC-GRACE solutions to degree 15 are shown in Fig. 5-11; Fig. 5-12 shows the geoid variations from the combined COSMIC and GRACE solution and from CSR RL04 solution to degree 15. Comparing Fig. 5-11 and Fig. 5-12, the COSMIC-only solution shows clear geoid highs and lows over European, eastern Pacific, India continent and southern Africa, which resembles those given by the CSR RL04 solution but still contains the aliasing artifacts over southern Pacific and Bering Sea. We note that the COSMIC-GRACE solution can reduce the geoid signature artifacts of the COSMIC-only solution due to better observation data coverage. The combined solution closely resembles the CSR RL04 solution and this is due to the large weights of CSR RL04 coefficients in the combination. We still need to carry out more quantitative assessments of accuracy and spatial resolution of COSMIC gravity solutions using the terrestrial-based data.

The relative differences of the COSMIC-only and COSMIC-GRACE geopotential coefficients with respect to the CSR RL04 coefficients are given in Fig. 5-13. A large portion of the recovered geopotential coefficients are smaller than 1 which is considered as significantly close to the CSR RL04 solution. The COSMIC-GRACE greatly enhances the COSMIC-only solution especially in some terms of geopotential coefficients listed in Table 5-3. This would be explained by the combination of two different inclination satellite observation data. Fig. 5-14 shows the relative differences of the combined solution coefficients with respect to the CSR RL04 coefficients and most of them are less than 1. From Fig. 5-15, we can note that the relative differences of zonal coefficients derived from COSMIC-GRACE solution are larger than COSMIC-GRACE solution using analytical orbit perturbation approach after degree 6. The cause could be taced back to the lower degree geopotential coefficients which are more sensitive to the accuracy of accelerations.

We also compute calibrated standard errors of COSMIC-derived geopotential coefficients using the method given in Hwang et al. (2008). A calibrated standard error is obtained by multiplying the un-calibrated standard error by the scaling factor. Fig. 5-16 compares the calibrated error degree variances from CSR RL04, COSMIC-only using AOP approach, COSMIC-only and COSMIC-GRACE using acceleration approach, and combined solutions. From the comparison, one can see that the combined solution yields smaller error degree variances than those from CSR RL04 solution. The calibrated error degree variances of COSMIC-only and COSMIC-GRACE derived by acceleration approach turn out to be smaller than them of COSMIC-only solution derived by analytical orbit perturbation approach. However, it may not be necessary to say that the time-varying gravity field recovered from acceleration approach would be better than that recovered from analytical orbit perturbation approach. In this study, the COMSIC observation data combined with GRACE shows a good potential to recover the low degree time-varying gravity field.

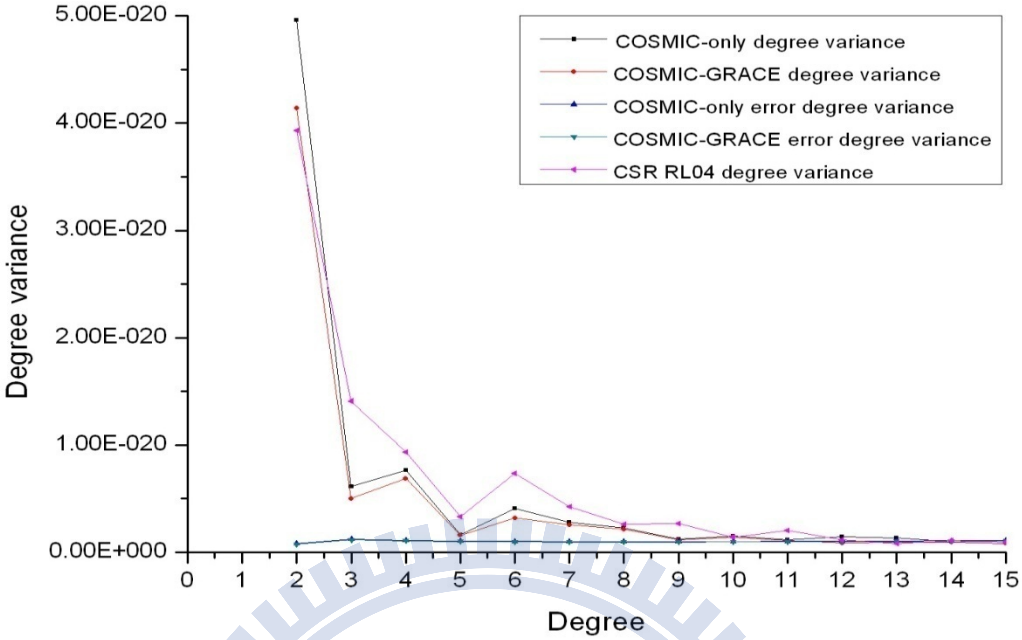

Fig. 5-10: Degree variances and formal error degree variances of time-varying geopotential coefficients from the COSMIC-only, COSMIC-GRACE and CSR RL04 solutions

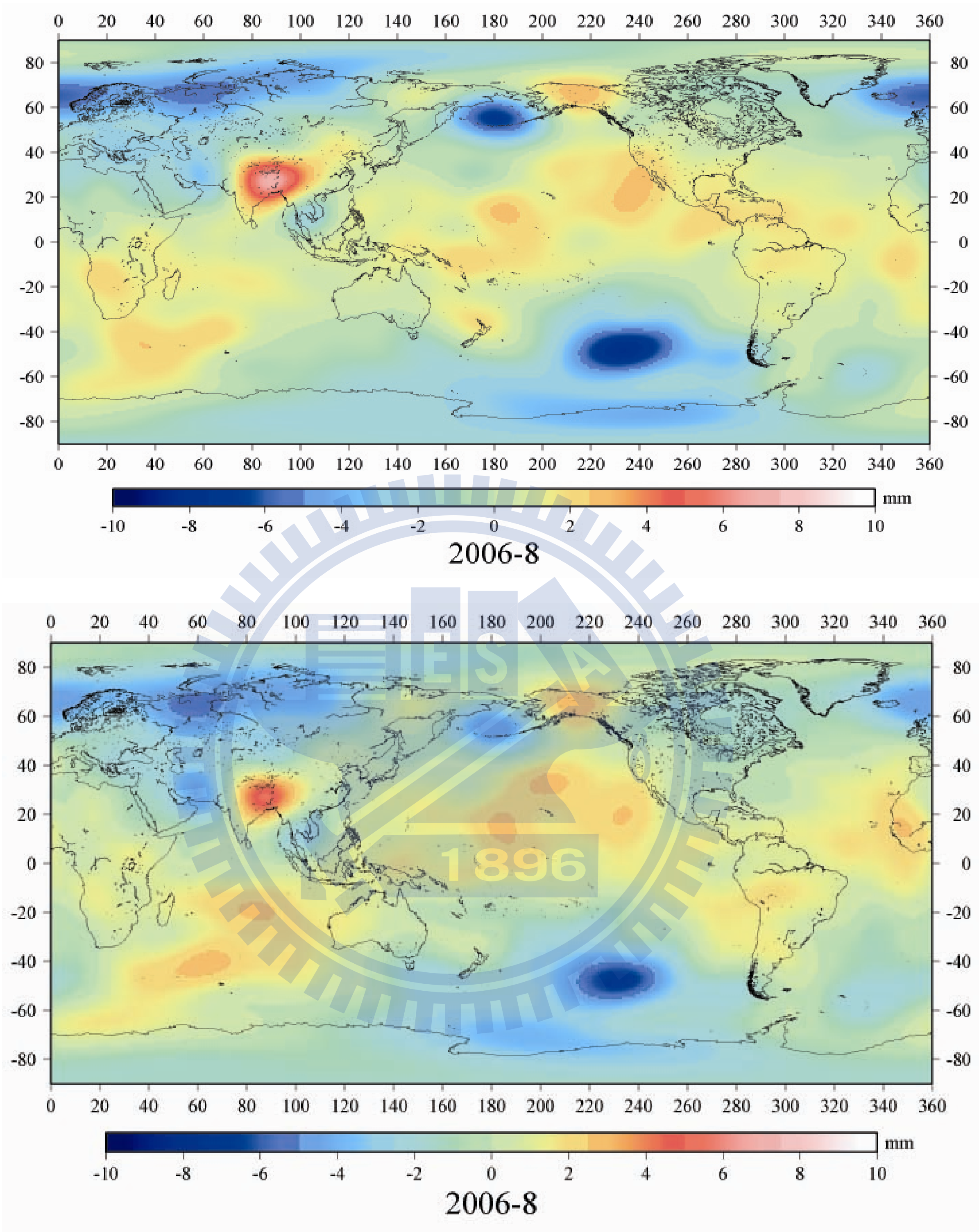

Fig. 5-11: Geoid variations to spherical harmonic degree 15 from COSMIC-only solution (top) and from COSMIC-GRACE solution using residual acceleration approach

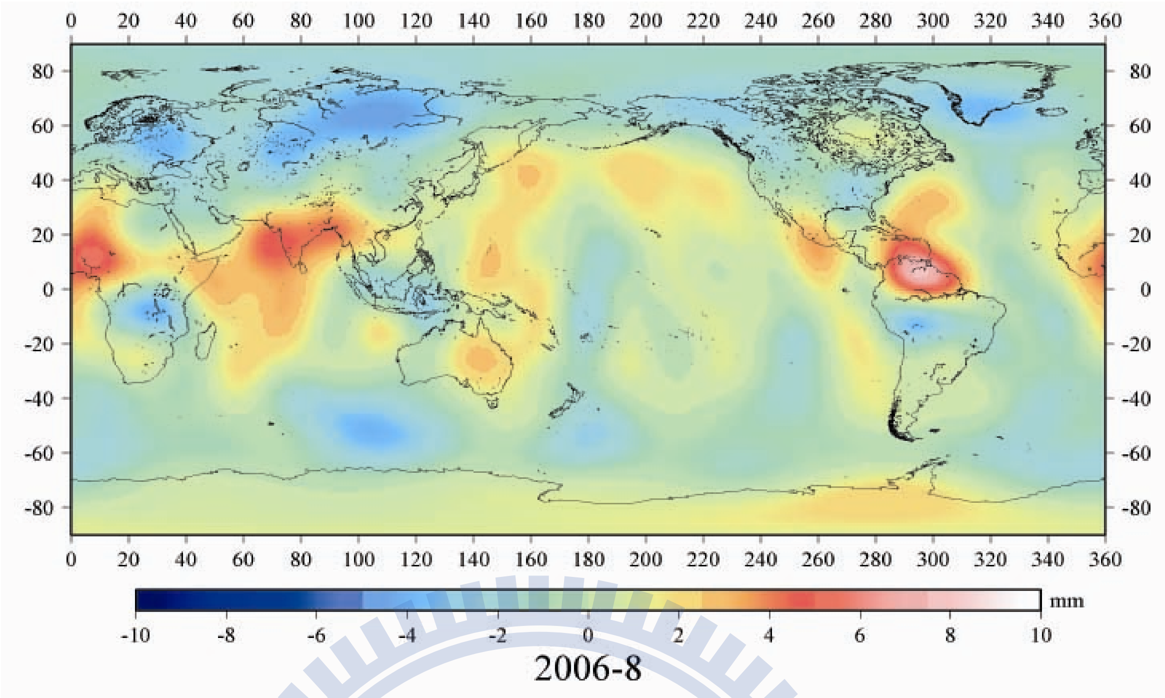

Fig. 5-12: Geoid variation to spherical harmonic degree 15 from the combined solution

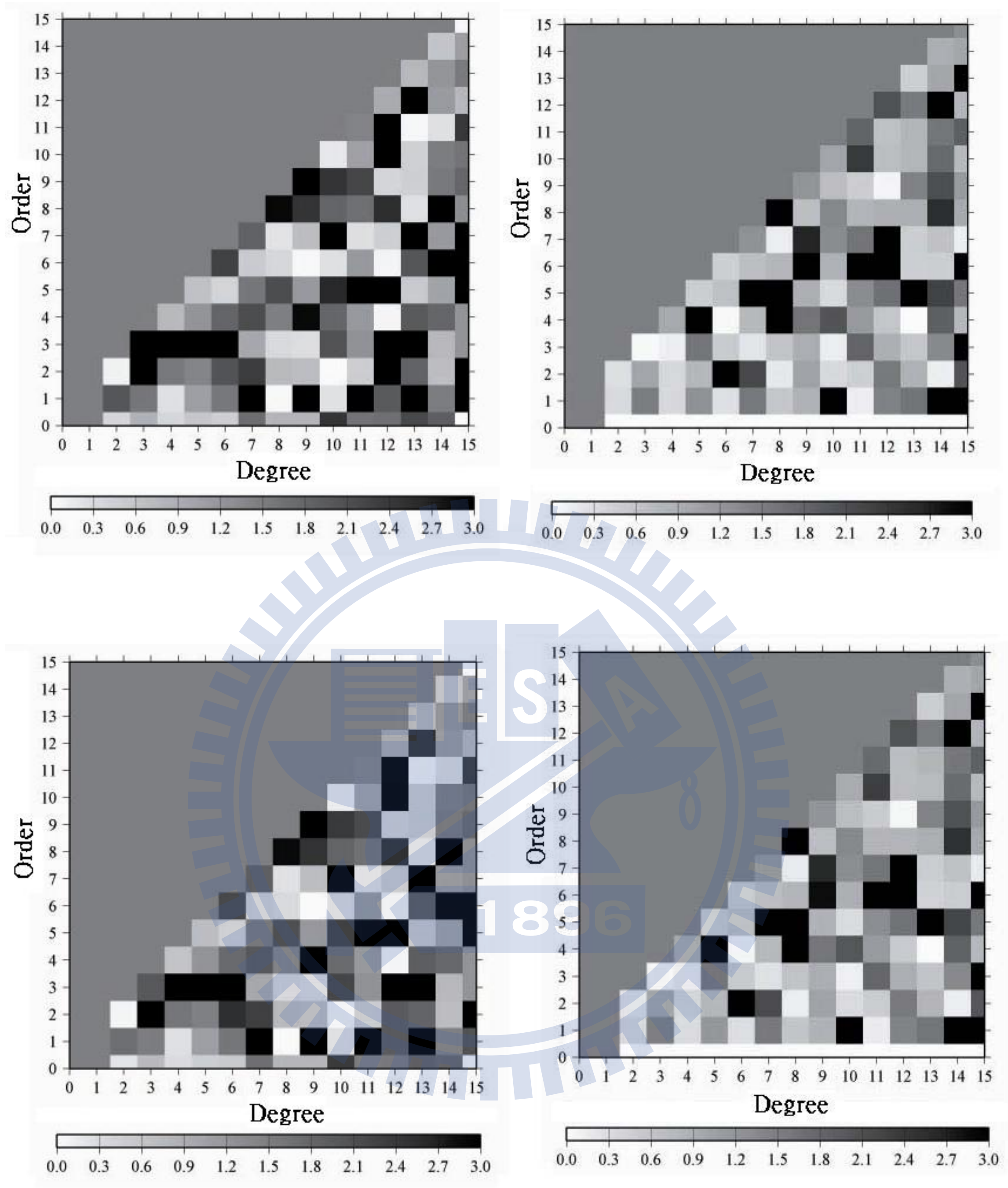

Fig. 5-13: Relative differences of the COSMIC-only (top) and COSMIC-GRACE geopotential coefficients with respect to the CSR RL04 coefficients of gravity variation for $\Delta\overline{C}_{nm}$ (left) and $\Delta\overline{S}_{nm}$ up to degree 15

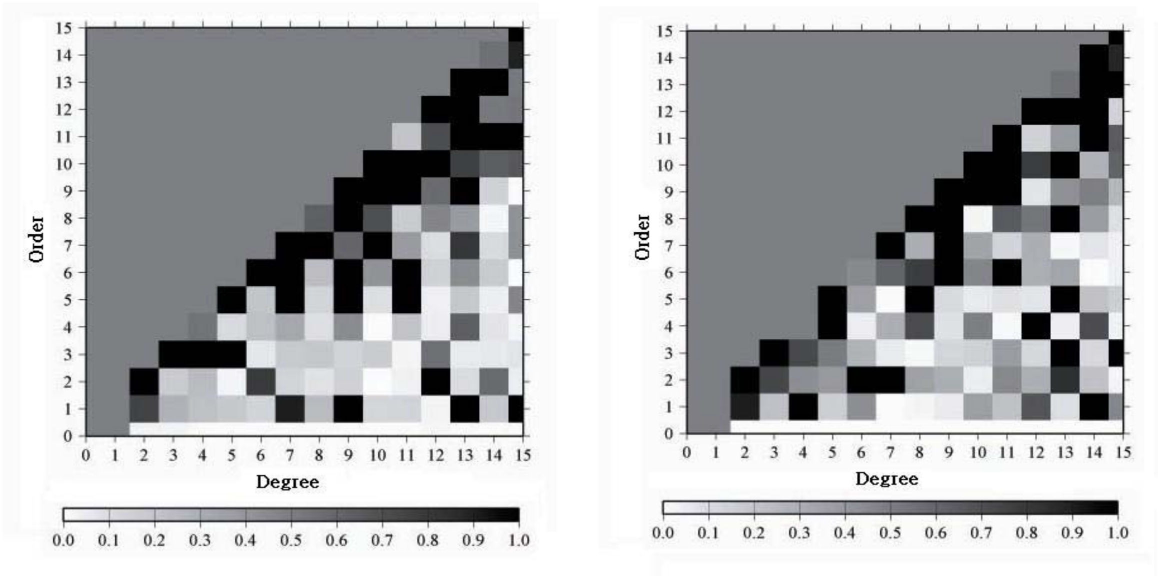

Fig. 5-14: Relative differences of the combined solution coefficients with respect to the CSR RL04 coefficients for $\Delta\overline{C}_{nm}$ (left) and $\Delta\overline{S}_{nm}$ up to degree 15

Table 5-3: Relative errors of geopotential coefficients from COSMIC-only and COSMIC-GRACE solutions

coefficient	COSMIC-only solution	COSMIC-GRACE solution
$\Delta\overline{C}_{3,3}$	55.287	1.987
$\Delta\overline{C}_{9,1}$	1088.755	4.61
$\Delta\overline{S}_{9,6}$	20.110	2.854
$\Delta\overline{C}_{12,2}$	29.133	1.953
$\Delta\overline{C}_{13,1}$	499.183	3.902
$\Delta\overline{C}_{13,12}$	16.223	2.491
$\Delta\overline{C}_{15,1}$	30.375	2.074
$\Delta\overline{C}_{15,7}$	22.240	1.278

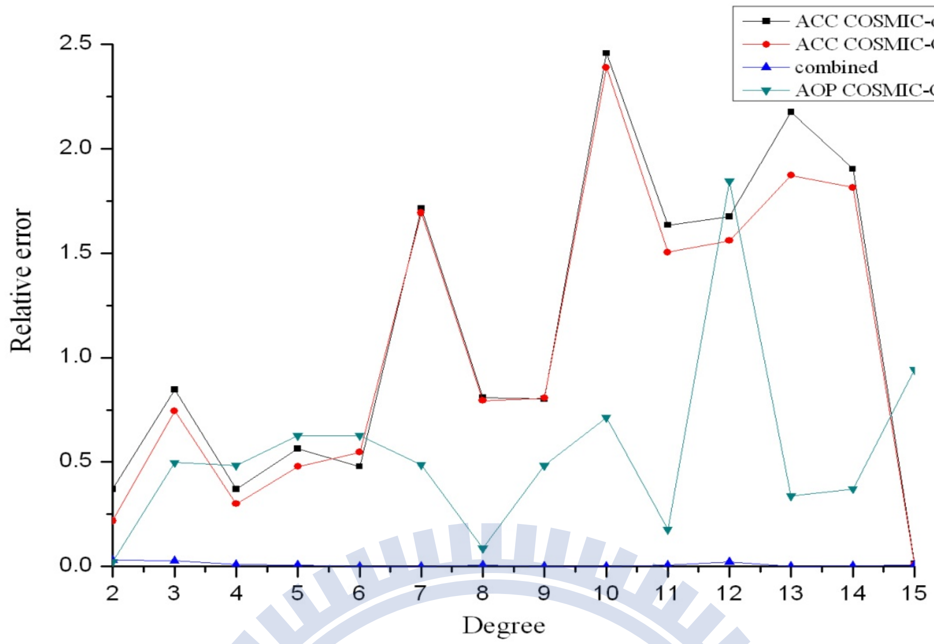

Fig. 5-15: Relative differences for the zonal coefficients from ACC, AOP, CSR RL04 and combined solutions

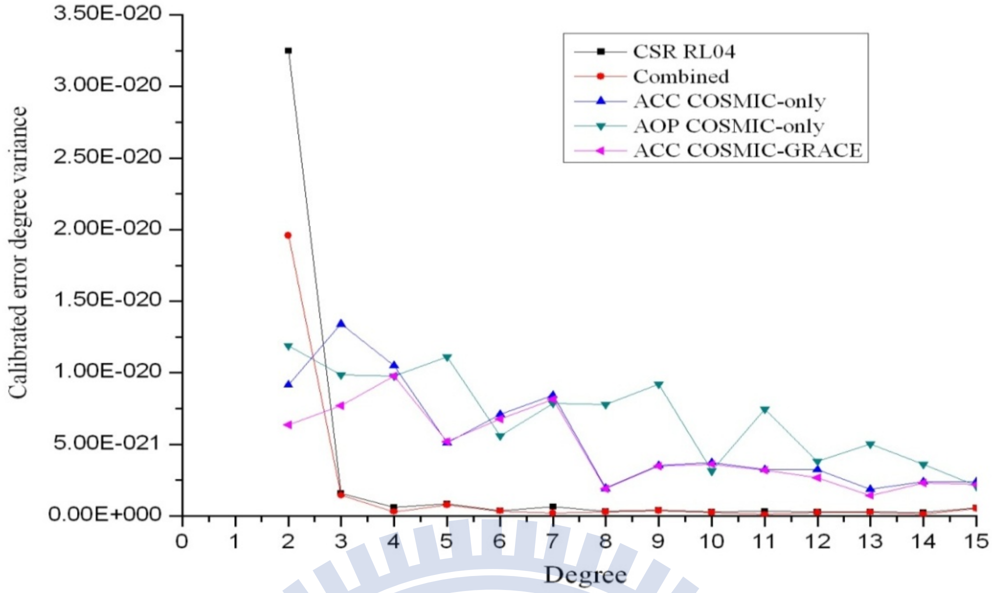

Fig. 5-16: Calibrated error degree variances from ACC, AOP, CSR RL04 and combined solutions

Chapter 6

Low-degree gravity change

6.1 Introduction

In Chapters 4 and 5, we have presented two methods to process the COSMIC and GRACE hl-SST data to recover the temporal gravity field using one month of observations. Therefore, we use these two methods to compute the monthly solutions: the NCTU AOP solution by the analytical orbital perturbation method, and the NCTU ACC solution by the residual acceleration method. The six COSMIC and two GRACE POD data from September 2006 to December 2007 were processed to obtain 16 monthly solutions. Section 6.2 will describe COSMIC and GRACE POD data processing. The time series of low degree (up to degree/order 5) NCTU AOP, ACC solutions and the combined solutions (up to degree/order 15) with GRACE KBR solutions will be discussed in Section 6.3. Finally, Section 6.4 focuses on variations of low-degree zonal harmonic coefficients, including $\Delta\overline{C}_{20}$, $\Delta\overline{C}_{30}$ and $\Delta\overline{C}_{40}$. These results will be compared with the SLR and CSR RL04 solutions.

6.2 Data of COSMIC and GRACE

Following the procedure mentioned in Chapter 3, the reduced-dynamic and kinematic orbits of both COSMIC and GRACE satellites were determined using 16 months of zero-differenced measurements by Bernese 5.0 from September 2006 to December 2007. The original sampling intervals of COSMIC, GRACE kinematic and reduced-dynamic orbits are 30-s. The force models for both COSMIC and GRACE are listed in Table 3-1 and the prior static gravity field is from the GGM03S model.

Because of unknown reasons, COSMIC GPS observations in certain days were missing or not completed. Table 6-1 presents the numbers of files received from each

COSMIC satellite and the numbers of kinematic orbit computed from the original data from September 2006 to December 2007. The unusable kinematic orbit data take the blame for the bad attitude control, bad GPS observation quality or simply missing observations. Fig. 6-1 shows the monthly RMS differences between dynamic and kinematic orbits of COSMIC and GRACE satellites in the radial, along-track and cross-track directions. The averaged RMS differences in these three directions for each COSMIC and GRACE satellite are listed in Table 6-2. Comparison of the RMS differences between COSMIC and GRACE in August 2006 shown in Table 5-1 suggests that the RMS differences of each COSMIC satellite are at the same level but smaller due to the better attitude control and the higher satellite operating altitudes. We will use these dynamic and kinematic orbits to recover monthly temporal gravity field solutions following the procedures for the analytical orbital perturbation and residual acceleration approaches.

Table 6-1: Numbers of observation files and usable kinematic orbit files from September 2006 to December 2007

Month	FM1	FM2	FM3	FM4	FM5	FM6
2006.9	26[a]/26[b]	15/14	26/26	27/27	29/29	23/23
2006.10	27/24	30/27	27/27	28/25	28/28	25/24
2006.11	28/28	16/16	30/29	29/29	28/27	29/25
2006.12	27/27	26/26	26/26	29/29	29/29	22/21
2007.1	29/29	30/29	27/27	29/29	29/28	20/20
2007.2	26/26	27/27	28/27	28/28	28/28	16/14
2007.3	29/29	6/6	31/31	28/23	30/30	30/30
2007.4	30/29	13/13	30/29	23/18	29/29	20/20
2007.5	31/30	12/10	30/28	23/21	30/29	31/31
2007.6	30/30	22/21	25/25	30/30	30/30	26/26
2007.7	30/30	29/29	16/14	30/30	31/27	31/31
2007.8	31/31	18/18	17/17	30/29	31/30	29/28
2007.9	28/27	8/8	7/7	30/30	29/28	7/7
2007.10	28/15	27/27	21/21	31/31	31/31	0/0
2007.11	29/28	13/13	7/4	30/30	28/26	12/12
2007.12	27/27	27/27	23/23	31/29	29/27	28/27

a: Number of observation files
b: Number of usable kinematic orbit files

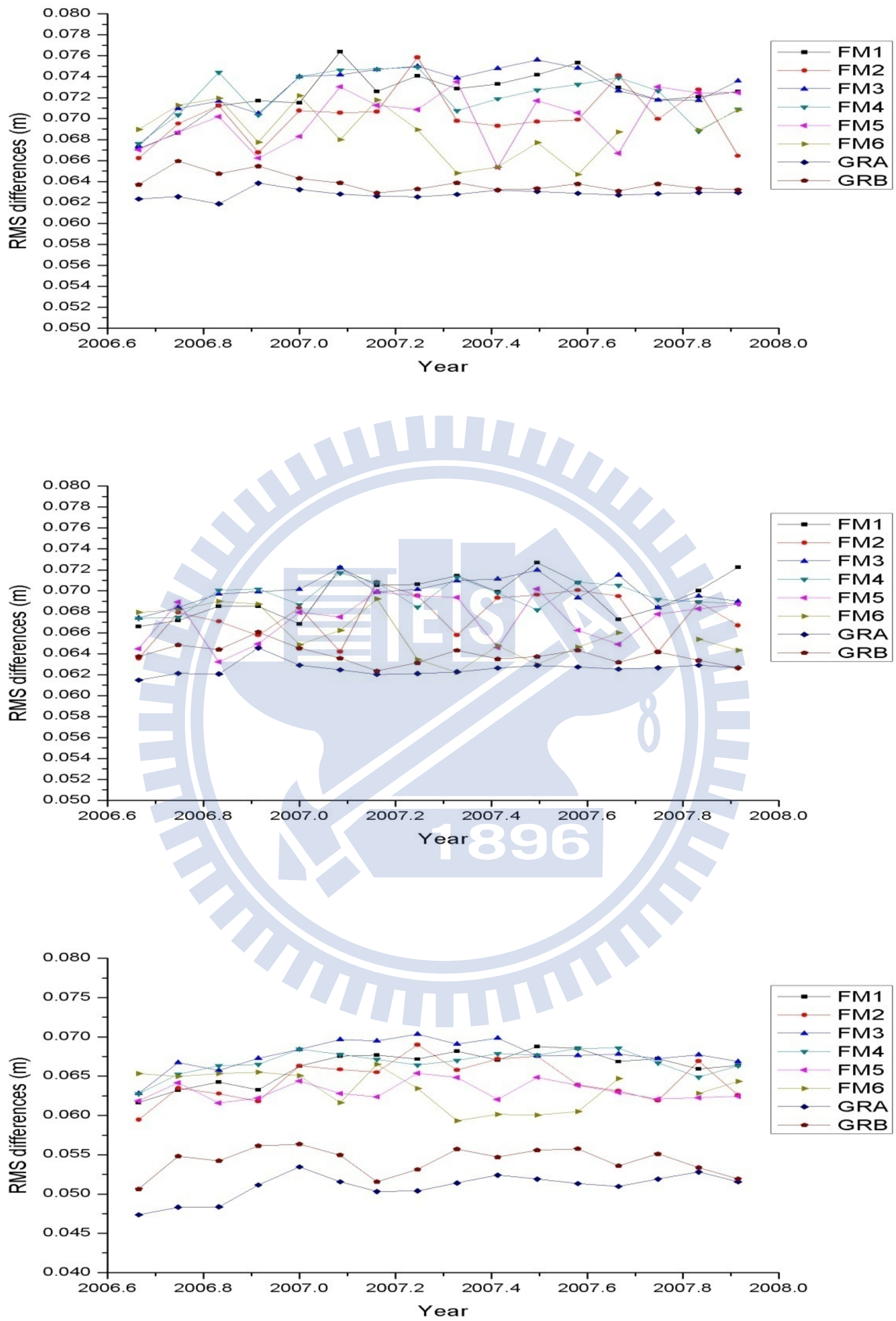

Fig. 6-1: The monthly RMS differences between dynamic and kinematic orbits of COSMIC and GRACE satellites in radial (top), along-track and cross-track (bottom) directions from September 2006 to December 2007

Table 6-2: Averaged RMS differences between kinematic and dynamic orbits from September 2006 to December 2007 (unit: cm)

Satellite	radial	alone-track	cross-track
FM1	7.24	6.96	6.66
FM2	7.02	6.76	6.46
FM3	7.30	7.00	6.78
FM4	7.25	6.95	6.68
FM5	7.00	6.73	6.31
FM6	6.88	6.59	6.33
GRA	6.28	6.26	5.01
GRB	6.38	6.38	5.42

6.3 Time series of monthly gravity solutions

In order to investigate the temporal variation of gravity field, we process the COSMIC and GRACE data from September 2006 to December 2007 at almost one month interval. The NCTU solutions contain a series of monthly estimates of the temporal gravity field variation with respect to the GGM03S model based on four years (January 2003 through December 2006) of GRACE KBR and GPS data from the RL04 processing. To focus on changes of low-degree geopotential coefficients, we adopted degrees 5 as the maximum degree in harmonic expansion for gravity recovery using COSMIC and GRACE hl-SST data. Figs. 6-2 and 6-3 show the time series of geoid variations to spherical harmonic degree 5 and 15 of CSR RL04 solutions from September 2006 to December 2007. Some hydrological signals are clearly visualized over the Amazon, India, central Africa, Russia, North America and Greenland. The maximum variations can be observed in spring (April) and autumn (September to October) and this pattern is consistent from one year to another.

Figs. 6-4 and 6-5 present the time series of the geoid variations to spherical harmonic degree 5 from the NCTU AOP and ACC solutions from September 2006 to December 2007. In general, the NCTU AOP and ACC solutions show similar magnitudes of geoid variations and show clear geoid highs and lows compared with CSR RL04 solutions with small phase differences. Compared with the CSR RL04 results shown in Fig. 6-2, not all monthly NCTU AOP and ACC solutions are of the same quality. For example, the AOP solutions for December of 2006; January, February and April of 2007 still show some artifacts at latitudes higher than 72º, which may be caused by lack of the measurements and ACC solutions as well for November and December of 2006, and February, April, June, August, September, October and December of 2007. The geoid signatures of the same month shown in the NCTU ACC solution are usually smaller than in the NCTU AOP solution. The reason may be that the numerical differentiation for acceleration derivation will increase the noise and we should use more terms of empirical model to absorb the noise.

The combined COSMIC-GRACE solutions are also carried out. The time series of the geoid variations to spherical harmonic degree 15 of combined NCTU AOP and ACC solutions from September 2006 to December 2007 are shown in Figs 6-6 and 6-7. We can indicate that the combined NCTU AOP and ACC solutions closely resemble the CSR RL04 solutions. Some geoid signatures are enhanced in some large mass redistribution areas like Amazon, India, and North America etc.. This is due to the large weights of GRACE coefficients in the combination. Comparing with Figs. 6-3, 6-6 and 6-7, we note that the combined NCTU AOP solutions show greater enhancements of geoid signatures than NCTU ACC solutions.

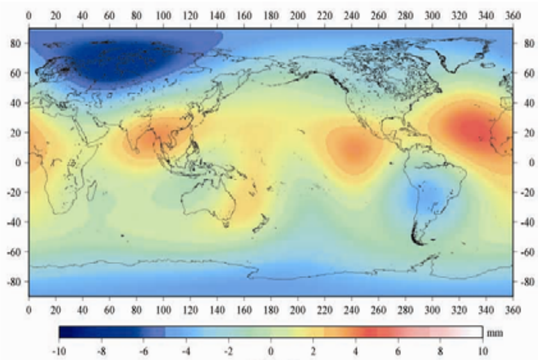

2006-9

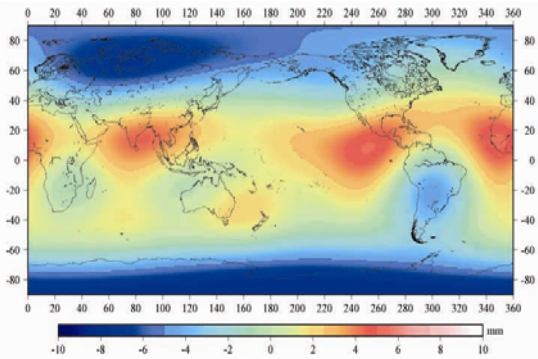

2006-10

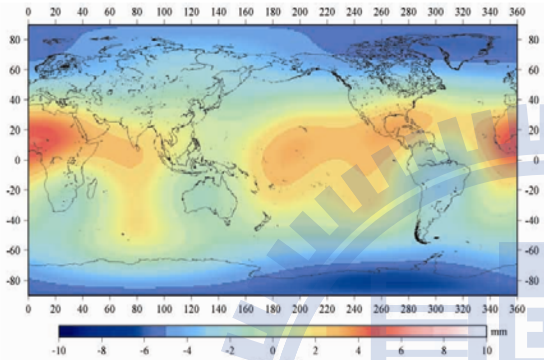

2006-11

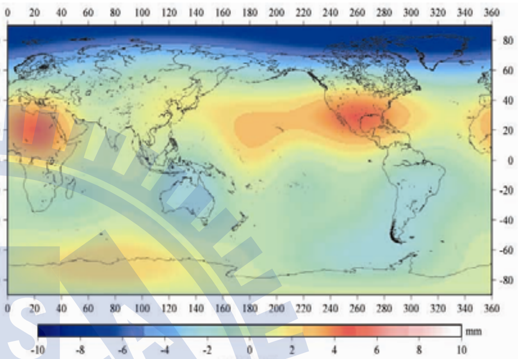

2006-12

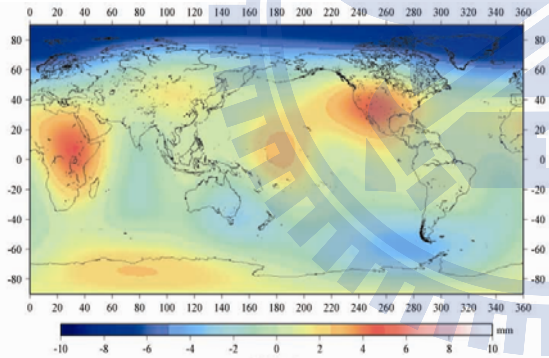

2007-1

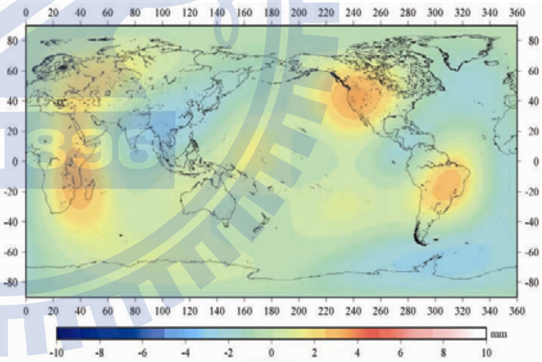

2007-2

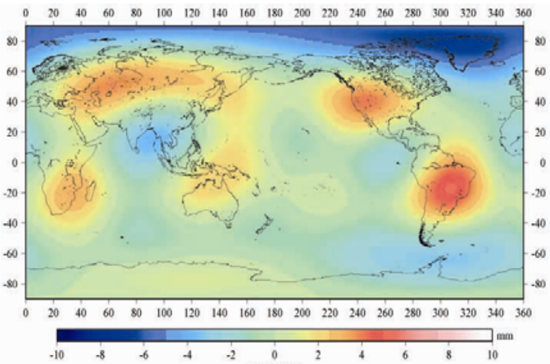

2007-3

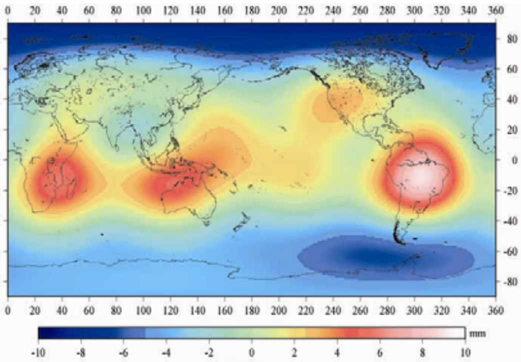

2007-4

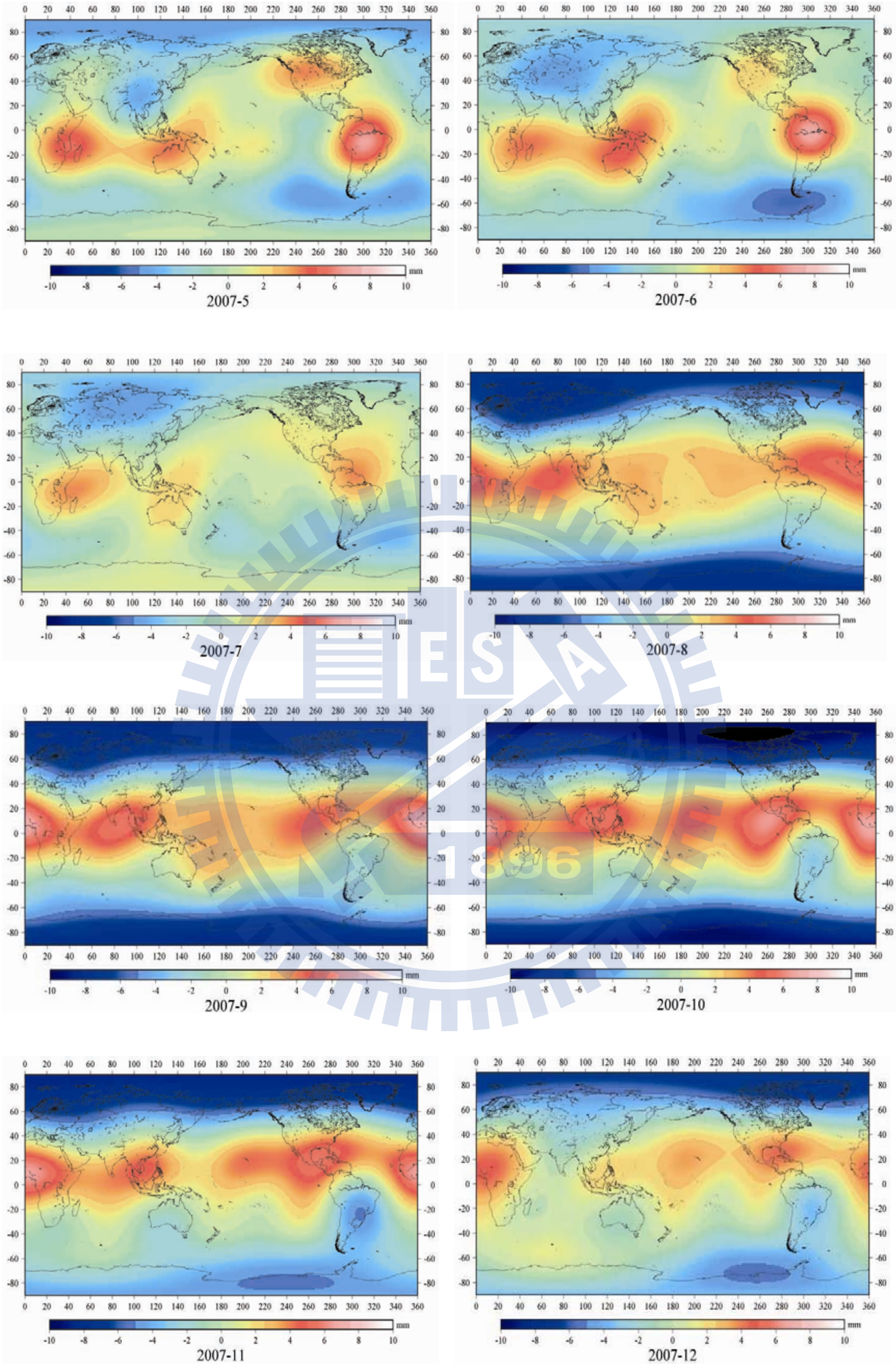

Fig 6-2: Maps of geoid variations up to degree 5 of CSR RL04 solutions from September 2006 to December 2007

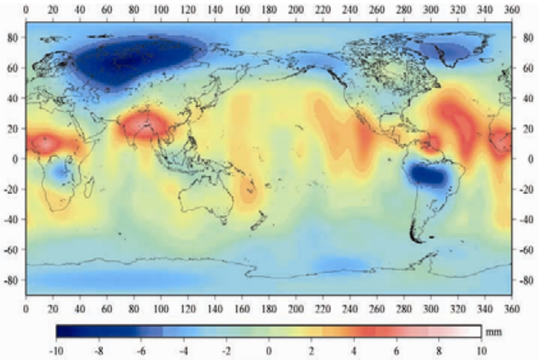

2006-9

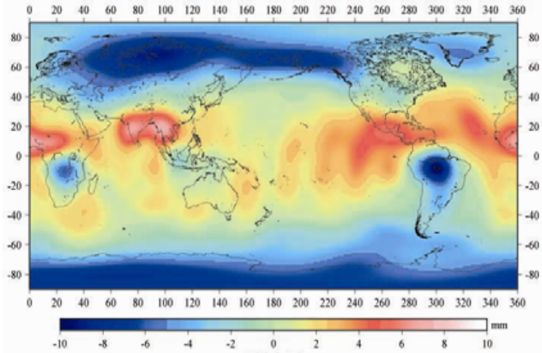

2006-10

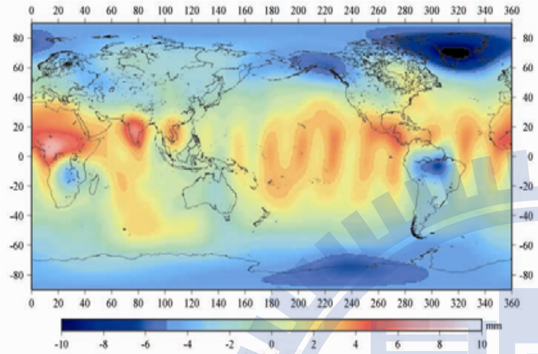

2006-11

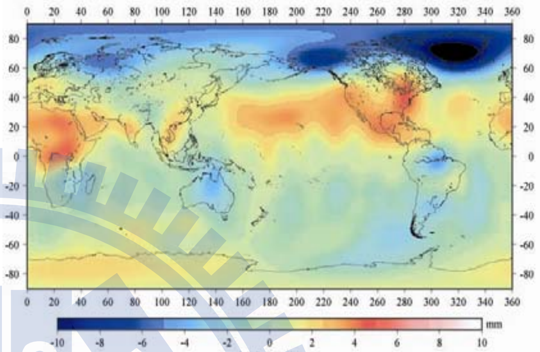

2006-12

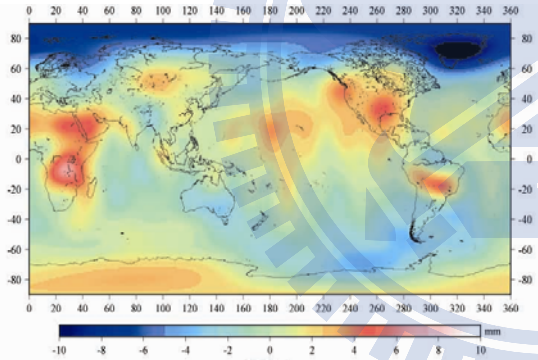

2007-1

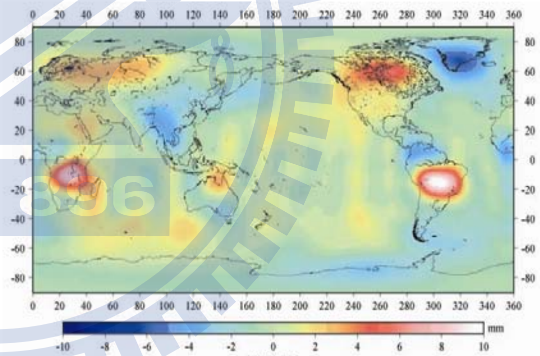

2007-2

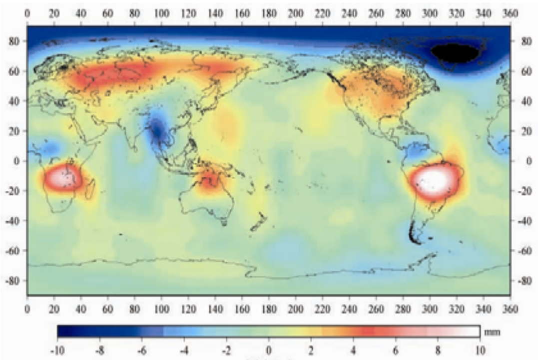

2007-3

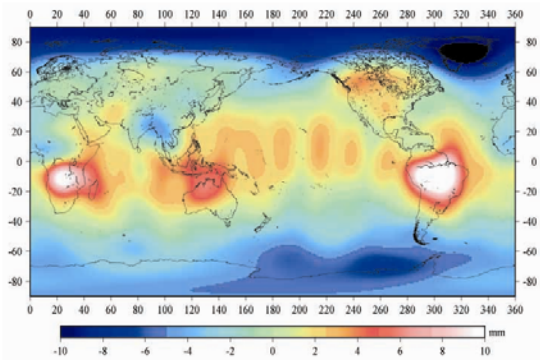

2007-4

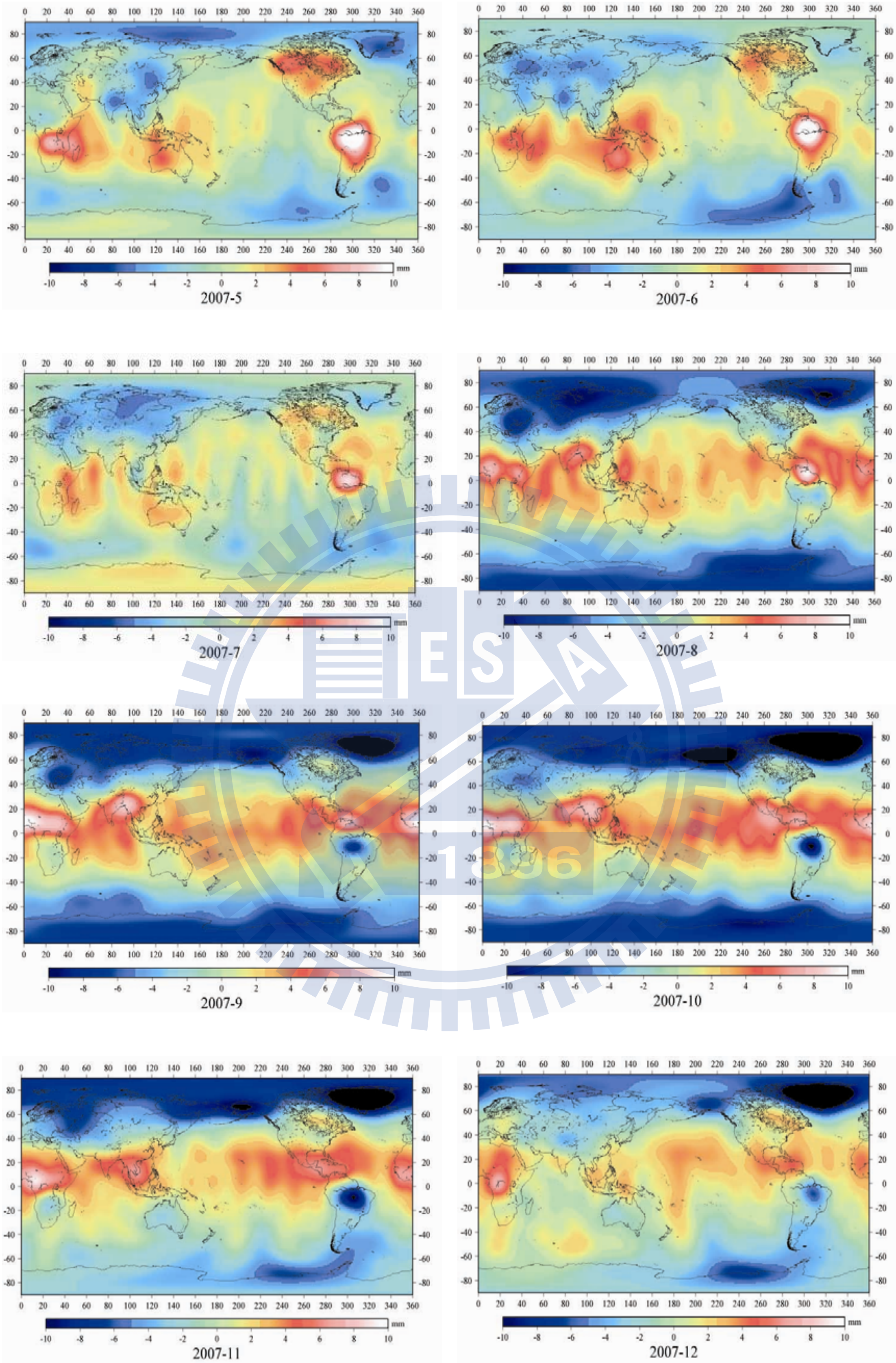

Fig 6-3: Maps of geoid variations up to degree 15 of CSR RL04 solutions from September 2006 to December 2007

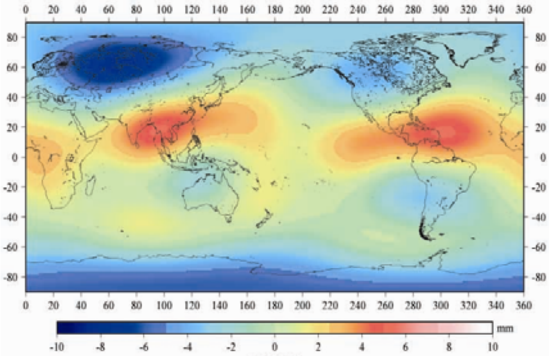
2006-9

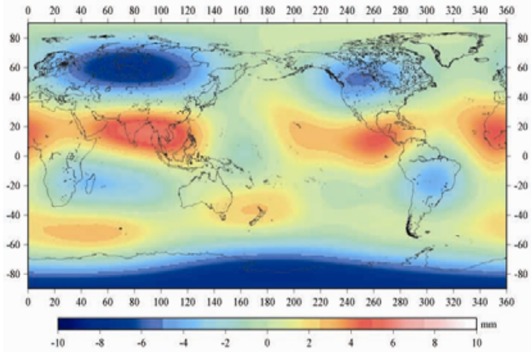
2006-10

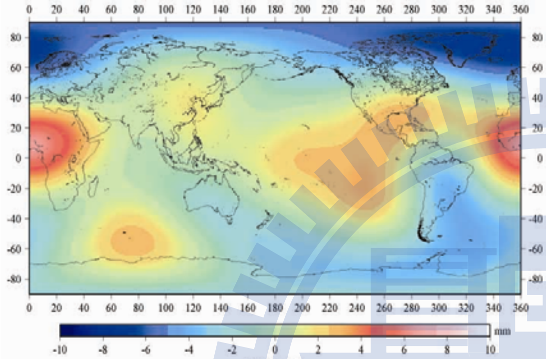
2006-11

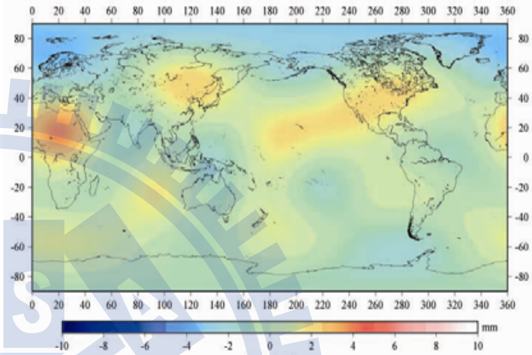
2006-12

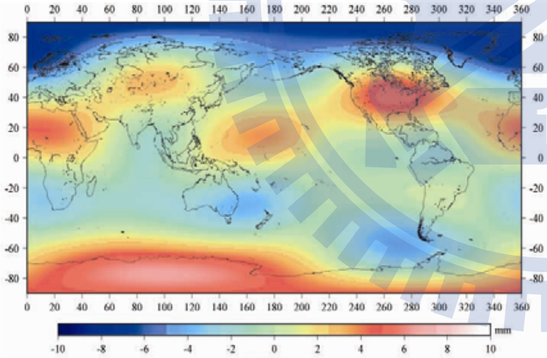
2007-1

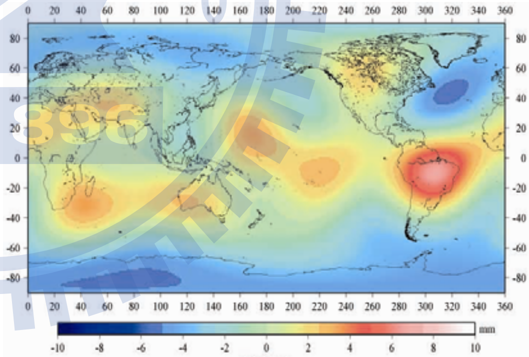
2007-2

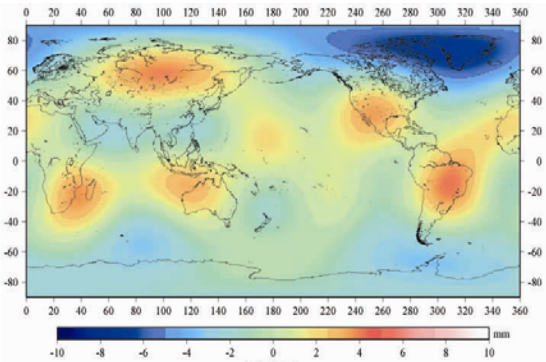
2007-3

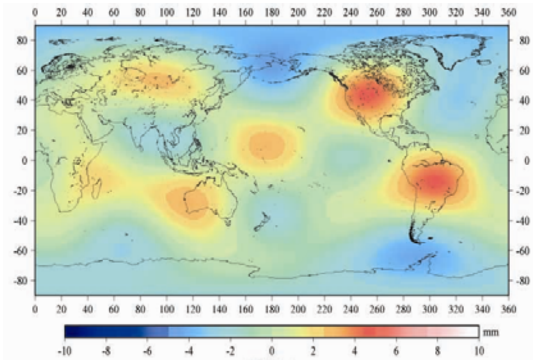
2007-4

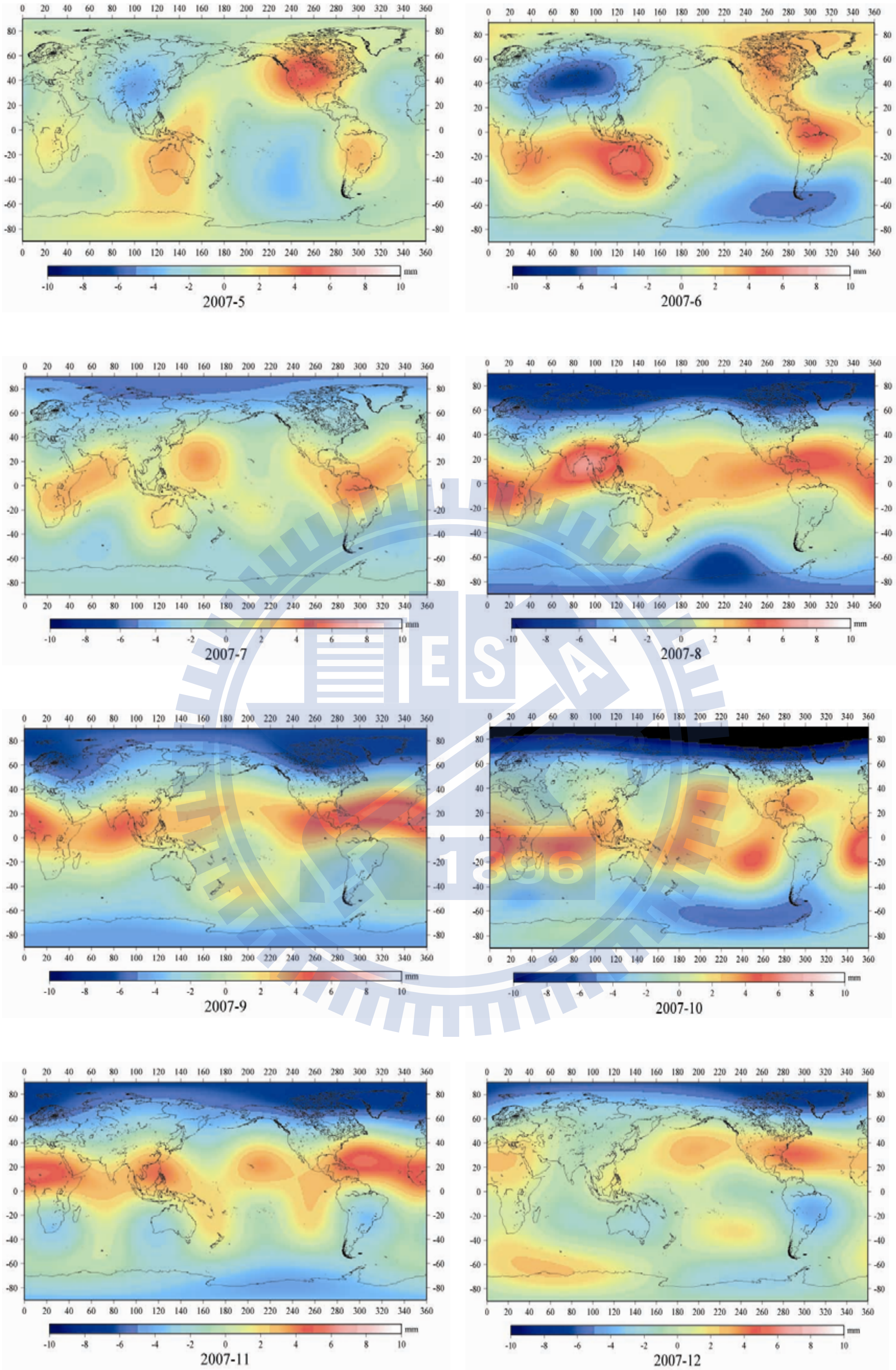

Fig 6-4: Maps of geoid variations up to degree 5 of NCTU AOP solutions from September 2006 to December 2007

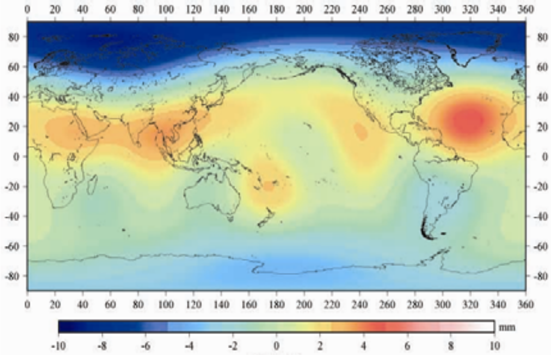
2006-9

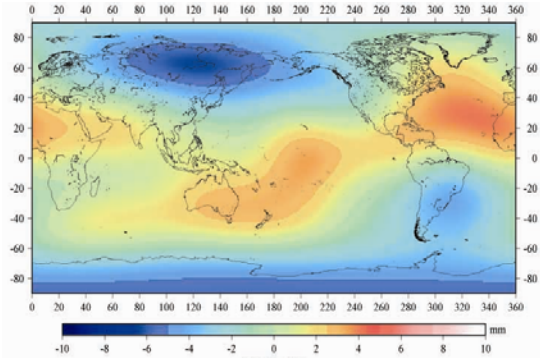
2006-10

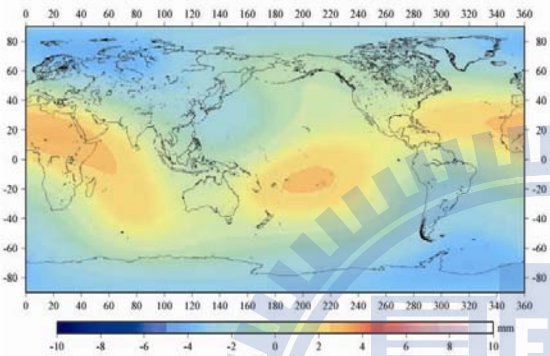
2006-11

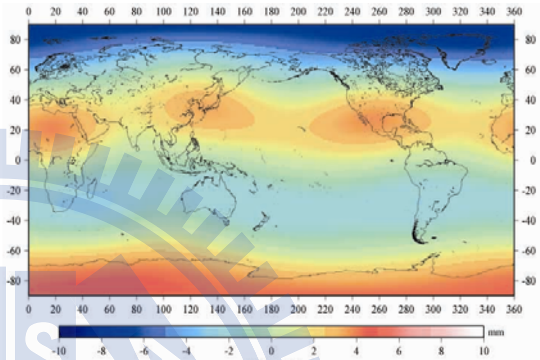
2006-12

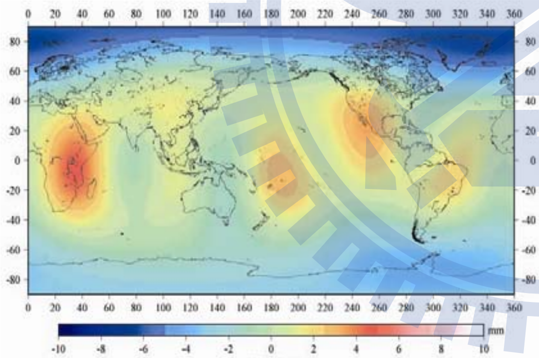
2007-1

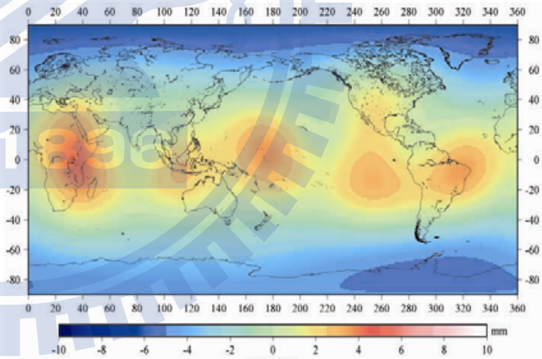
2007-2

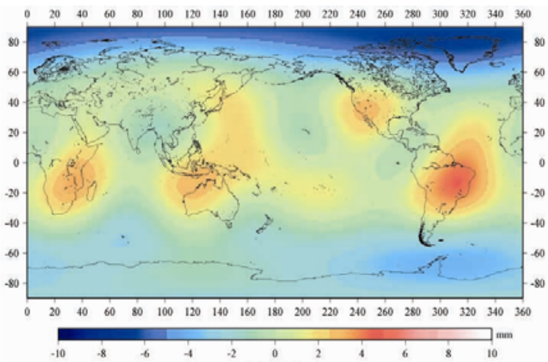
2007-3

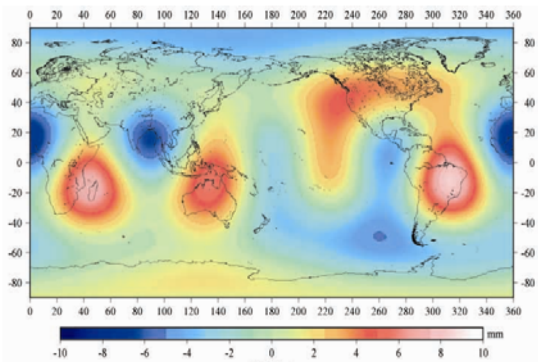
2007-4

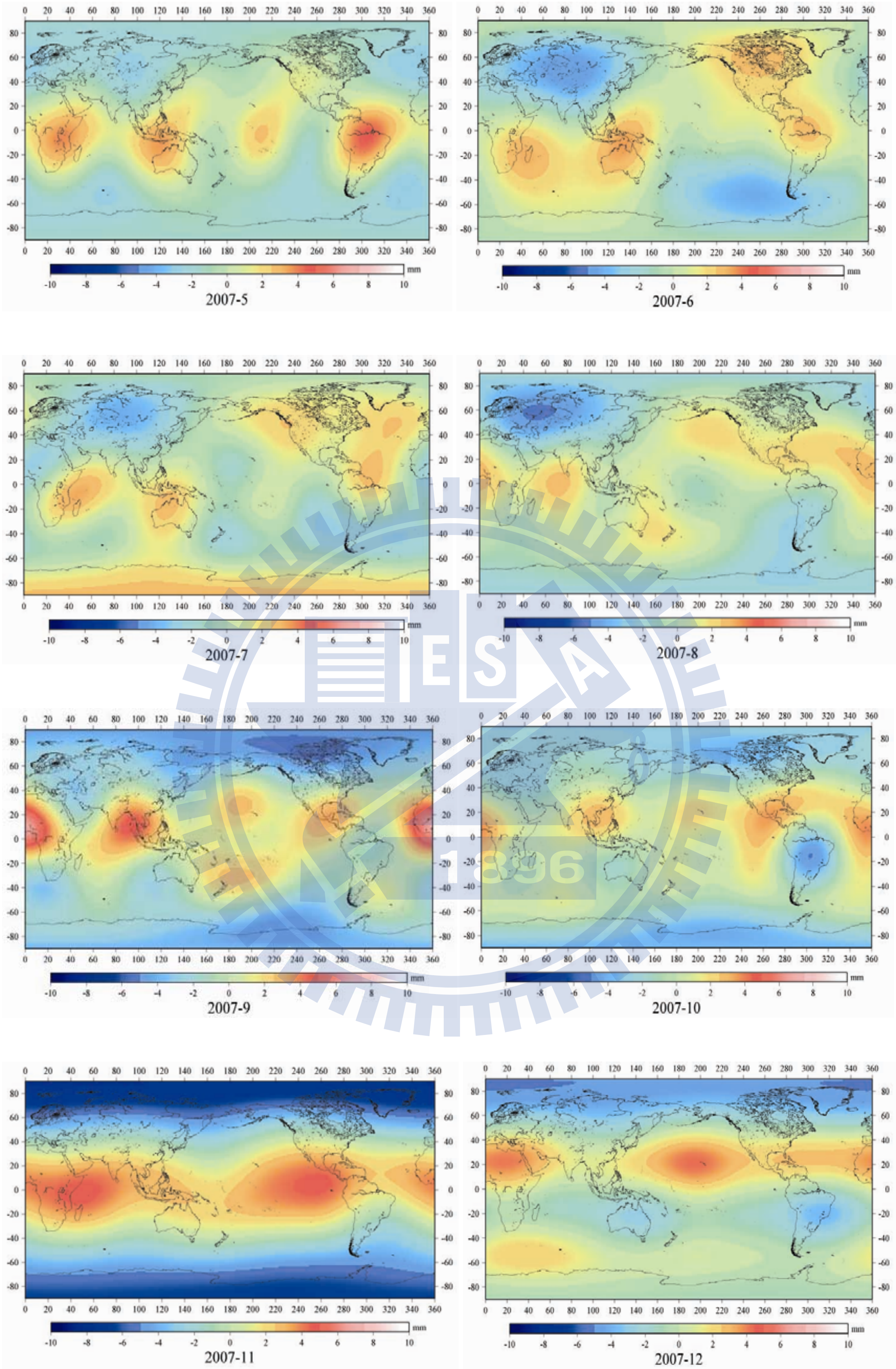

Fig 6-5: Maps of geoid variations up to degree 5 of NCTU ACC solutions from September 2006 to December 2007

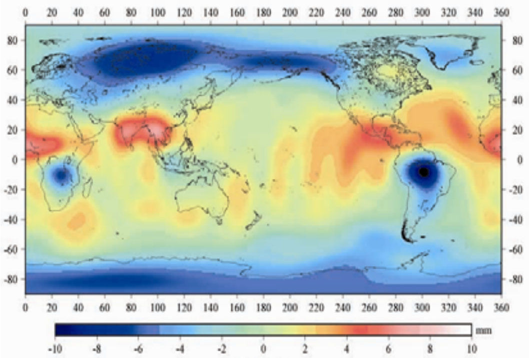

2006-9

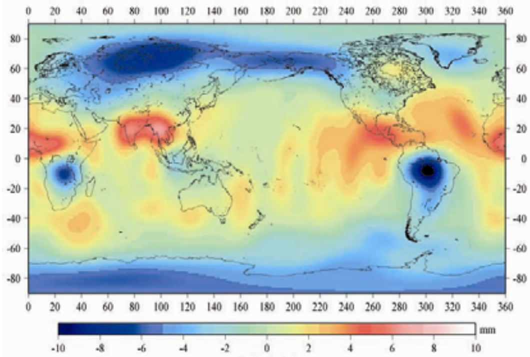

2006-10

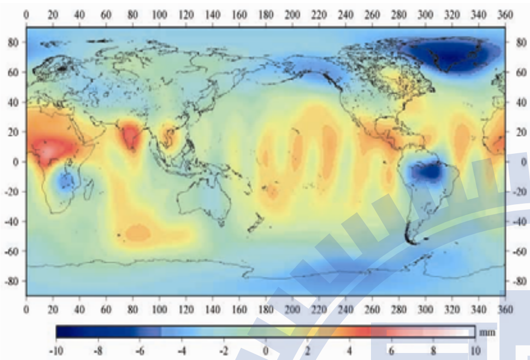

2006-11

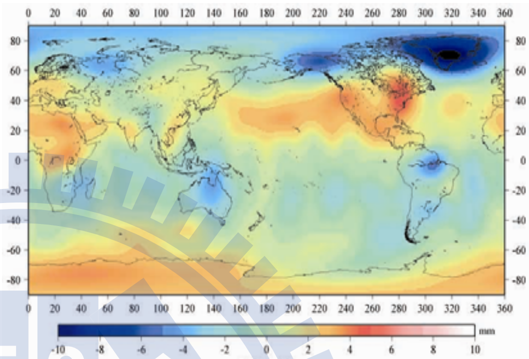

2006-12

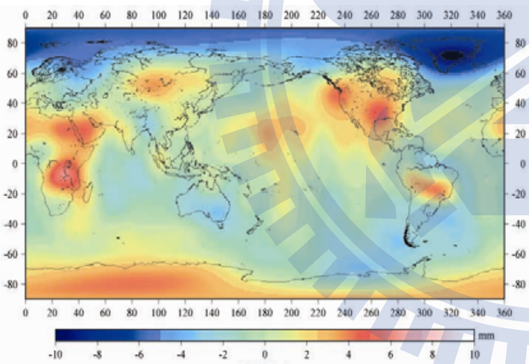

2007-1

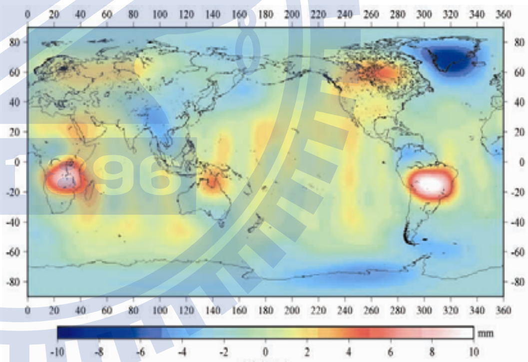

2007-2

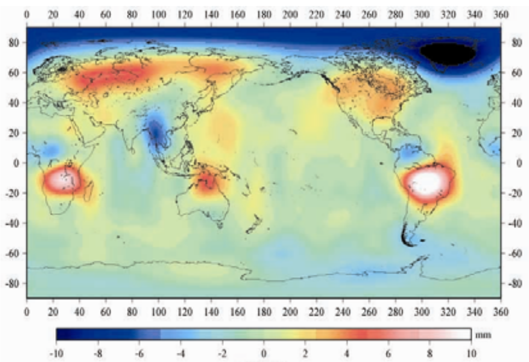

2007-3

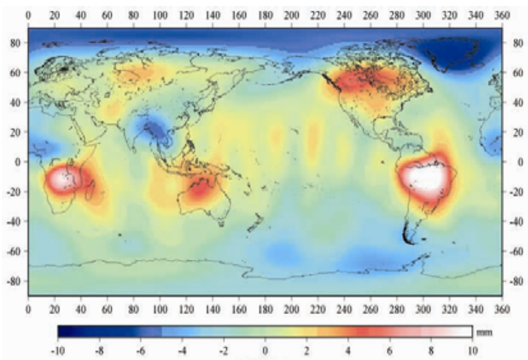

2007-4

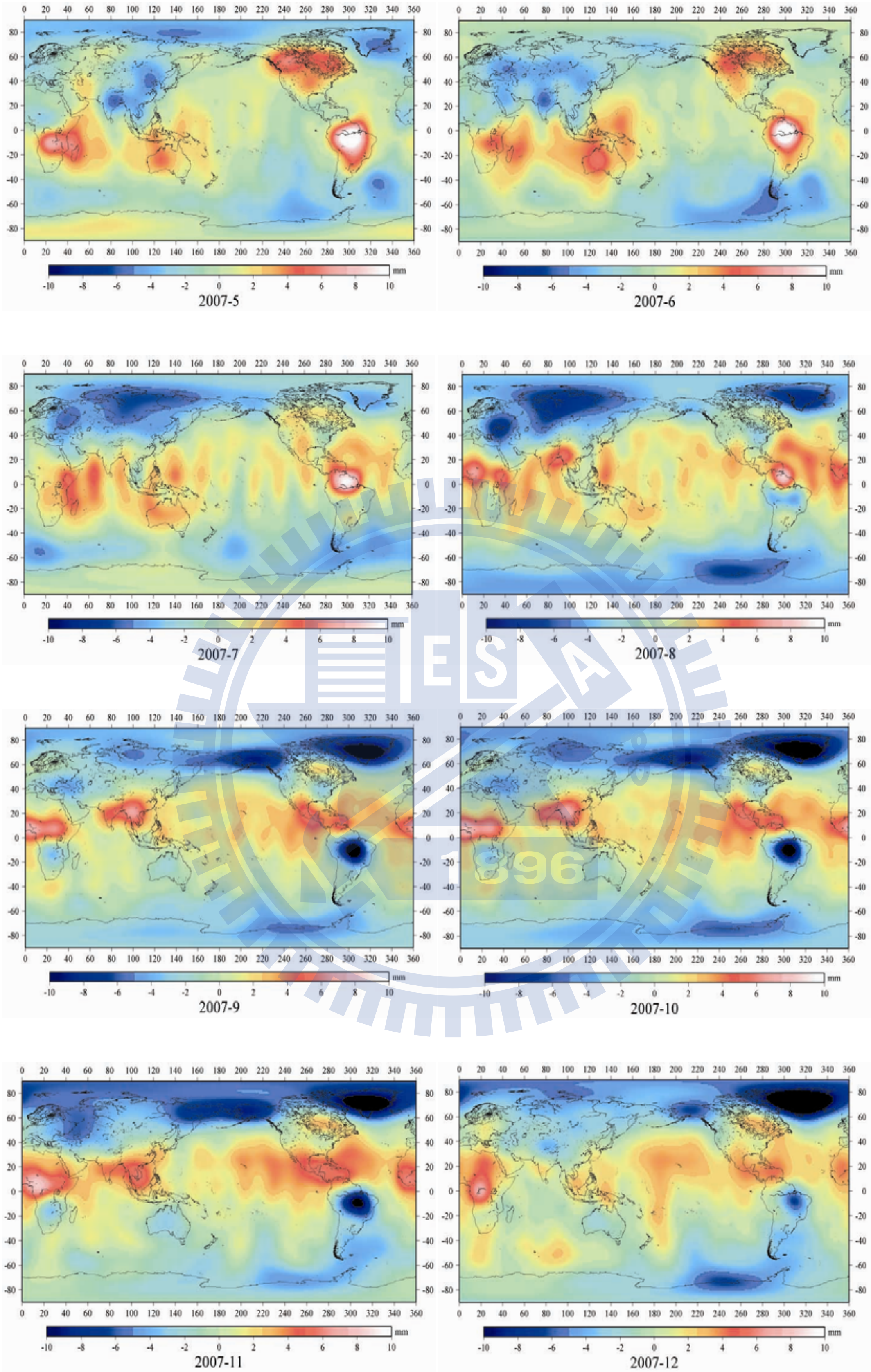

Fig 6-6: Maps of geoid variations up to degree 15 of combined NCTU AOP solutions from September 2006 to December 2007

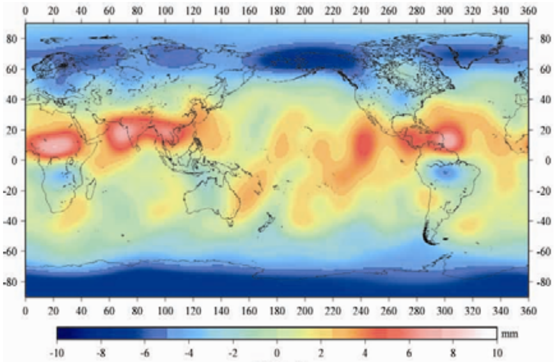

2006-9

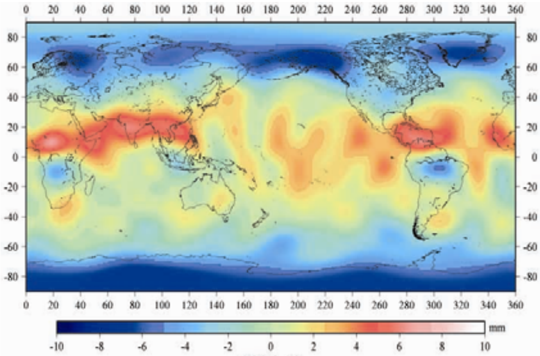

2006-10

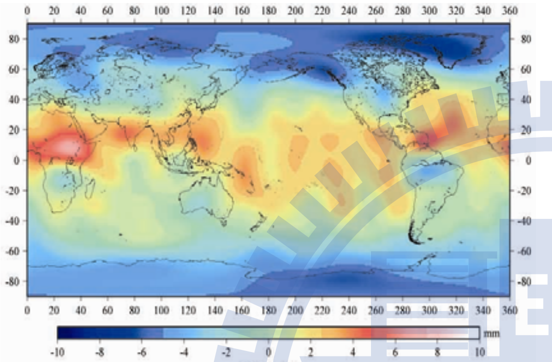

2006-11

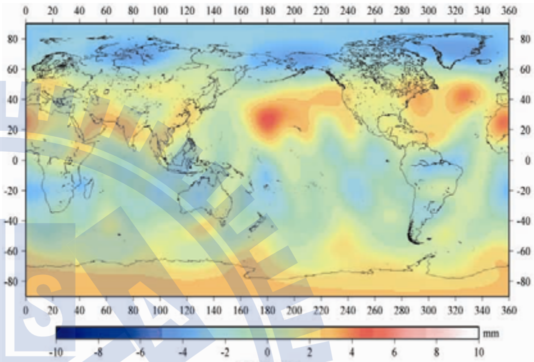

2006-12

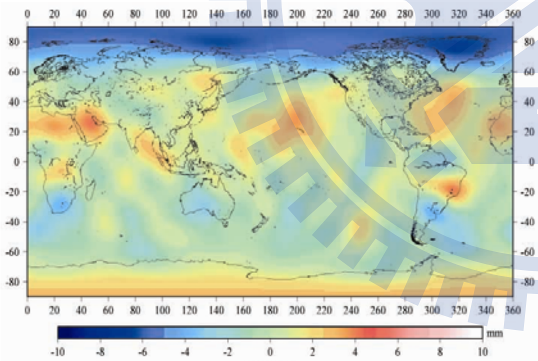

2007-1

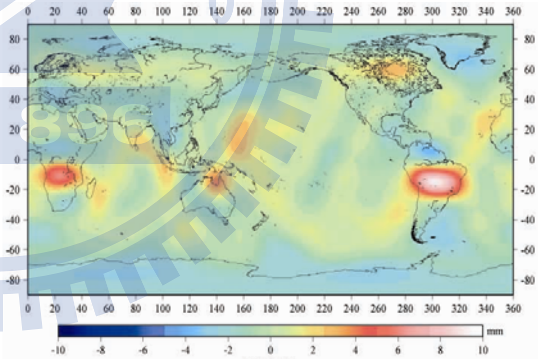

2007-2

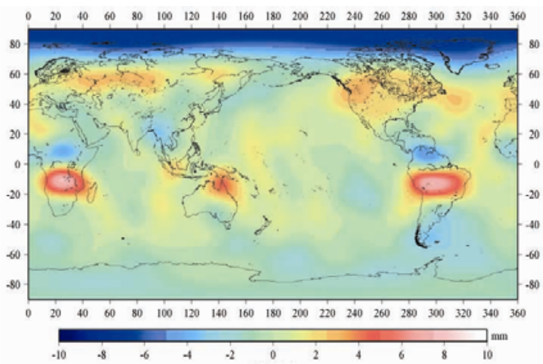

2007-3

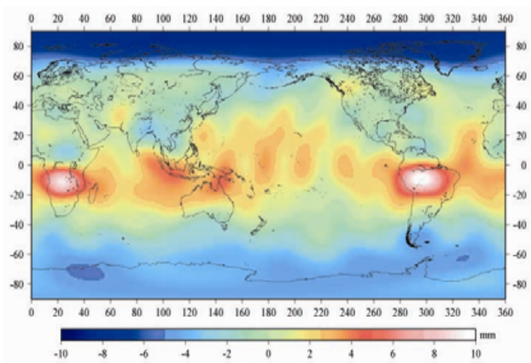

2007-4

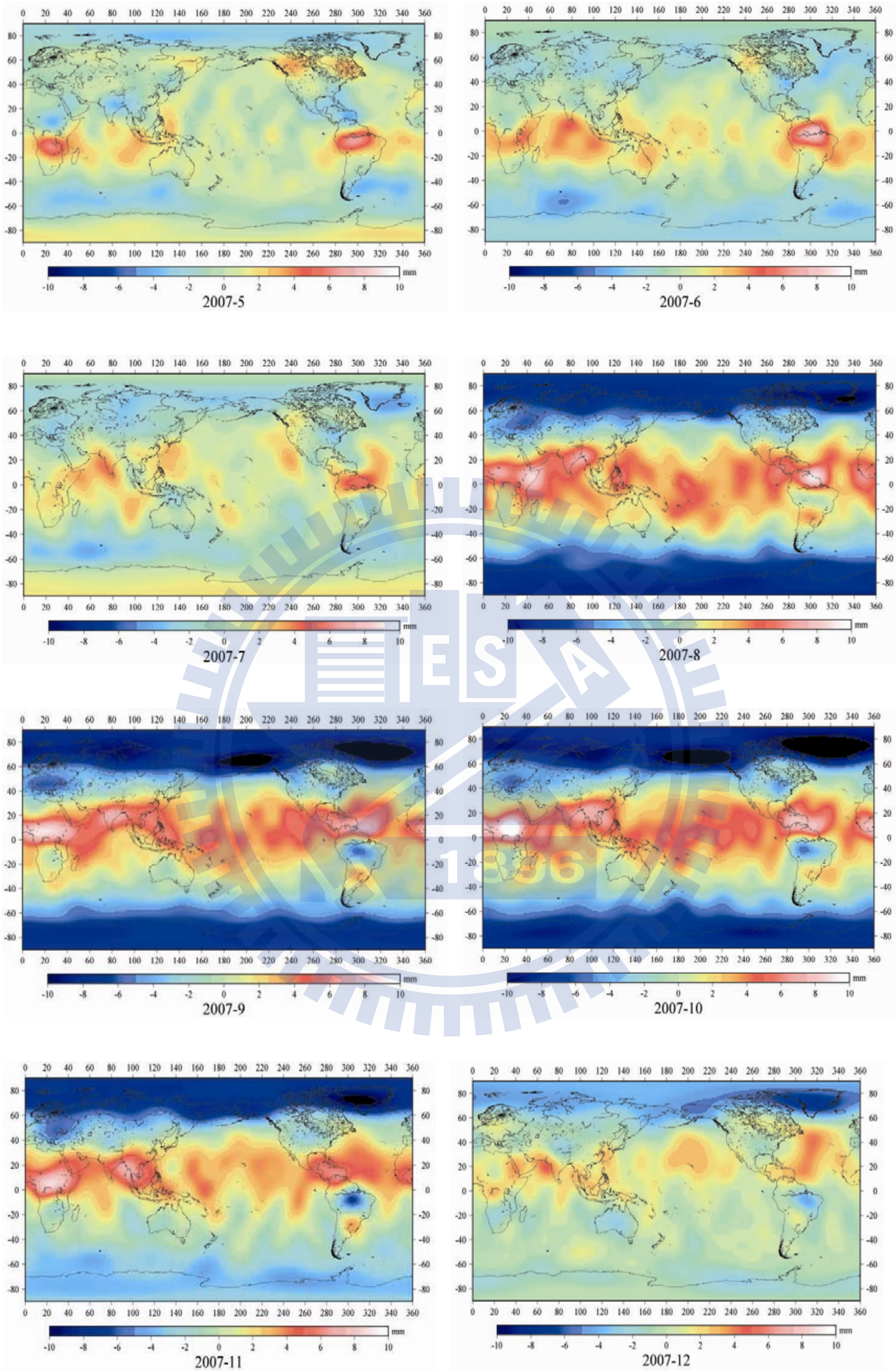

Fig 6-7: Maps of geoid variations up to degree 15 of combined NCTU ACC solutions from September 2006 to December 2007

6.4 Low-degree zonal coefficients

The studies for long term time series of low degree geopotential coefficients become an important issue for application of satellite geodesy. The conventional J_n and the fully normalized zonal coefficient $\overline{C}_{n0}$ are related by

$$J_n = -C_{n0} = -\sqrt{2n+1}\overline{C}_{n0} \tag{6-1}$$

The second coefficient J_2 is called Earth's mean tide-free dynamic oblateness (Cox and Chao 2002):

$$J_2 \equiv \left[C-(A+B)/2\right]/MR^2 = -C_{20} = -\sqrt{5}\overline{C}_{20} \tag{6-2}$$

where A, B, C present the Earth's mean principle moments of inertia, M is the mean mass of Earth and R is the mean radius of Earth.

From the variation of the coefficient J_2 one can study atmospheric mass variation, oceanic mass redistribution and ground water-level change, which are vital to the understanding of global change. By observing the LEO orbital node acceleration using SLR, one can determine precise variation of the coefficient J_2 (Cheng and Tapley 1999; Cox and Chao 2002). The rate estimate of J_2 from SLR data is decreasing from 1979 to 1998, and then increasing since 1998 until around 2005 and decreasing after 2005 due to the significant inter-annual variation (Cheng and Tapley 2008). The long term variations of zonal terms J_2 and J_3 can be used to explain mantle compositions and post-glacial rebound. The long and short period variations of J_2 and J_3 are related to solid Earth, oceanic and atmospheric tidal or non-tidal change, and seasonal mass change of hydrology. The time variations of even zonal coefficients

$\dot{J}_n(n=2,4,6,...)$ are sensitive to the mantle composition and the variations of odd terms $\dot{J}_n(n=3,5,7,...)$ are sensitive to the glacial mass balance (Ivins et al. 1993). Cheng et al. (1997) have used 8 SLR satellite observations, including those from Starlette, Lageos 1 and 2, Ajisai, Etalon 1 and 2, Stella and BE-C, to analyze low-degree zonal coefficients to obtain $\dot{J}_2=(-2.7\pm0.4)\times10^{-11}/\mathrm{yr}$, $\dot{J}_3=(-1.3\pm0.5)\times10^{-11}/\mathrm{yr}$, $\dot{J}_4=(-1.4\pm1.0)\times10^{-11}/\mathrm{yr}$, $\dot{J}_5=(2.1\pm0.6)\times10^{-11}/\mathrm{yr}$, and $\dot{J}_6=(0.3\pm0.7)\times10^{-11}/\mathrm{yr}$.

The second zonal coefficient C_{20} is rather difficult to estimate from GRACE data, particularly due to the polar orbit design and the presence of several long-tidal aliases (Ries et al. 2008). The combination of satellite data of different inclinations such as COSMIC-GRACE will not only effectively improve the accuracy of zonal geopotential coefficients but also the tesseral terms (Zheng et al. 2008). In Section 6.2, we choose the GGM03S model as a reference Earth's gravity field model so the reference C_{20} is also chosen from the same model. Fig. 6-8 shows the time series of C_{20} change from CSR RL04 and SLR solutions from September 2006 to December 2007. The file containing monthly estimates of C_{20}, reference C_{20} (the value is -0.48416948×10^{-3}) and the error estimates of C_{20} by 5 SLR satellites (LAGEOS-1 and 2, Starlette, Stella and Ajisai) can be available at the JPL ftp site (ftp://podaac.jpl.nasa.gov/grace/doc/ TN-05_C20_SLR.txt) (Cheng et al. 2004). The background gravity model used in the SLR analysis is consistent with the CSR RL04 processing. Large differences of $\Delta\overline{C}_{20}$ occurred in April, September and October of 2007. Time series of $\Delta\overline{C}_{20}$ change from the ACC, AOP, CSR RL04 and SLR solutions from September 2006 to December 2007 are given in Fig 6-9. The rates of

$\Delta\overline{C}_{20}$ from SLR, AOP, ACC, and CSR RL04 are $(-0.94\pm0.45)\times10^{-10}$, $(-1.06\pm0.86)\times10^{-10}$, $(0.15\pm0.78)\times10^{-11}$ and $(-1.98\pm0.86)\times10^{-10}$, respectively. These results suggest that the AOP solution and the SLR solution provide a more similar magnitude of variation with a smaller phase difference than CSR RL04 and ACC solutions. For the $\Delta\overline{C}_{30}$ and $\Delta\overline{C}_{40}$ changes, the three solutions (CSR RL04, AOP and ACC) have almost the same phase and similar magnitude of variation (see Fig. 6-10 and 6-11). The rates of $\Delta\overline{C}_{30}$ from CSR RL04, AOP and ACC solutions are $(-1.58\pm6.07)\times10^{-11}$, $(-5.13\pm7.09)\times10^{-11}$, and $(-7.07\pm8.14)\times10^{-11}$, and the rates of $\Delta\overline{C}_{40}$ are $(3.46\pm3.06)\times10^{-11}$, $(-0.20\pm2.91)\times10^{-11}$, and $(2.33\pm3.01)\times10^{-11}$, respectively.

In conclusion, the NCTU AOP and ACC solutions produce improved low-degree zonal coefficients because they use satellite data of different inclinations.

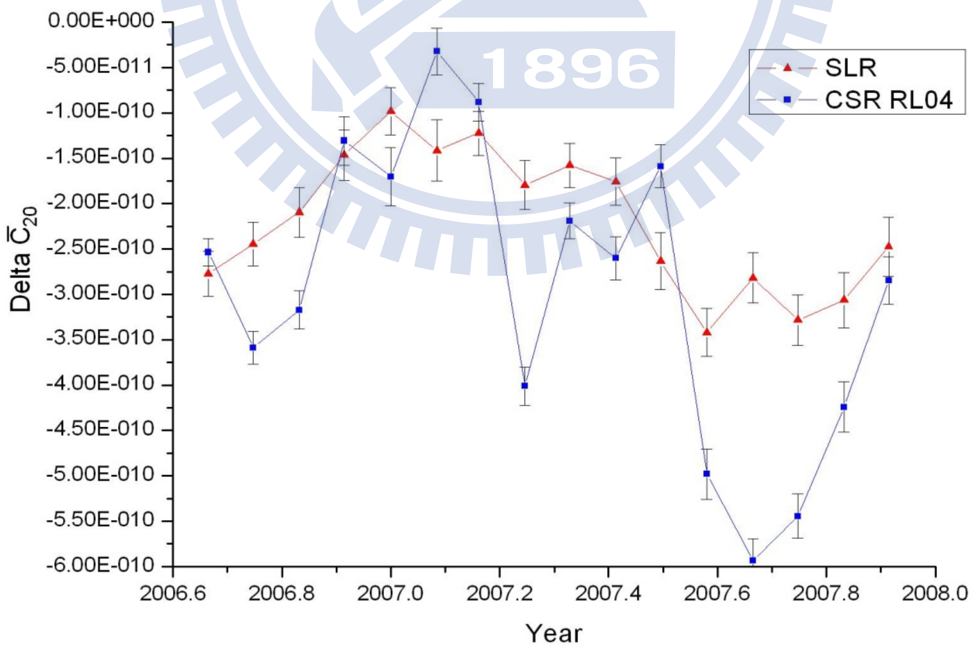

Fig 6-8: Time series of $\Delta\overline{C}_{20}$ from CSR RL04 and SLR solutions from September 2006 to December 2007

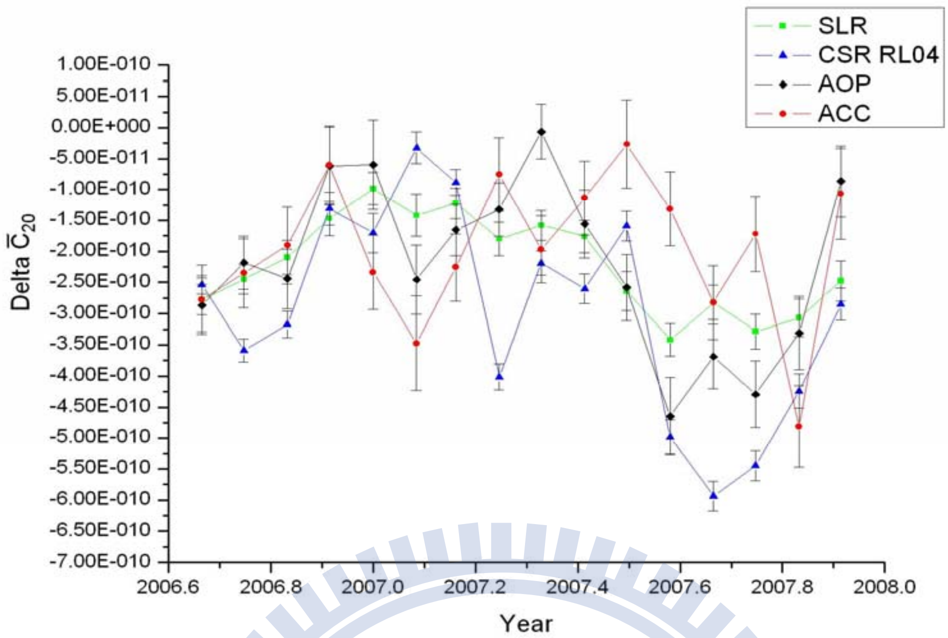

Fig 6-9: Time series of $\Delta\overline{C}_{20}$ from SLR, CSR RL04, NCTU AOP and NCTU ACC solutions from September 2006 to December 2007

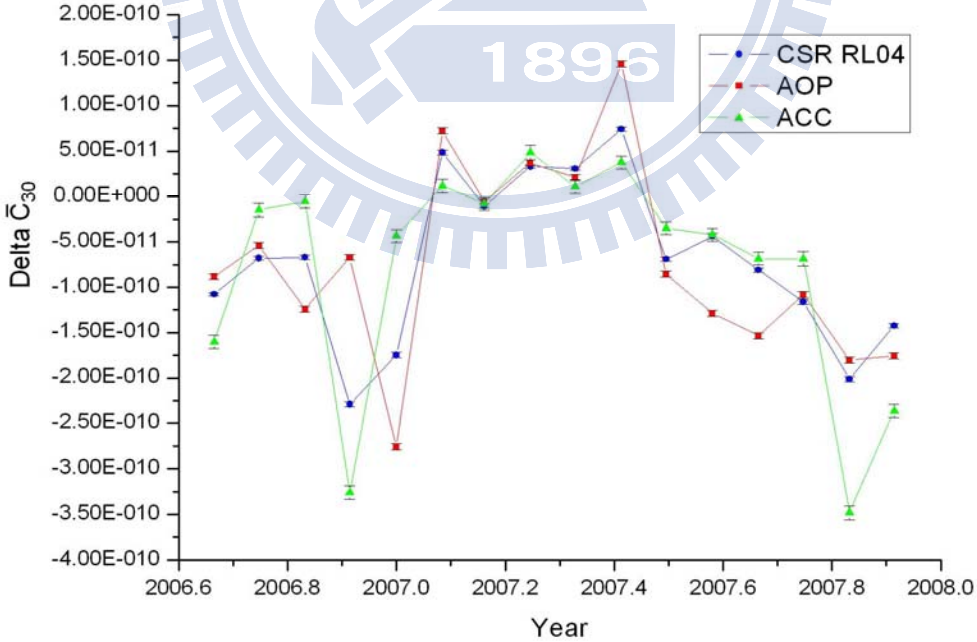

Fig 6-10: Time series of delta $\Delta\overline{C}_{30}$ from CSR RL04, NCTU AOP, and NCTU ACC solutions from September 2006 to December 2007

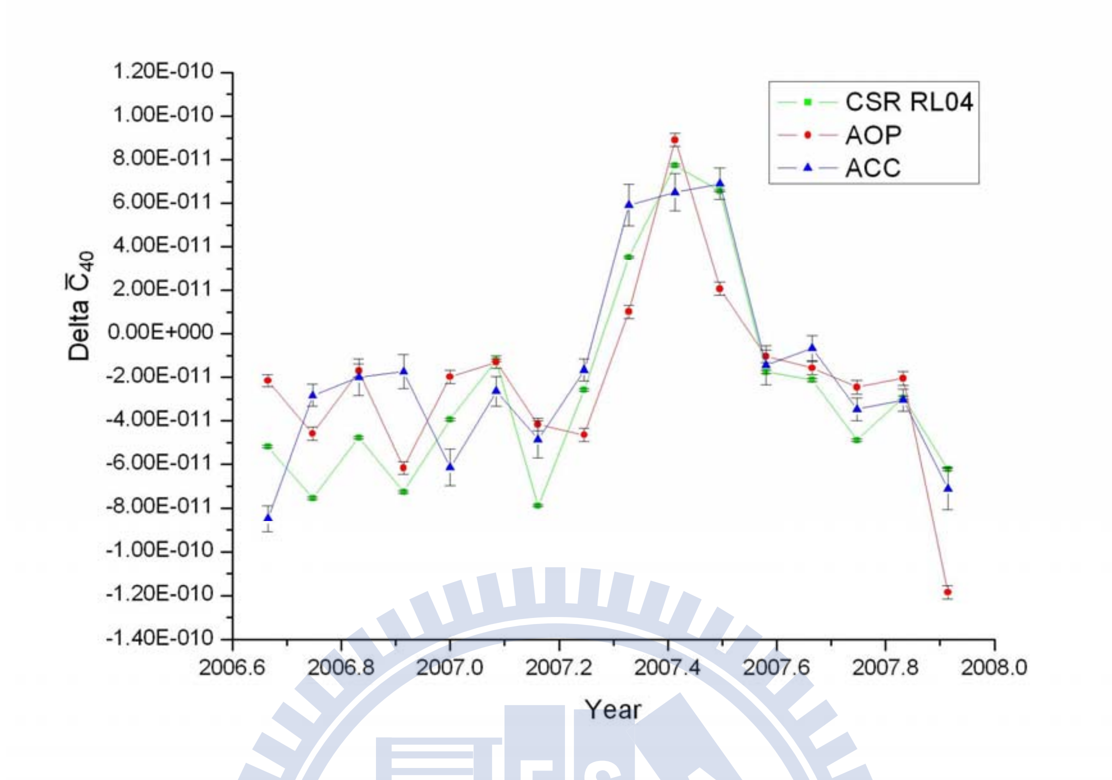

Fig 6-11: Time series of delta $\Delta\overline{C}_{40}$ from CSR RL04, NCTU AOP, and NCTU ACC solutions from September 2006 to December 2007

Chapter 7

Summary, Conclusions, and Recommendations

7.1 Summary and Conclusions

The primary contribution of this research is to use the combination of satellite hl-SST data of different inclinations to recover the temporal gravity fields, particularly the low-degree ones. This research is divided into four major parts. In the first part, we refined the COSMIC and the GRACE hl-SST data processing methodology for kinematic and dynamic POD (chapter 2). Secondly, we further developed the analytical orbital perturbation approach to process the COSMIC and the GRACE positional data to recover the temporal gravity field (chapter 4). Thirdly, the acceleration data derived from the COSMIC and the GRACE positional data are applied to the temporal gravity recovery procedure using the residual acceleration approach (chapter 5). Finally, we conducted an analysis of the time series of low-degree geopotential coefficients using the COSMIC and the GRACE hl-SST data, and validated such results by the CSR RL04 and SLR solutions.

The main results are summarized as follows.

(1) Precise kinematic and dynamic orbits of the COSMIC and the GRACE satellites are computed, with accuracies at the cm level.

(2) Detailed and precise force modeling for COSMIC LEOs is achieved.

(3) Time-varying gravity changes are estimated with a sufficient confidence from COSMIC only and combined COSMIC and GRACE GPS tracking data, based on the analytical orbit perturbation theory.

(4) An alternative method of gravity recovery based on satellite accelerations is developed. The result is as good as the result from the analytical orbit perturbation theory. In the case of combined COSMIC and GRACE GPS data, both methods

produce changes in geopotential coefficients with smaller error degree variances and more evident gravity change signatures than the ones given by the GRACE-only solutions.

(5) Time series of second, third and fourth zonal geopotential coefficients are determined from COSMIC and GRACE GPS data and they are consistent with the SLR results. The rates of $\Delta\overline{C}_{20}$ from SLR, AOP, ACC, and CSR RL04 are $(-0.94\pm045)\times10^{-10}$, $(-1.06\pm0.86)\times10^{-10}$, $(0.15\pm0.78)\times10^{-11}$ and $(-1.98\pm0.86)\times10^{-10}$, respectively. The rates of $\Delta\overline{C}_{30}$ from CSR RL04, AOP and ACC solutions are $(-1.58\pm6.07)\times10^{-11}$, $(-5.13\pm7.09)\times10^{-11}$, and $(-7.07\pm8.14)\times10^{-11}$, and the rates of $\Delta\overline{C}_{40}$ are $(3.46\pm3.06)\times10^{-11}$, $(-0.20\pm2.91)\times10^{-11}$, and $(2.33\pm3.01)\times10^{-11}$, respectively.

7.2 Recommendations for future work

To further improve accuracies in orbit determination and gravity recovery, there are several topics that need to be investigated in future works.

(1) Improving COSMIC kinematic orbits

This can be achieved by (1) using ambiguity fixing, (2) combing GPS data from the two POD antennas (3) using improved attitude data (collaborating with NSPO) and (4) using improved PCV estimates (Hwang et al. 2009).

(2) Improving the COSMIC and the GRACE dynamic orbits

Compared to the method used in this study, an improved method is to use the double-differenced GPS carrier-phase observations with sufficient numbers of ground stations. But this will require a higher computational capacity.

(3) Improving the accuracy of acceleration derivation

In this study, we use the numerical differential method to derive the acceleration from positional data. There are at least two different variants of acceleration approaches such as the point-wise acceleration method and average acceleration method. These methods to derive observed acceleration should be investigated.

(4) Accuracy assessment of the COSMIC and combined solutions

More quantitative assessments of accuracy and spatial resolution of the COSMIC and combined gravity solutions are yet to carry out, for example, using terrestrial based gravity measurements at locations with major gravity changes.

Reference

Balmino G, Barriot JB (1989) Numerical integration techniques revised, Manuscripta geodaetica, 15, 1-10.

Balmino G, Schrama E, Sneeuw N (1994) Compatibility of first-order circular orbit perturbations theories; consequences for cross-track inclination functions, J Geod, 70, 554-561.

Bertiger W, Bar-Sever Y, Christensen E, Davis E, Guinn J, Haines B, Ibanez-Meier R, Lee J, Lichten S, Melbourne W, Muellerschoen R, Munson T, Vigue Y, Wu S,Yunck T, Schutz B, Abusali P, Rim H, Watkins M, Willis P (1994) GPS precise tracking of TOPEX/Poseidon: Results and implications, J Geophys Res, 99(C12), 24449-24464.

Bettadpur S (2007) UTCSR level-2 processing standards document for Level-2 product release 0004, Center for Space Research, Univ of Texas, Austin, USA.

Beutler G, Rothacher M, Schaer S, Springer TA, Kouba J, Neilan RE (1999) The international GPS service (IGS): an interdisciplinary service in support of Earth sciences. Adv Space Res, 23, 631–635.

Bock H (2003) Efficient methods for determining precise orbits of low Earth orbiter using the global positioning system, Ph. D dissertation, Astronomical Institute, Univ of Berne, Berne, Switzerland.

Byun S, Schutz BE (2001) Improving satellite orbit solution using double-differenced GPS carrier phase in kinematic mode, J Geod, 75, 533-543.

Case K, Kruizinga GLH, Wu SC (2004) GRACE level 1B data product user handbook, JPLD-22027, http://podaac.jpl.nasa.gov/grace/documentation.html.

Chang LH (2003) Force modeling for ROCSAT-3 satellite orbits, master thesis, Dept. of Civil Engineering, National Chao Tung Univ , Hsinchu, Taiwan, ROC.

Chao BF, Pavlis E, Hwang C, Liu CC, Shum CK, Tseng CL, Yang M (2000) COSMIC: geodetic applications in improving Earth's gravity model, Terr Atm Ocean Sci (TAO), 11, 365-378.

Cheng M, Tapley B (1999) Seasonal variations in low-degree zonal harmonics of the Earth’s gravity field from satellite laser ranging observations, J Geophys Res, 104, 2667-2681.

Cheng M, Tapley BD (2004) Variations in the Earth's oblateness during the past 28 years, J Geophys Res, 109, B09402.

Cheng M, Tapley BD (2008) Recent variations in J2 from SLR and GRACE, GRACE science team meeting, San Francisco, CA, USA.

Colombo O (1984) Altimetry, orbits and tides, NASA TM 86180, Greenbelt, Maryland, USA.

Cox C, Chao BF (2002) Detection of a large-scale mass redistribution in the terrestrial system since 1998, Science, 297 (5582), 831-833.

Dach R, Hugentobler U, Fridez P, Meindl M (2007) Bernese GPS Software - Version 5.0. Astronomical Institute, Univ of Bern, Switzerland.

Ditmar P, Kuznetsov V, van der Sluijs AAV, Schrama E, Klees R (2006) DEOS_CHAMP-01C_70: a model of the Earth's gravity field computed from accelerations of the CHAMP satellite. J Geod, 79, 586-601.

Dunn C, Bertiger W, Bar-Sever Y, Desai S, Haines B, Kuang D, Franklin G, Harris I, Kruizinga G, Meehan T, Nandi S, Nguyen D, Rogstad T, Thomas JB, Tien J, Romans L, Watkins M, Wu SC, Bettadpur S, Kim JR (2003) Instrument of GRACE: GPS augments gravity measurements, GPS World, 14, 16–28.

Engelis T (1987) Radial orbit error reduction and sea surface topography determination using satellite altimetry, Dept. of Geodetic Science and Surveying, Rep. No. 377, Ohio State Univ, Columbus, Ohio, USA.

European Space Agency (1999) Gravity field and steady-state ocean circulation missions, Reports for mission selection, the four candidate Earth explorer core missions, SP-1233(1), European Space Agency, Noordwijk, Netherland.

Förste C, Flechtner F, Schmidt R, König R, Meyer U, Stubenvoll R, Rothacher M, Barthelmes F, Neumayer H, Biancale R, Bruinsma S, Lemoine J, Loyer S (2006) A mean global gravity field model from the combination of satellite mission and altimetry/gravimetry surface data – EIGEN-GL04C. Poster presented at EGU, General Assembly 2006, Vienna, Austria.

Gerald C, Wheatley P (2003) Applied numerical analysis 7th ed., Addison Wesley Longman Inc.

GFZ homepage. http://www-app2.gfz-potsdam.de/pb1/op/grace/index_GRACE.html.

GSFC (1989) Mathematical Theory of the Goddard Trajectory Determination System, Goddard Space Flight Center, Greenbelt, Maryland, USA.

Hedin A (1991) Extension of the MSIS thermosphere model into the middle and lower atmosphere, J Geophys Res, 96, 4649-4662.

Heiskanen W A, Moritz H (1985) Physical Geodesy, reprint, Inst. of Physical Geodesy, TU Graz, Austria.

Hwang C (1995) Orthonormal function approach for Geosat determination of sea surface topography, Mar Geod, 18, 245-271.

Hwang C, Lin MJ (1998) Fast integration of low orbiter's trajectory perturbed by Earth's nonsphericity, J Geod, 72, 578-585.

Hwang C (2001) Gravity recovery using COSMIC GPS data: application of orbital perturbation theory, J Geod, 75, 117-136.

Hwang C, Hwang LS (2002) Satellite orbit error due to geopotential model error using perturbation theory: applications to ROCSAT-2 and COSMIC mission, Comput Geosci, 28, 357-367.

Hwang C, Lin TJ, Tseng TP, Chao BF (2008) Modeling orbit dynamics of FORMOSAT-3/COSMIC satellites for recovery of temporal gravity, IEEE Transactions on Geoscience and Remote Sensing (TGRS), 46(11), 3412-3423.

Hwang C, Tseng TP, Lin TJ, Švehla D, Schreiner B (2009) Precise orbit determination for FORMOSAT-3/COSMIC, J Geod, 83, 477-489.

Hwang LS (2002) Precision orbit determination and gravity models from tracking data of Low-Earth-Orbiting (LEO) satellites, Ph. D dissertation, Dept of Civil Engineering, National Chao Tung Univ, Hsinchu, ROC.

Ivins R, Sammis C, Yoder C (1993) Deep mantle viscous structure with prior estimate and satellite constraint, J Geophys Res, 98, 4579-4609.

Jäggi A, Hugentobler U, Beutler G (2006) Pseudo-stochastic orbit modeling techniques for low-Earth orbiters. J Geod, 80, 47-60.

Jäggi A, Hugentobler U, Bock H, Beutler G (2007) Precise orbit determination for GRACE using un-differenced and doubly differenced GPS data, Adv Space Res, 39, 1612-1619.

Jekeli C (1999) The determination of gravitational potential differences from satellite-to-satellite tracking. Celes Mech Dynam Astron, 75, 85–101.

Jekeli C, Garcia R (1997) GPS phase accelerations for moving-base gravimetry. J Geod, 71, 630-639.

Kang Z, Tapley B, Bettadpur S, Ries J, Nagel P, Pastor R (2006) Precise orbit determination for the GRACE mission using only GPS data, J Geod, 80, 322–331.

Kang Z, Nagel P, Pastor R (2003) Precise orbit determination for GRACE, Adv Space Res, 31, 1875–1881.

Kaula WM (1966) Theory of satellite geodesy. Blaisdell Publishing Co, Walthamn, Massachusetts, USA.

Koch K (1987) Parameter estimation and hypothesis testing in linear model, Springer, Berlin, Germany.

Long A, Cappellari Jr. J, Velez C, Fuchs A (1989) Goddard trajectory determination system, Mathematical Theory, Revision 1, Flight Dynamics Division, National Aeronautics and Space Administration, USA.

Luthcke S, Rowlands D, Lemoine FG, Klosko SM, Chinn D, McCarthy JJ (2006) Monthly spherical harmonic gravity field solutions determined from GRACE inter-satellite range-rate data alone, Geophys Res Lett, 33, L02402.

McCarthy D (1996) IERS Standards, IERS Technical Note 21, http://www.iers.org/MainDisp.csi?pid=47-25786.

Meskó A (1984). Digital filtering: Applications in geophysical exploration for oil. Pitman Pub. Ltd., London, UK.

Montenbruck O, Gill E (2001) Satellite orbit - models, methods, and application, Springer, Berlin, Germany.

Montenbruck O, Garcia-Fernandez M, Williams J (2006) Performance comparison of semicodeless GPS receivers for LEO satellites, GPS Solut, 10, 249–261.

Nerem RS, Klosko SM (1995) Secular variations of zonal harmonics and polar motion as geophysical constraints. In Rapp RH, Cazenave AA, Nerem RS (eds) Global Gravity and Its Temporal Variations. IAG Symp 116, Boulder.

Pavlis D et al. (1996) GEODYN operational manual, 5 volumes, Hughes/STX Corp., Greenbelt, Maryland, USA.

Ray R D (1999) A global ocean tide model from TOPEX/POSEIDON altimetry: GOT99.2, Goddard Space Flight Center, Greenbelt, Maryland, USA.

Reigber C, Bock R, Forste C, Grunwaldt L, Jakowski N, Luhr H, Schwintzer P, Tilgner C (1996) CHAMP phase B executive summary. GeoForschungs -Zentrum (GFZ), Potsdam, Germany.

Reigber C, Schmidt R, Flechtner F, König R, Meyer U, Neumayer K, Schwintzer P, Zhu SY (2005) An Earth gravity field model complete to degree and order 150 from GRACE: EIGEN-GRACE02S, J Geodyn, 39, 1-10.

Reubelt T, Austen G, Grafarend EW (2004) Harmonic analysis of the Earth's gravitational field by means of semi-continuous ephemerides of a low Earth orbiting GPS-tracked satellite, Case study: CHAMP. J Geod, 77, 257-278.

Ries J, Cheng M, Bettadpur S, Chambers D (2008) Low-degree geopotential harmonics from SLR and GRACE. GRACE science team meeting, San Francisco, CA, USA.

Rim H (1992) TOPEX Orbit Determination using GPS tracking system. Ph. D dissertation, Dept of Aerospace Engineering and Engineering Mechanics, The Univ of Texas at Austin, USA.

Schreiner B (2005) COSMIC GPS POD and limb antenna test report. Internal report of UCAR, USA.

Schmidt R, Flechtner F, König R, Meyer Ul., Neumayer K-H., Reigber C, Rothacher M, Petrovic S, Zhu SY, Güntner A (2007) GRACE time-variable gravity accuracy assessment, IAG Symp, 130, 230-243.

Schutz L, Tapley B, Abusali P, Rim H (1994) Dynamic orbit determination using GPS measurements from TOPEX/Poseidon, Geophys Res Lett, 21(19), 2179-2182.

Seeber G (2003) Satellite Geodesy, 2nd Ed., Walter de Gruyter, Berlin, Germany.

Sinclair A (1997) Data Screening and Normal Point Formation: A Restatement of the Herstmonceaux Normal Point Recommendation, http://cddisa.gsfc.nasa.gov/cstg/npt_algo.html.

Švehla D, Rothacher M (2003) Kinematic and reduced–dynamic precise orbit determination of low Earth orbiters, Adv in Geos, 1(1), 47-56.

Švehla D, Rothacher M (2004) CHAMP and GRACE in Tandem: POD with GPS and K-Band Measurements. Joint CHAMP/GRACE Science Meeting, 6–8 July 2004, GeoForschungsCentrum Potsdam (GFZ), Germany.

Tapley B (1997) The gravity recovery and climate experiment (GRACE). EOS, Trans. AGU 78, 46, Suppl-163.

Tapley B, Bettadpur S, Ries J, Thompson P, Watkins M (2004) GRACE measurements of mass variability in the Earth system, Science, 305, 503-505.

Tapley B, Ries J, Bettadpur S, Chambers D, Cheng M, Condi F, Gunter B, Kang Z, Nagel P, Pastor R, Pekker T, Poole S, Wang FG (2005) GGM02 - An improved Earth gravity field model from GRACE, J Geod, 79, 467-478.

Tapley B, Ries J, Bettadpur S, Chambers D, Cheng M, Condi F, Poole S (2007) The GGM03 Mean Earth Gravity Model from GRACE, Proc of AGU fall meeting 2007.

Torge W (1989) Gravimetry, Walter de Gruyter & Co., Berlin, Germany.

Visser PNAM (2005) Low-low satellite-to-satellite tracking: a comparison between analytical linear orbit perturbation theory and numerical integration, J Geod, 79, 160–166.

Visser PNAM, Sneeuw N, Gerlach C (2003) Energy integral method for gravity field determination from satellite orbit coordinates, J Geod, 77, 207–216.

Visser PNAM, van den Ijssel J, Koop R, Klees R (2001) Exploring gravity field determination from orbit perturbations of the European Gravity Mission GOCE, J Geod, 75, 89–98.

Wagner CA (1983) Direct determination of gravitational harmonics from low-low GRAVSAT data. J Geophys Res, 88(B12), 10309–10321.

Wolff M (1969) Direct measurements of the Earth's gravitational potential using a satellite pair. J Geophys Res, 74, 5295–5300.

Wu BH, Fu CL, Liou YA, Chen WJ, Pan HP (2005) Quantitative analysis of the errors associated with orbit uncertainty for FORMOSAT-3. In: Proceedings of the international symposium on remote sensing (ISRS), Korea, 87–90.

Xu PL, Fukuda Y, Liu Y (2006) Multiple parameter regularization: numerical solutions and applications to the determination of geopotential from precise satellite orbits. J Geod, 80, 17–27.

Zheng W, Shao C, Luo J, Xu H (2008) Improving the accuracy of GRACE Earth's gravitational field using the combination of different inclinations, Prog Nat Sci, 18, 555-561.

Zhu S, Reigber C, König R (2004) Integrated adjustment of CHAMP, GRACE, and GPS data, J Geod, 78, 103-108.

Appendix A: Acronyms

ACC	Residual acceleration approach
AOCS	Attitude and Orbit Control System
AOP	Analytical orbital perturbation approach
CES	Coarse Earth and Sun Sensor
CHAMP	CHAllenging Minisatellite Payload
CMT	Center of Mass Trim Assembly
CODE	Center for Orbit Determination in Europe
COSMIC	Constellation Observing System for Meteorology, Ionosphere and Climate
CSR	Center for Space Research
DORIS	Doppler Orbitography and Radio positioning Integrated by satellite
GOCE	Gravity Field and Steady-State Ocean Circulation Explorer
GPS	Global Positioning System
GRACE	The Gravity Recovery and Climate Experiment
GST	Greenwich sidereal time
hl-SST	high-low satellite-to-satellite tracking
ILRS	International Laser Ranging Service
JPL	Jet Propulsion Laboratory
KBR	K-Band Ranging System
LEO	Low Earth orbiter
LEOM	Lagrange's equation of motion
ll-SST	low-low satellite-to-satellite tracking
LRR	Laser Retro-Reflector
NSPO	National Space Organization
POD	Precise Orbit Determination
PRARE	Precise Range and Range Rate Experiment
PCV	phase center variation
RTN	radial, along-track and cross-track
SAD	solar arrays drive
SCA	Star Camera Assembly
SGG	Satellite Gravity Gradiometry
SLR	Satellite Laser Ranging
TDF	Tracking Data Formatter

UCAR the University Corporation for Atmospheric Research

USO Ultra Stable Oscillator

Curriculum Vitae

Position

Department of Civil Engineering

National Chiao-Tung University

1001 University Road, Hsinchu 300

Taiwan, ROC

Phone: (886) 35712121#54990

Fax: (886) 35716257

Email: ltl.cv92g@nctu.edu.tw

WWW: http://space.cv.nctu.edu.tw

Date of Birth

August 9, 1977.

Place of Birth

Yunlin County, Taiwan.

Education

B.S., Civil Engineering, National Chiao-Tung University, June 1999

M.S., Civil Engineering, National Chiao-Tung University, June 2002

- Major: Satellite Geodesy and GIS
- Thesis: Georeference and GIS Systems for Image Acquisition of ROCSAT-2 Satellite Mission
- Advisor: Dr. Cheinway Hwang and Dr. Tienyaun Shih
-

Major Field of Research

Satellite geodesy, Physical geodesy

List of Publications

Referred Journal Articles

Hwang, C, YS Hsiao, and TJ Lin, A digital elevation model of Taiwan and accuracy assessment, Cadastre Survey, 22 (2), 1-19, 2003. (in Chinese)

Hwang, C, TP Tseng and TJ Lin, C.L. Fu, D. Svehla, Precise orbit determination for FORMOSAT-3/COSMIC and gravity application, Chinese Journal of Physics, 28(6), 924-933, 2006. (in Chinese)

Hwang, C, TJ Lin and TP Tseng, BF Chao, Modeling orbit dynamics of FORMOSAT-3/COSMIC satellites for recovery of temporal gravity, IEEE Transactions on Geoscience and Remote Sensing, 46(11), 3412-3423, 2008.

Hwang, C, TP Tseng, TJ Lin, D Svehla, and B Schreiner, Precise orbit determination for FORMOSAT-3/COSMIC, J. Geod, 83, 477-489, 2009.

Hwang, C, TP Tseng, TJ Lin, D Švehla, Hugentobler, and BF Chao, Quality assessment of FORMOSAT-3/COSMIC and GRACE GPS observables: analysis of multipath, ionospheric delay and phase residual in orbit determination, GPS Solut, 14 , 121-131, 2010.

Conference Paper/Presentation

Hwang, C and TJ Lin, Georeference and GIS systems for image acquisition of ROCSAT-2 satellite mission, Proceedings of the 21th Conference on Surveying, Hsinchu, 2002.

Hwang, C, CG Wang, LS Hwang, TJ Lin, LS Chang, YS Lee, and SC Hsu, Orbit and gravity determinations using ROCSAT3/COSMIC GPS data: status 2004. Fall Meeting, American Geophysical Union, San Francisco, December 13-17, 2004.

Hwang, C, TJ Lin, CG Wang, YS Lee and LS Chang, Force modeling for FORMOSAT-3/COSMIC satellites: application to time-varying gravity determination, Scientific Assembly of International Association of Geodesy, and Dynamic Planet 2005, Cairns, Australia, August 22-26, 2005.

Lin, TJ, C Hwang, TP Tseng, Temporal gravity field recovery using FORMOSAT-3/COSMIC kinematic orbit data, FORMOSAT-3/COSMIC

Workshop 2006, Taipei, 2006.

Hwang, C, TP Tseng and TJ Lin, CL Fu, D. Svehla, Precise Orbit Determination For FORMOSAT-3/COSMIC And Gravity Application, Fall Meeting, American Geophysical Union, San Francisco, December 11-15, 2006. (invited)

Hwang, C, TJ Lin and TP Tseng, Recovery and analysis of Earth's gravity field using FORMOSAT-3/COSMIC GPS data, IUGG XXIV General Assembly, Perugia, Italy, July 2-13, 2007.

Shen, YC, C. Hwang, TJ Lin and JH Geng, FORMOSAT-3/COSMIC baseline solution using GPS data, Proceedings of the 26th Conference on Surveying, Yilan, Taiwan, 2007.

Lin TJ and C. Hwang, Recovery of time-varying gravity using GPS data of COSMIC, GRACE and CHAMP, poster paper presented in GGEO 2008 meeting, Crete, Greece, June 23-27, 2008.

Lin TJ and C Hwang, Low-degree gravity change from the GPS data of FORMOSAT-3 and GRACE, WPGM 2010, Taipei, Taiwan, June 22- 25, 2010.

Technical Reports

Chen C.S. and TJ Lin, The gravity surveying work on the first level leveling points, Report of Ministry of the Interior Program, 2002. (in Chinese)

Hwang, C and TJ Lin, Determination and analysis of Earth's gravity field using COSMIC GPS data, Report of National Space Organization 5-year Program, 2003-2007. (in Chinese)

Hwang, C, TJ Lin, TP Tseng, and N. Tangdamrongsub, Precise orbit determination and analysis of Earth's gravity field using COSMIC GPS data, Report of GPS Science and Application Research Center 3-year Program, 2008-2010.